Geosciences Theses   Department of Geosciences

12-17-2019

Comparative Analysis of Water Storage Dynamics and Storage-Discharge Relations among Variably Urbanized Catchments within South River Watershed, DeKalb County, GA

Eimienwanlan Ibhagui

Follow this and additional works at: https://scholarworks.gsu.edu/geosciences_theses

COMPARATIVE ANALYSIS OF WATER STORAGE DYNAMICS AND STORAGE-

DISCHARGE RELATIONS AMONG VARIABLY URBANIZED CATCHMENTS WITHIN

SOUTH RIVER WATERSHED, DEKALB COUNTY, GA

by

EIMIENWANLAN IBHAGUI

Under the Direction of Luke A. Pangle, Ph.D.

ABSTRACT

The study of watershed storage is critical for understanding watershed hydrologic functions, ecosystem dynamics, and biogeochemical processes. However, few studies have quantified how much water lies in the subsurface in urban watersheds. In this study, dynamic storage was estimated, and storage-discharge relations evaluated in Atlanta, GA among variably urbanized watersheds. Streamflow data from 2012-2016 was utilized and the simple dynamical systems model employed. Dynamic storage values in these watersheds are small: ~3mm to ~9mm. The small dynamic storage values observed across the watersheds are linked to watershed urbanization; however, other subsurface properties of the watersheds may also account for this small storage values. Storage-discharge relations across all the watersheds are non-linear, except the most developed sub-watershed (35% impervious surface area). Two less urbanized sub-watersheds (21% and 26% impervious surface area), showed high streamflow sensitivity. Overall, this study shows that the simple dynamical system model performs well in urbanized watersheds and the South River Watershed can be regarded as a dynamical system.

INDEX WORDS: Area-slope relationship, Baseflow, Dynamic storage, Hypsometric index, Recession analysis, Storage-discharge relation, Simple dynamical system, Streamflow sensitivity

COMPARATIVE ANALYSIS OF WATER STORAGE DYNAMICS AND STORAGE-

DISCHARGE RELATIONS AMONG VARIABLY URBANIZED CATCHMENTS WITHIN

SOUTH RIVER WATERSHED, DEKALB COUNTY, GA

by

EIMIENWANLAN IBHAGUI

A Thesis Submitted in Partial Fulfillment of the Requirements for the Degree of

Master of Science

in the College of Arts and Sciences

Georgia State University

2019

COMPARATIVE ANALYSIS OF WATER STORAGE DYNAMICS AND STORAGE-

DISCHARGE RELATIONS AMONG VARIABLY URBANIZED CATCHMENTS WITHIN

SOUTH RIVER WATERSHED, DEKALB COUNTY, GA

by

EIMIENWANLAN IBHAGUI

Committee Chair: Luke Pangle

Committee: Jeremy Diem

Richard Milligan

Electronic Version Approved:

Office of Graduate Studies

College of Arts and Sciences

Georgia State University

December 2019

DEDICATION

This thesis is dedicated first to my late father, Mr. Lawrence Ibhagui, who always prayed for me to excel in my academic pursuits. Secondly, to my mother, Mrs. Regina Uwayeme Ibhagui (Nee Akhigbe), for her constant support and ceaseless prayers.

To two special people in my life: my wife, Oluwatosin Ibhagui (Nee Odubade), and my son, Eronmosele Jonathan Ibhagui. The love, patience, sacrifice, and understanding you both demonstrated while researching and writing this thesis are unquantifiable. Indeed, I would never have completed this project if I have not had you both beside me, supporting and spurring me on. I love you infinitely!

ACKNOWLEDGMENTS

First and foremost, I would like to thank God Almighty for the grace, good health, privilege, and opportunity to pursue this master's program. To Him be all the glory and adoration.

I want to acknowledge the unquantifiable and intellectual assistance, guidance, and support provided by my thesis advisor and committee chair, Dr. Luke Aaron Pangle, from whom I have learned so much. His classes I took inspired me a great deal, and I have come to love catchment hydrology and water science in general. Thank you for your patience and understanding throughout this project. I am immensely grateful. To the other thesis committee members, Professor Jeremy Diem and Dr. Richard Milligan, I say thank you. I appreciate you both for taking the time to read and provide invaluable suggestions for this work. Thanks to the immediate past graduate director, Dr. Lawrence Kiage, for his fatherly role in the course of my study here at GSU and the Chair, Professor Katherine Hankins.

It would be remiss of me not to mention the assistance rendered by the current graduate director, Professor Kabengi (Dr. K, as students like to address her) in the latter days of my program. Not to forget our amiable laboratory coordinator and teaching assistant (TA) supervisor, Atieh Tajik, for her tremendous support for all the semesters I worked as a TA, advising and helping me to transition culturally. I want to thank the excellent faculty and non-faculty members of the Geosciences Department; the former made learning exciting, fun, and interesting, while the latter – Basirat, Bone, and Julia (recently) – ensured my administrative needs were appropriately and swiftly addressed. I thank all my fellow graduate students (past and present) for their camaraderie and cooperation. To mention a few, thank you, Richard Ajewole (fellow Akokite), Fatai Balogun, Abdulkabir Adeniyi Adekunle (aka KB), and Fabian Zowam (I enjoyed those nocturnal moments in the Geospatial Lab figuring out the best approach to our Remote Sensing projects). Also, thank

you, Dr. Daniel Gebregiorgis Yirgaw (graduate students go-to person), for your help on MATLAB. Thank you to Corporate Environmental Risk Management (CERM), Chattahoochee River Keeper (CRK), and Atlanta Regional Commission (ARC) for the opportunity to learn hydrology outside the four walls of the classroom. My most profound appreciation goes to Georgia State University (GSU), the Geosciences Department in particular, for giving me admission and funding, and thus the opportunity to study in a culturally diverse and intellectually stimulating academic environment.

It is often said that it takes a village to train a child. So, I owe a huge debt of gratitude to other people worthy of mentioning. I want to acknowledge and thank my elder brother, Oseiwe Dwight Ibhagui (Engr.), especially. I am eternally grateful to you for your sacrifice and vision for your siblings. You laid the foundation upon which all my academic structure is built. Only God can reward you for your benevolence. To my elder sisters: Patricia, Esther, Blessing, and Evelyn, I am thankful for your encouragement, love, and prayers always. To my younger brother and friend, Oyakhilome Wallace Ibhagui (Ph.D.), I say thank you for the many academic advise, encouragement, and suggestions since our days at the University of Lagos, Akoka.

To all my Christian family members at the Redeemed Christian Church of God (RCCG) Family Praise Chapel (FPC), Decatur, I say thank you for your immense support, spiritually and otherwise. Thank you, Bro. Adebayo and family. Indeed, it has ended in praise!

TABLE OF CONTENTS

LIST OF TABLES

LIST OF FIGURES

1   INTRODUCTION

1.1   Population and Urbanization

The continuous increase of the world's population and migration of people from rural to urban areas have prompted increased attention to the temporal and spatial dynamics of underground stored water and ways of quantifying the resource for proper management, planning, and sustainable development. Globally, more people nowadays are living in cities compared to previous decades. As of 2018, 55% of the world's population resided in urban areas, and it is projected to increase to 68% by 2050 when countries from the global south (less developed) become urbanized (United Nations, 2019). In North America, including the United States, more than 82% of the population lives in urban areas. The U.S. Census Bureau considers an area as urban if it has a population $\geq$ 50,000 or population density that is in the range of 190-390 persons/km^2 (ppskm – persons per square kilometer). The southern region of the U.S., which comprises sixteen states, has been experiencing rapid population growth (O'Driscoll, Clinton, Jefferson, Manda, & McMillan, 2010).

The Atlanta metropolitan area is one of the urbanized cities in the southeast, as well as the entire U.S. The Atlanta region has been experiencing massive and continuous population growth over several decades (Lo & Yang, 2002; Smucygz, Clayton, & Comarova, 2010). As reported by Rose & Peters (2001), the population witnessed a jump of approximately 191%, increasing from 1.1 to 3.2 million persons between 1960 and 1999, while Diem, Hill, & Milligan (2018) reported a population growth of roughly 141% for 29 counties from 2.2 million persons in 1980 to 5.3 million persons in 2010. A population demographic report released by the Atlanta Regional Commission (ARC, 2018) estimated the population of the Atlanta region, comprising Cherokee, Clayton, Cobb, DeKalb, Douglas, Fayette, Fulton, Gwinnett, Henry, Rockdale counties and the

City of Atlanta, to be 4.56 million. This is an increase of 1.7% from the previous year's population size of 4.48 million. Population density (persons/area) has been used as a proxy for urbanization (Brandes, Cavallo, & Nilson, 2005). Urbanization leads to changes in the natural landscape and local climate, resulting in urban heat island (UHI) phenomenon, reduced evapotranspiration due to loss of vegetation, increased impervious surface cover, land cover/land use change, and alteration or re-engineering of the urban hydrologic cycle (O'Driscoll, Clinton, Jefferson, Manda, & McMillan, 2010). As population increases, land development becomes inevitable. Water resources are stressed in urban areas due to increased demand for diverse domestic, recreational, industrial, and commercial applications.

1.2   Impervious Surface

The hydrologic consequences of urbanization are commonly attributed to watershed imperviousness. In separate studies, Stankowski (1972) and Zhou, He, Nigh, & Schulz (2012) found impervious surface and human population/population density to be strongly correlated. High streamflow velocity, increased volume of surface runoff (quick flow), and elevated peak flows are the hydrologic outcomes of increased imperviousness. Others are flashy streams, frequent flooding, reduced infiltration, point and non-point sources of pollution of streams and rivers resulting in poor water quality, stream scouring, and declined groundwater recharge with a concomitant reduction in storage, ultimately leading to decreased baseflow (Rosburg, Nelson, & Bledsoe, 2017). Although urbanization has modified natural recharge mechanisms, it does not always lead to reduced recharge, as it is often believed (Lerner, 2002). In a study of water fluxes in a residential area, Ragab, Rosier, Dixon, Bromley, & Cooper (2003) found that between 6% and 9% of annual rainfall actually infiltrated the road surface in the United Kingdom contrary to the assumption among hydrologists and city planners that infiltration is 0% and runoff is 100% of

precipitation. In a formerly glaciated, highly urbanized catchment in Canada (the watershed is 75% developed), Meriano, Howard, & Eyles (2011) found that approximately 6% of total rainfall contributed to groundwater recharge. These results contradict the commonly held view about infiltration and groundwater recharge in urban settings (Rose & Peters, 2001; Rosburg, Nelson, & Bledsoe, 2017).

Notwithstanding, impervious surfaces are hardened, solid land surfaces that prevent water from infiltrating the soil and percolating more in-depth into the subsurface, thus significantly reducing, if not preventing entirely, the recharge or replenishment of groundwater. Examples of impervious surfaces in urban areas are rooftops, asphalted roads, compacted or sealed soils, shopping malls, paved areas, and bridges. As noted by Arnold & Gibbons (1996), the impervious surface is a significant indicator of the degree of urbanization and environmental quality. Watersheds with more impermeable surface experience high speed at which pollutant loads are transported to water bodies (the first flush phenomenon) and aquatic habitat displacement due to stream impairments in urban catchments. Different impervious thresholds have been reported that can cause impairment of streams. For example, Schueler (1994) found that an increase of 10% impervious area of a watershed increased stream scouring and temperature (due to the loss or reduction of tree cover). Ourso & Frenzel (2003) reported that 4.4-5.5% imperviousness of the drainage area in their study in urbanized Anchorage, Alaska resulted in stream impairment.

There is an ongoing debate concerning what parameter to use between Directly Connected/Effective Impervious Area (DCIA/EIA) and Total Impervious Area (TIA) in the modeling of watersheds to better quantify the effects of urbanization on catchment hydrology. EIA refers to impervious surfaces that are directly connected to drainage networks or conveyance systems for effective transportation of stormwater from their origin e.g., culverts, curbs, gutters,

or runoff from parking lots that are connected to surface waters or treatment plants (Ebrahimian, Wilson, & Gulliver, 2016). On the other hand, TIA represents a proportion or percentage of an area that is developed (Arnold & Gibbons, 1996) like driveways, roof/rooftops, sidewalks, bridges, and compacted/sealed soils. Several investigators of urban imperviousness have developed empirical equations that connect EIA and TIA. Shuster, Bonta, Thurston, Warnemuende, & Smith (2005) proposed a power-law relationship between EIA and TIA of the form $EIA = 0.15(TIA)^{1.41}$ and Wenger, Peterson, Freeman, Freeman, & Homans (2008) suggested a linear relationship between the two variables from their study in Etowah River Basin, Atlanta: $EIA = (1.046 \times TIA) - 6.23$, where EIA and TIA are in percent, and EIA = 0, for TIA values < 6.23%. Both empirical relationships have a similar coefficient of determination ($R^2 = 0.98$), implying a solid association, although their contrasting functional forms suggest that the relationship may be modulated by basin-specific features of the impervious surface cover.

Figure 1 is an illustration that summarizes the relationship, by percentage, between impervious and pervious areas, and the degree to which an area is sewered (e.g., piped), typical of an urbanized watershed. Qualitatively, it shows that as the percentage of sewered and impervious areas increase, the time of concentration decreases (the time it takes water to exit a catchment from a remote location upslope). That is, rainwater reaches a stream or river quickly after a storm event. Conversely, it takes event water a longer arrival time as the percent pervious (e.g., vegetated) and natural detention (e.g., lake) areas increase. Urban catchments are heavily reticulated (sewer pipes, septic tanks, drinking water pipes, et cetera). For example, Rose (2003) reported that the highly urbanized Peachtree Creek watershed in Atlanta, Georgia, is underlain by sewage and stormwater pipes that cover 3400km. In some other catchments, there are water withdrawal plants (WWPs) and wastewater treatment plants (WWTPs). Leakages from these aging, dilapidated, and old

infrastructures, as well as discharge from these facilities, contribute to groundwater recharge, thus complicating urban hydrologic systems. Furthermore, urbanization reduces vegetation in and around riparian corridors. This reduced vegetation affects the temperature of streams as fewer tree covers are available to shield them from harsh solar radiation.
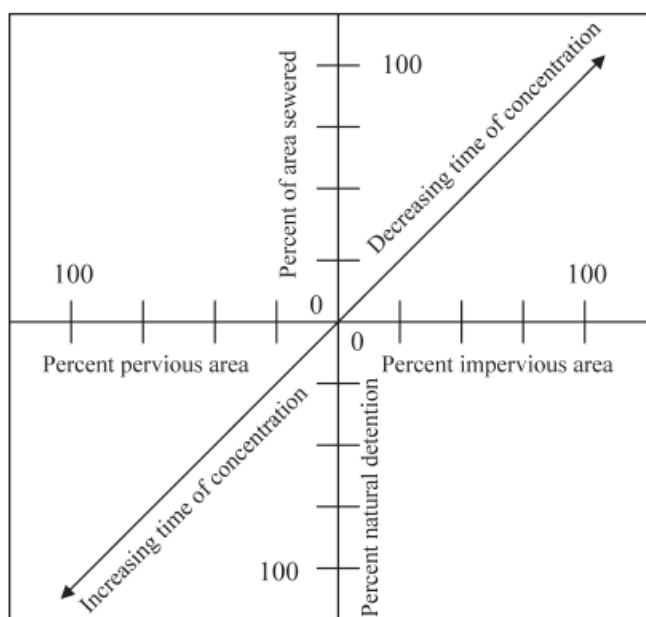
Figure 1. Relationship between impervious and pervious areas, and sewerage (pipes). Source: (Shuster et al., 2005).

The several adverse effects of impervious surfaces in urban areas are collectively referred to as urban stream syndrome. Impervious surface tremendously affects socio-economic, hydrologic, and ecologic systems in urban areas, as well as on urban water budget and groundwater systems. For instance, economists use impervious cover to set rates for stormwater utilities; engineers utilize impervious area as an important variable to predict downstream hydrology and design stormwater management practices; ecologist use the knowledge of impervious cover to categorize and manage urban streams, and watershed managers depend on this metric plus other hydrologic parameters to model changes in stream health, manage surface water intake points by preventing point and non-point pollution, and groundwater for future development (Walsh et al.,

2005; Wickham, Wade, & Norton, 2014). Apart from vegetation that intercepts rainfall in urban settings, bridges built at different elevations above the land surface intercept rainfall. Some of the resultant flow exit openings on the bridge designed for expansion and contraction, and fall unto pervious areas, while others evaporate. Besides, very tall commercial and residential buildings with open spaces at the top intercept rainfall and act as a temporary storage reservoir which later returns (evaporate) to the atmosphere.

1.3   Land Cover and Land Use (LCLU)

Water quality evaluation, planning, and management activities have made the knowledge of land cover and land use important for hydrologic analysis. The term land cover refers to what landscape feature is present on the surface of the earth. Categories commonly include surface water (lakes, rivers, streams), vegetation (crops, tree canopies, forest), wetland, and human-made materials like concrete highways or asphalted/paved roads. On the other hand, land use refers to the activities performed on the land, i.e. the interaction with the natural environment. For instance, a parcel of land could be used for agriculture, commerce, housing, or transportation. The conversion of land from one form to another (e.g., agriculture to urban/suburban development) is termed land use change. The detection of this change is commonly investigated using aerial and satellite imageries and applying Geographic Information System (GIS) or remote sensing techniques. In the context of hydrology, it is vital to understand how land cover change impacts a catchment's rainfall-runoff characteristics for a better watershed decision making and planning.

1.4   Baseflow

A hydrograph – a time series plot of discharge – can be conceptualized as consisting of two parts: quick flow and baseflow. In urban areas, quick flow or direct runoff results from the rapid transmission of rainwater over impervious surfaces following a rain event to a nearby waterbody.

In non-urban settings, quick flow is caused by multiple possible mechanisms. One mechanism involves infiltration of precipitation in near-stream areas, which leads to rapid pressure head difference in riparian, unconfined aquifers and causes water to discharge into the stream quickly. A second mechanism is referred to as Hortonian (after Robert Horton), or infiltration excess overland flow, whereby the rate of precipitation exceeds the rate at which the surficial soil can be infiltrated. A third mechanism is commonly called saturation-excess overland flow and results due to the temporary expansion of a zone of completely water-saturated soil up to the land surface. A temporary rivulet rapidly transmits water over the land surface to the stream channel.

Baseflow is defined as the release of water from the subsurface into a stream channel or that component of streamflow that emanates from groundwater storage or other delayed sources (Hall, 1968; Price, 2011). Alternatively, baseflow may be identified as that flow occurring during rainless periods between precipitation events. The so-called baseflow persists during storm events and is supplemented by the mechanisms of quick flow described above. An inverse relationship exists between urbanization and baseflow. As an area becomes urbanized due to the increase in impervious surface area, less water infiltrates and percolates into the subsurface, causing baseflow reduction and water table decline due to limited groundwater recharge (Rose & Peters, 2001). Baseflow is often studied in hydrological research because of its diverse application in water resources planning and management. The extraction of baseflow from streamflow time series is performed by hydrograph separation, and it entails three basic techniques: analytical, empirical, and isotope/tracer-based methods (Stewart, 2015). Although these hydrograph separation techniques have been criticized for being arbitrary, subjective (the first two methods), and uncertain (the latter method), they are still widely utilized in hydrologic investigations. Despite the uncertainty associated with them, isotope/tracer-based methods are considered by far as the most

objective measurement of baseflow and quick flow components of total streamflow (Bosch, Arnold, Allen, Lim, & Park, 2017; Stewart, 2015). A metric commonly used to quantify baseflow is the baseflow index (BFI). It is the ratio of the volume of baseflow to the volume of streamflow (Price, 2011). High BFI is suggestive of a stream dominated by groundwater discharge. In urban catchments, several studies have examined baseflow to understand how it is impacted and its generation processes (Brandes et al., 2005; Kauffman, Belden, Vonck, & Homsey, 2009; Rose, 2007; Rose & Peters, 2001). The magnitude of baseflow and BFI depend on climatic conditions, evapotranspiration, and catchment water storage (Bosch et al., 2017; Zecharias & Brutsaert, 1988).

1.5   Catchment Water Storage

In hydrology, a catchment, interchangeably used either as a watershed, basin, or drainage area, is an area of land from which all water drains, running downslope from an upslope area, to a common point. This point can be any surface water body such as river, pond, stream, lake, or an estuary. According to Black (1997), a catchment has two broad functions: ecological and hydrological. The former refers to the provision of habitat for fauna and flora, which are biological elements of ecosystems, in addition to locations and pathways for critical chemical reactions to occur. Hydrologically, a catchment has three primary functions: capture/collect, detain/store, and discharge/release water. Firstly, in a precipitation event (rainfall or snowmelt, for example), the catchment collects water and facilitates its entry into the ground in the area where it falls. Depending on factors such as topography (elevation and slope), soil type, geology, climate, and vegetation, the water infiltrates the soil and percolates deeper to recharge aquifer/groundwater. Equally, catchments store rainwater within the soil column and aquifer until full saturation is attained wherein release in the form of runoff to a surface water body becomes inevitable. Thus, between "collecting" and "releasing" of water from a catchment is "storing."

Catchment storage modulates flooding and contributes to streamflow during extreme weather conditions (e.g., drought) to sustain streams and ensure ecosystem functioning (Aulenbach & Peters, 2018). Also, storage controls mean travel and residence times of water in the subsurface (Katsuyama, Tani, & Nishimoto, 2010). Biogeochemical processes in the hyporheic zone and hydrological processes that occur in catchments are facilitated by storage (Tetzlaff, McNamara, & Carey, 2011), as well as the provision of plant-available water. The hyporheic zone is a distinct environment in streams where groundwater and surface water interact, or exchange of flow takes place, and it is a vital component of the lotic system (Hayashi & Rosenberry, 2002). The volume of water stored within a catchment defines the state of the hydrologic system at that scale (Tetzlaff et al., 2011). Consequently, catchment water storage may be utilized as a metric to compare catchments (McNamara et al., 2011). In recognition of the critical roles that storage plays in catchment hydrologic processes, there has been a clarion call for hydrologist to renew interest and devote energy, resources, skills and time to the study of catchment water storage (McNamara et al., 2011; Tetzlaff et al., 2011) to gain understanding on catchment discharge dynamics and dominant hydrologic processes. This clarion call seems to have been heeded with the publication of several studies on catchment storage dynamics using rainfall-runoff models, recession analysis and storage-discharge relationship among other methods: Ajami, Troch, Maddock, Meixner, & Eastoe (2011); Aulenbach & Peters (2018); Berghuijs, Hartmann, & Woods (2016); Bhaskar & Welty (2015); Buttle (2016); Carrer, Klaus, & Pfister (2019); Creutzfeldt et al. (2014); Dralle et al. (2018); Hector et al. (2015); McNamara et al. (2011); Peters & Aulenbach (2011); Pfister et al. (2017); Sayama, McDonnell, Dhakal, & Sullivan (2011); Maria Staudinger et al. (2017); Tetzlaff et al. (2011); and Teuling, Lehner, Kirchner, & Seneviratne (2010). Chapter 2 provides a review

of some catchment water storage studies, particularly those that have utilized the approach in this research.

1.5.1 Storage Definitions

Catchment storage estimation and comparison depend on the type of storage. Storage varies spatiotemporally, seasonally, and topographically. In hydrologic literature, storage has different definitions (Dralle et al., 2018; Maria Staudinger et al., 2017; Tetzlaff et al., 2011). The definition given to a particular type of storage is a reflection of the methodology used to derive it (hydrodynamic or a transport concept) (Maria Staudinger et al., 2017). Here, three types of storages are described.

i. *Dynamic Storage*: This is the volume of porous geologic material that ranges from being fully saturated to variably desaturated over the time of scale of a typical inter-storm period (e.g., one to several days in our humid subtropical climate). In space, the dynamic storage is often conceived of as those depths below ground, including the variably-wetted soil and the zone where the water table surface regularly fluctuates.

ii. *Immobile Storage*: This is the volume of water within a catchment that has residence time that is generally orders of magnitude greater than the dynamic storage. In space, the immobile storage might be associated with (1) the deepest layers of an unconfined aquifer, where hydraulic gradients are very small, and not exhibiting much temporal variation, or (2) water stored within very fine-textured sediments (e.g., clay and silts) that are mixed throughout the soil and/or aquifer, and that have significantly lower hydraulic conductivity than surrounding geologic material.

iii. ***Total Storage***: The sum of dynamic and immobile storage. Most empirical analyses to date indicate that immobile storage is often the majority fraction of total storage within low-order watersheds.

Dynamic storage controls catchment hydrodynamics and so can be quantified using rainfall-runoff models. The quantification of catchment storage can give insight into the sensitivity of catchments to extreme events and pollution. Model-based estimates of catchment storage are uncertain because of our inability to validate them with actual data-based estimates. Additionally, bedrock topography is complex, and there are uncertainties associated with bottom boundary conditions of catchment-scale storage (Dralle et al., 2018; Kobayashi & Yokoo, 2013; Tetzlaff et al., 2011).

Measuring and predicting the amount of water stored within a catchment is infrequently done, even studying the storage dynamics is often overlooked (McNamara et al., 2011; Tetzlaff et al., 2011), yet this is the water released from the subsurface that eventually becomes baseflow in stream channels. Despite numerous baseflow studies in urban catchments as listed in Section 1.4, there is a far lesser number of studies on the behaviors and dynamics of storage at the catchment level in urban settings (Bhaskar & Welty, 2015). One study, however, that has investigated this topic in an urban catchment is that by Bhaskar & Welty (2015) where they used a hybrid approach (environmental isotopes and a hydrologic model) to analyze subsurface storage in three urbanized catchments in Baltimore, Maryland. However, the study did not estimate or quantify dynamic catchment water storage. Thus, there is still a lack of study on catchment water storage dynamics, storage-discharge relations, and spatiotemporal patterns in streamflow recession characteristics (Karlsen et al., 2019) at the catchment scale in urban settings. As a result, this research attempts to bridge this knowledge gap by applying the simple dynamical systems approach proposed by Kirchner (2009), hereinafter referred to as SDS model, which utilizes the water balance equation

and streamflow sensitivity function [g(Q)] to estimate catchment dynamic storage and examine storage-discharge relationships in South River Watershed (SRW) and its sub-watersheds in the Piedmont physiographic province of Atlanta, Georgia. The sensitivity function describes the behavior of discharge (Q) to changes in storage (S) and is derived from the streamflow recession analysis technique of Brutsaert & Nieber (1977).

The current study is partly motivated by previous work by Diem et al. (2018) in the SRW. It was one of the eight catchments in their study of multiple decades of streamflow changes in the Atlanta metropolitan area where they compared these drainage basins by utilizing population and land cover datasets, as well as diverse streamflow variables to examine streamflow trends due to the impacts of urbanization. In the study, the authors found that SRW behaved anomalously among similarly or more urbanized catchments, displaying high runoff ratio, high flow days (even in summer), and high baseflow index (BFI) which they attributed to the combined contribution of effluent discharge from two wastewater treatment plants (WWTPs) within the basin. This is opposite the results presented by Schwartz & Smith (2014) from the catchments they studied in a similar climatic and physiographic setting as SRW, where they showed that urban catchments exhibited low BFI. Contrasting results from studies in urban catchments suggest that the investigation of catchment water storage and how it controls streamflow (baseflow) generation using a different tool might give a better understanding of catchment functioning and the dominant hydrologic processes in these watersheds. Here, the relationship between dynamic storage and discharge is investigated among nested watersheds located in SRW, which is situated in the Upper Ocmulgee River Basin (ORB).

1.6   Research Questions and Objectives

The overarching goal of this research is to utilize streamflow data and the SDS model to quantify dynamic storage in each catchment. The questions this study seek to answer are as follows: (i) what is the amount of dynamic storage in an urbanized catchment, and how does it vary across different catchment scales? (ii) how do streamflow recession curves behave in a set of nested urban catchments? (iii) what inference can be drawn from the storage-discharge relationship across the nested catchments in terms of hydrological processes and what is the variation of the discharge sensitivity function [g(Q)] across an urban-suburban gradient? Specific objectives of this study are to (1) provide a comprehensive characterization of the catchments in terms of bedrock geology, land cover categories, population, and soil types; (2) examine the geomorphologic (hypsometry and slope-area relationship) and hydrologic descriptors (flow duration curves and baseflow index) of the catchments; and (3) determine the functional form of storage-discharge relationship and compute dynamic storage for the catchments.

2   LITERATURE REVIEW

2.1   Recession Analysis

Recession analysis has a long history in hydrology (Brutsaert & Nieber, 1977; Hall, 1968). Hydrograph recession behavior was usually observed by plotting discharge (Q) against time (t). The approach required the determination of the onset of the recession (i.e., recession start time), which could introduce bias in the result, especially for multiple events. This problem was resolved by Brutsaert & Nieber (1977) when they proposed a power-law relationship between the negative time derivative of discharge and the mean discharge over the same time increment: $-dQ/dt = aQ^b$, where 'a' is related to the catchment properties such as hydraulic conductivity and porosity, while 'b' is a function of Q and determines the shape (slope) of the recession curve. For early recession, b = 3, and b = 3/2 for late recession. A plot of $-dQ/dt$ against Q on a log-log scale is called "recession plot." The authors determined the parameters 'a' and 'b' of the power-law function by using the lower envelope of the recession plot. They reasoned that it was least affected by evapotranspiration and represented the release of stored water from the subsurface to streams.

In developing the SDS model, Kirchner (2009) applied the Brutsaert & Nieber (1977) recession analysis technique to obtain recession parameters. However, he did not use the lower envelope of the recession plot because it has been demonstrated to be associated with random variability, measurement noise (Rupp & Selker, 2006), and impacted by evapotranspiration (Teuling et al., 2010). Removing this portion of the dataset would introduce bias in the estimate of mean $-dQ/dt$ and Q. He overcame this problem by applying the central tendency of $-dQ/dt$ (binned means) to obtain recession parameters and derived a sensitivity function, g(Q). Individual hourly data points of $-dQ/dt$ and Q were binned into ranges of discharge. The mean and standard error for each parameter within the bin was computed under the condition that the standard error (SE)

in the negative time derivative of discharge must be less than or equal to half its mean. Further, Kirchner (2009) used a polynomial quadratic function to fit the binned data because he found it to be both flexible and smooth to capture essential attributes of the data and allows extrapolation beyond the range of the binned data. The SDS model is described in greater detail in Chapter 4.

Stoelzle, Stahl, Morhard, & Weiler (2014) conducted an intercomparison study of three recession analysis methods (RAMs) and three parameter-fitting methods to a power-law model, to distinguish specific catchment behavior. These methods are ordinary least squares regression (Vogel & Kroll, 1992), lower bound/envelope method (Brutsaert & Nieber, 1977), and least squares regression, weighted by inverse variance on the binned means (Kirchner, 2009). They applied the method to twenty predominantly forested catchments. Results showed enormous variation, up to two orders of magnitude, of recession parameter values, and recession characteristics. The authors attributed this variation to differences in the specificity and distinctiveness of each RAM. Nevertheless, the study showed that the Brutsaert & Nieber (1977) lower envelope approach estimated storage depletion better than the other two techniques. The explanation offered for this observation was that the Brutsaert & Nieber (1977) method focused on the late recession period (lower envelope) and excluded early recession time (upper envelope), which can lead to shorter recession times and poor estimation of storage depletion.

Chen, Kumar, Basso, & Marani (2018) extended this intercomparison study by introducing an experimental approach which they called "control set up" and added another method to the ones evaluated in the study by Stoelzle et al. (2014) – the event-based method of Basso, Schirmer, & Botter (2015). Rather than use the ensemble of points to characterize recession flow, this method investigates each recession period, defined as the time interval of two days after precipitation events until the next storm begins, and with a continuous reduction in streamflow for at most five

days. The authors applied all four methods to forty-five catchments across seven states in the southeastern U.S to examine the performance of the different recession schemes. They compared observed with reconstructed streamflow based on the sensitivity function, g(Q), they generated. The results showed that the binning method by Kirchner (2009) and the event-based method by Basso et al. (2015) were superior in obtaining storage-discharge relation and reconstructing streamflow. In contrast, the lower envelope method of Brutsaert & Nieber (1977) performed poorly. Their result confirmed that of Stoelzle et al. (2014) in terms of the variability of recession parameter values and recession characteristics. Nonetheless, the superiority portrayed by the binning approach of Kirchner (2009) over the lower envelope method of Brutsaert & Nieber (1977) may be attributed to differences in catchment areas. The maximum catchment area in the study by Chen et al. (2018) was $25km^2$, whereas for Stoelzle et al. (2014), it was between $26km^2$ and $954km^2$. Kirchner (2009) noted that his method must breakdown for large catchments due to high lag time (the time interval between rainfall and discharge peaks), but what is unknown is the size of the catchment that will bring this about.

2.2   The Simple Dynamical System (SDS) Model and Catchment Water Storage

2.2.1   The Simple Dynamical System Model

Under the assumption that discharge to stream channels in catchments is a function of the amount of stored water within them, recession analysis has been used to investigate dynamic catchment storage (Troch et al., 2013; Wittenberg, 1999). The method has also been applied in the development of a functional form for storage-discharge relation, and estimation of groundwater recharge volume in a mountainous catchment (Ajami et al., 2011). By combining the relationship between recession rate and discharge with the water balance equation (which measures the time rate of change of water storage in a catchment), Kirchner (2009) formulated the simple dynamical

systems (SDS) model in which a catchment is considered as a first-order dynamical system. He assumed that discharge (Q) is a single-valued function of storage (S), and the calculations use discharge data when it can be reasonably assumed that discharge is significantly greater than evapotranspiration (E) and precipitation (P) (i.e., Q >> E and P).

The merits of this approach are that it is data-driven, does not involve baseflow separation, and the functional form of the storage-discharge relationship is not assumed a priori based on overly simplified assumptions. So, it enables a broad category of relationships between storage and discharges to be derived based on the observed functional form of the discharge sensitivity function, g(Q). The SDS model is a known conceptual, lumped, parsimonious model that requires no calibration and is used to estimate dynamic storage and characterize storage-discharge relations in various catchments. In addition, the approached has been applied extensively across diverse scales, geology, hydroclimatic, and physiographic settings Further, it has been demonstrated to work as much as other complex, highly parameterized models (Kirchner, 2009; Krier et al., 2012) even at scales up to approximately 3,000km^2 (Hailegeorgis, Alfredsen, Abdella, & Kolberg, 2016). Hence, the method has shown that rainfall-runoff models may not necessarily have to be complex which in a way answers Jakeman & Hornberger's (1993) question: "how much complexity is warranted in a rainfall-runoff model?" The methodology is described at great length in Chapter 4. However, Kirchner (2009) tested the SDS model to hourly streamflow data from two catchments (Severn and Wye) in Plynlimon, mid-Wales, United Kingdom to estimate catchment sensitivity to changes in storage, quantify dynamic storage, simulate hydrograph from S-Q relation, estimate catchment sensitivity to antecedent moisture, characterize recession time constants, estimate catchment-averaged precipitation rates and infer evapotranspiration patterns in what he broadly called 'doing hydrology backward'.

By using recession analysis and fitting data to a power-law function, Melsen, Teuling, van Berkum, Torfs, & Uijlenhoet (2014) demonstrated that one season of five months was adequate to determine sensitivity function parameters for the simulation of high flows in the Rietholzbach catchment in Switzerland. According to the authors, this season should be one with the least evapotranspiration (winter season). Their result showed that hysteresis exists in the storage-discharge relation, which contradicted the result of Teuling et al. (2010), where they had concluded that there was no 'strong hysteresis' between storage and discharge in a previous study at the same catchment. This new revelation led Melsen et al. (2014) to state that the SDS model does not yield a physically realistic representation of the separate hydrological processes in the catchment and so oversimplifies reality, which induces 'model structural uncertainty' in the results. In their published work, Teuling et al. (2010) noted that the assumptions in the SDS model do not mean that the catchment properties and fluxes are analogous spatially, neither do they imply that minor processes, pipe flow, for example, are less important in controlling catchment hydrological response. Rather, they imply that processes at the catchment scale are dependent on storage under negligible evapotranspiration, precipitation, and snowmelt, which means that saturated (passive) and unsaturated (active/dynamic) storages in the catchment are hydraulically connected.

Krier et al. (2012) applied Kirchner's (2009) approach to twenty-four geologically diverse sub-catchments of the Alzette catchment in Luxembourg with a maximum size of 1,092km^2 to derive precipitation time series for each catchment. Their results show that the model performed well, leading them to conclude that the approach could be effectively utilized in catchments with heterogeneous lithology. After separating the hydrograph into its component fast-flow and slow-flow respectively, as suggested by Stewart (2015), and employing stream water electrical conductivity (EC) as a tracer, Rusjan & Mikoš (2015) applied the SDS model to each flow type to

generate catchment sensitivity function. The reason for the separation was because stream formation was influenced by bypassing flow due to low hydraulic conductivity in their study area, the Padez catchment in Slovenia. Also, their study catchment had limestone bedrock with significant flow through dissolution channels. The authors demonstrated that both the recession analysis method and the two-component hydrograph separation technique could be applied to simulate streamflow to account for the impact of fast flow in a catchment where subsurface storage does not solely generate streamflow.

Adamovic, Braud, Branger, & Kirchner (2015) assessed the SDS model in characterizing four catchments of the Ardeche Basin in France, ranging in size from 16 to 103km^2. They obtained good results for discharge simulation under wet conditions, but poor result under dry conditions. The poor SDS performance was linked to disturbed water balance terms and high influences of actual evapotranspiration (AET) and discharge measurement errors. Hailegeorgis et al. (2016) examined the SDS model in four nested catchments in a mountainous and snow-influenced boreal catchment in Gaula watershed in central Norway and its sub-catchments having a maximum catchment area of 3090km^2 to evaluate the performance of the model. It was discovered that the model reproduced both the observed streamflow hydrographs (NSE = 0.83) and flow duration curves. Nevertheless, the authors noted the vulnerability of the model to parameter uncertainty and identifiability problems, which they linked to the lower envelope of the recession plot and minimum length of recession segments. Although Kirchner (2009) stated that his model would fail at large catchments, this result shows otherwise and contradicts the findings of Stoelzle et al. (2014). Li & Nieber (2017) modified the SDS model by normalizing g(Q) with initial storage condition of the catchment for improvement of model performance in both dry and wet seasons, and to accommodate hysteresis. The latter has been observed in watershed-scale storage-discharge

relationships (Weill et al., 2013; Xu, Saiers, Wilson, & Raymond, 2012) due to different storage compartments and flow paths, although not many direct observations of this phenomenon have been recorded since total catchment storage is not directly observable. Li & Nieber (2017) applied the model to the Sagehen Creek watershed in Sierra Mountains, California. They found that it performed better than Kirchner's (2009) original model in simulating discharge, although there were still some observed errors attributed to the non-unique spatial distribution of water storage in the catchment.

2.2.2 Catchment Water Storage

Catchment water storage varies spatially and temporally, and subsurface flow is heterogeneous and complex. This makes point and plot scale measurements of water storage using soil moisture and groundwater table level insufficient to characterize storage dynamics. The size of a catchment is about a million times (10^6) more than the scale these measurements are made. Thus, catchment water storage measurement is generally difficult, and infrequently estimated, much less reported (McNamara et al., 2011; Tetzlaff et al., 2011). To overcome this challenge, techniques such as geophysics (microgravity), conservative tracers/isotopes, gravimetry (Creutzfeldt et al., 2014), remote sensing (GRACE, Gravity Recovery And Climate Experiment) satellite (Krakauer & Temimi, 2011; Riegger & Tourian, 2014) and models (Dralle et al., 2018; Krakauer & Temimi, 2011) have been employed to provide estimates of catchment water storage. These methods can measure dynamic storage, which is the subject of this research. Here, Kirchner's (2009) simple dynamical systems (SDS) model is applied.

Kirchner (2009) used the SDS model at the Severn and Wye catchments in mid-Wales, which possess a humid climate and are dominated by grassland and conifer plantations. Using hourly rainless nighttime streamflow data from these catchments, he found that the Wye catchment

responded abruptly to precipitation and yielded a dynamic storage value of 62mm, whereas the less responsive Severn produced a dynamic storage of 98mm. Teuling et al. (2010) investigated whether the Rietholzbach catchment in Switzerland behaves like a simple dynamical system by applying the model. Unlike Kirchner (2009), they used a piecewise regression and two-parameter sensitivity function (power-law) model to infer dynamic catchment storage. They found the estimate of yearly average dynamic storage at the Rietholzbach catchment to be 104mm, while over the whole 32-year period of record, the maximum estimated storage was 205mm. The storage value was compared to measurements from a lysimeter and simulations made with a land surface model. Observed streamflow was simulated with good results (Nash-Sutcliffe efficiency, NSE = 0.60, 0.90, and 0.92 for August, February, and November, respectively). Evapotranspiration was found to be the dominant flux that controlled streamflow changes more than rainfall and snowmelt.

Ajami et al. (2011) applied the SDS model to estimate mountain block recharge (MBR) at three catchments in the Santa Catalina Mountains. They considered MBR to be equivalent to the lower bound of storage derived from the S-Q relationship. Using both linear and quadratic expressions of the S-Q function, they obtained MBR values ranging from 14.8mm to 25.7mm for observed streamflow data. Despite the different MBR estimates by the different models, they had the same order of magnitude. Birkel, Soulsby, & Tetzlaff (2011) used a nonlinear S-Q function and tracer-based conceptual lumped model to estimate dynamic storage for two catchments in Scotland. Their results showed that water storage varied with the catchment area. The catchment with an area of 3.6km^2 had an average dynamic (active) storage of 35mm, whereas the average dynamic storage for the bigger catchment with an area of 30.4km^2 was 15mm. Passive storage estimated using oxygen isotope showed that catchment storage is higher by an order of magnitude (500-900mm) than those estimated using both models with the smaller catchment still having the

largest storage value. The inequality of the dynamic storage values for these nested catchments was attributed to differences in model assumptions and conceptualization.

Chen & Wang (2013) used recession analysis to evaluate the effect of partial contributing storage due to unstable subsurface hydrologic connectivity on water S-Q relation in nine catchments in different climate regions in U. S. The authors found that the ratio of estimated storage to observed storage was somewhat stable during individual recession event across the catchments but correlated negatively with the water table depth and varied markedly among recession events. Partial contributing storage effect from hillslope, riparian, and stream zones was given as an explanation for this observation. The reduction in water table caused a corresponding decrease in the hydrologic connection among landscape zones (hillslope, riparian, and stream). Brauer, Teuling, Torfs, & Uijlenhoet (2013) applied three methods: hydrograph fitting, recession analysis, and direct-storage discharge fitting to investigate if the less humid lowland Hupsel Brook catchment in Netherland behaved like a simple dynamical system. They applied the SDS model and concluded that discharge depended on storage; however, the dependence was not well captured by a linear reservoir. It was demonstrated that the catchment did not always behave like a simple dynamical system as only 39% of the fitted monthly hydrographs yielded Nash-Sutcliffe Efficiencies > 0.5. Notably, the SDS model decreased with humidity (did not perform well under dry conditions). This poor model result was attributed to the seasonality effect of ET and sampling uncertainty on parameters of the storage-discharge relations for the methods used. From the direct storage-discharge fitting analysis, they observed that the change in storage from two soil moisture measurement sites (local storage change) was two to six times more than the change in storage calculated using water balance equation (catchment storage change) over the same period. The difference was ascribed to the location of the soil measurement sites, which are far away from

draining channels and tend to show a significant variation in groundwater level. A correction for this reduced the local storage change two to six times.

Bhaskar & Welty (2015) applied the SDS model to establish a relationship between storage and streamflow in three catchments ranging in area from 2.8km^2 to 14km^2 in Baltimore, Maryland, depicting an urban-to-rural gradient. The SDS approach showed that the most urbanized catchment displayed the highest discharge sensitivity and discharge response with respect to dynamic storage changes. Additionally, all the catchments exhibited a steep storage-discharge relationship except the most urbanized catchment. Buttle (2016) studied the characteristics of dynamic storage at five catchments in Ontario, Canada with similar topography, land cover (mainly forest and agriculture), climate, and hydrogeology using the SDS model and hydrogen isotope. They obtained dynamic storage values ranging from 30mm to 77mm for the catchments. Result also showed that there was no relationship between dynamic storage and catchment characteristics. However, dynamic storage was shown to be directly related to the ratio of the standard deviation of hydrogen isotope in streamflow to precipitation, implying that greater dynamic storage is linked to shorter mean transit times (MTTs) in the catchments - dynamic storage is inversely related to MTT.

Maria Staudinger et al. (2017) employed four methods, including the SDS model, to quantify dynamic storage in twenty-one prealpine and alpine catchments having mean elevation ranging from 500m to 2500m above sea level (a.s.l) in Switzerland. Their study generally illustrated that the storage estimates were identical across the catchments and that high elevation catchments can have large dynamic and mobile storage – the estimated storage from the SDS model was 12-974mm. Dralle et al. (2018) used a coupled mass balance and S-Q function to divide/partition storage into dynamic and indirect storages for two catchments (Elder Creek and Dry Creek) in the Northern California Eel River Critical Zone Observatory (ERCZO). The

outcome of the study was that direct and indirect storages for Elder Creek were 78mm and 400mm, respectively; no storage data was reported for Dry Creek because they had one-year data, but qualitatively, it had similar storages as Elder Creek. In addition, indirect storage constitutes most of the dynamic catchment storage even during wet periods and less variable relative to direct storage; by comparing with nearby field sites, their study demonstrated that indirect storage could be in the unsaturated zone and not necessarily in the saturated zone, but it is held under tension soils and bedrock. Carrer et al. (2019) utilized a combination of water balance with recession analysis and point measurement-based approach to partition dynamic storage into hydraulically connected and disconnected storage components in the experimental Weierbach catchment in Luxembourg. The former (connected) being the active storage that contributes to streamflow, whereas the latter (disconnected) is affected by ET and does not contribute. Dynamic storage in the range 64mm to 101mm was estimated between 2007 and 2014. When compared to point measurement estimation of storage, they found good agreement with the water balance approach for the hydrologically connected storage but not for the hydrologically disconnected storage. The authors attributed this difference to the overestimation of hydraulically connected storage, which they further supported by lower total dynamic storage than hydraulically connected storage dynamics during wet seasons.

Concerning model structure, Staudinger, Stahl, Seibert, Clark, & Tallaksen (2011) assessed its impact on low flow simulations and recession behavior in a 119km^2 headwater catchment in Norway under the Framework for Understanding Structural Errors (FUSE). The authors created and applied 79 models to a snow-dominated headwater catchment and found that summer low flow simulations were poorer than simulations of winter low flows. While most studies in this review confirmed this result, the SDS model performed well in some catchments located in dry areas, for

instance, in the study by Ajami et al. (2011). However, a visible area where the SDS model still needs to be tested is in urban catchments as only one study Bhaskar & Welty (2015) has applied the model in such a location. The current study differs from the previous one in that the authors did not quantify dynamic storage and used a power-law regression model in their study. Thus, this research applies the SDS model to quantify catchment dynamic water storage and develop sensitivity functions across nested variably urbanized catchments with increasing drainage area, which Kirchner (2009) suggests will assist in the understanding of how S-Q relationships differ across the landscape.

This literature review shows that recession analysis technique and the SDS model have been applied extensively across diverse hydroclimatic and hydrologic regions, as well as different catchment sizes to investigate storage-discharge behaviors, estimate dynamic storage, quantify groundwater recharge, study streamflow generation, obtain aquifer properties, evaluate models and obtain model parameters, and understand hydrological processes. The results vary because of different recession extraction procedures and model structures under different conditions. They also reveal that some catchments may exhibit hysteresis, while others may not, and that the application of different data fitting procedure even in the same catchment (e.g., Rietholzbach catchment in Melsen et al. (2014) and Teuling (2010)) can yield different results.

3   GENERAL DESCRIPTION OF THE STUDY AREA

3.1   Overview of the Piedmont Physiographic Province in Georgia

The study region is the Atlanta metropolitan area situated within the Piedmont physiographic province in GA, a region that has undergone general acute erosion (Aulenbach, Landers, Musser, & Painter, 2017). Atlanta is one of the most urbanized cities in the United States, with a rapidly growing population and sprawling urbanized and suburbanized locations (O'Driscoll et al., 2010; Rose & Peters, 2001). It has a humid, subtropical climate marked by warm summers and cold, wet winters with a mean annual temperature of 16℃. Precipitation is abundant and evenly distributed all year round. The average yearly precipitation is 50 inches, which is typical of the Southeastern United States (Aulenbach & Peters, 2018; Diem et al., 2018). Also, hydrological drought is a common occurrence in the region (Aulenbach & Peters, 2018). Developed/urbanized and forested areas are the predominant land use and land cover in Atlanta (Peters, 2009).

Furthermore, the province has a hilly configuration, and the geology is a mixture of complex, varied, and structurally deformed igneous and metamorphic rocks of the late Palaeozoic era (Gordon & Painter, 2018; Rose & Peters, 2001). These rocks are overlain by regolith, which has an average thickness of roughly 65ft and consists of sandy clay saprolite, alluvium, and Ultisol soils (Rose & Peters, 2001). The Piedmont physiographic province has a surficial aquifer system, as with the rest of the other provinces in Georgia (Gordon & Painter, 2018). These aquifers are unconfined and consist of residuum (soil, saprolite, stream alluvium, colluviums) and other surficial deposits that store groundwater that is accessed for various applications – domestic, commercial, agricultural et cetera. Because the bedrock found in this region is crystalline, the aquifers are often referred to as 'crystalline-rock aquifers' (Gordon & Painter, 2018). Much of the

groundwater moves within the regolith (Rose, 2007). According to Rose & Peters (2001), the average duration of groundwater storage within the aquifer system (i.e., residence time) in this province is between 20 years and 40 years before being discharged as baseflow into surface water bodies such as lakes, rivers, streams, and wetlands. As noted by O'Driscoll et al. (2010), hydrologic responses to urbanization in the Piedmont province generally are reduced baseflow.

3.2   South River Watershed

The specific study area is the South River Watershed (SRW), along with six of its sub-watersheds situated principally in DeKalb County in Atlanta, north-central Georgia, and bounded by the following counties: Fulton, Clayton, Henry, Rockdale, and Gwinnett, respectively. DeKalb shares similar attributes with the Atlanta region in terms of climate and geology, although there are variations. It encompasses an area of 694km^2 and is among the counties in the heart of the Metropolitan Statistical Area (MSA) of Atlanta as reported by Dai et al. (2019).

The 1910 census reported the county's population as 27,881 (Long and Baldwin, 1914). Recently, Dai et al. (2019) reported that the estimated population of the county as of 2016 was 740,321. A demographic report released by the Atlanta Regional Commission (ARC, 2018) for the Atlanta metropolitan region (ten counties including the City of Atlanta) between April 2017 and April 2018 showed that the county emerged third in terms of the addition of new residents among other counties, trailing behind Gwinnett County (second) and Fulton County (first) respectively. According to the report, DeKalb's population grew from 733,900 to 744,530 persons within twelve months, thus receiving about 10,630 new residents. This figure translates to a population growth of approximately 1.45% over this period, which mirrors the growth pattern of the entire Atlanta Metropolitan Region (1.79%) (Figure 2).
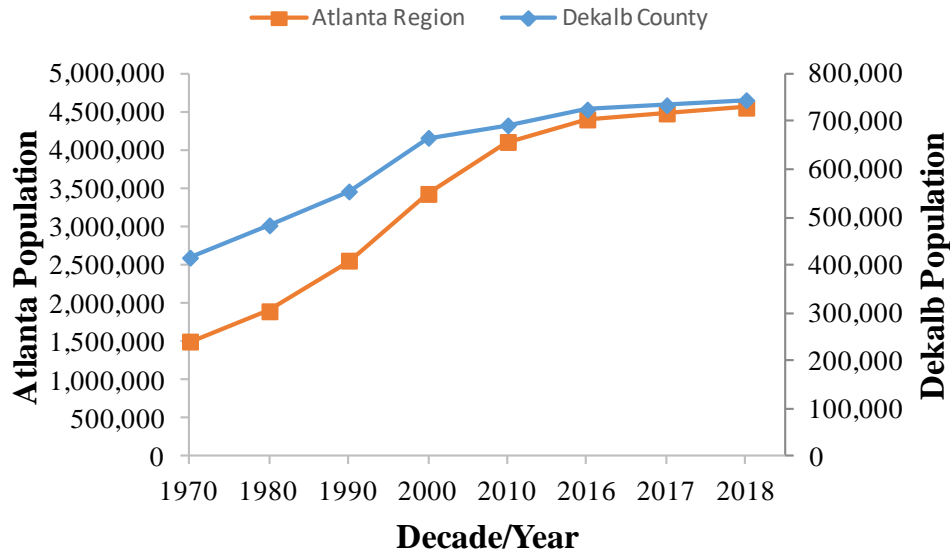
Figure 2. Population in Atlanta Metropolitan Region (10 counties and the City of Atlanta) and DeKalb County. Data source: Atlanta Regional Commission (ARC, 2018).

Topographically, the county has a gently rolling to a hilly landscape, which enhances drainage. The upland soils are mainly generated from gneiss, schist, and granite (Long & Badwin, 1914). These soils are well-drained with a loamy surface area and clayey subsoil. In contrast, lowland areas or flood plains are poorly drained to well-drained and loamy everywhere (Thomas, 1979). These are soils made up of alluvium that are products of fluvial processes. They are materials washed down from upland soils after the weathering of their parent rocks and are deposited along the stream during precipitation (Long & Badwin, 1914; Thomas, 1979). In the early stages of its development, land use in the county was predominantly agriculture – mainly cotton and dairy farming (Thomas, 1979). The persistent population growth from previous decades to date and the corresponding land use changes occasioned by urbanization have transformed the county from mostly agriculture and forest to a highly developed area.

South River begins at East Point in Fulton County and extends to Butts County. It flows from southwestern to southeastern DeKalb and exits at the extreme south-east corner of the county

to continue its flow through Rockdale County and joins Yellow River around Lake Jackson to form the Ocmulgee River. Hence, it belongs to the Altamaha-Ocmulgee-Oconee (AOO) river basin. Unlike Peachtree Creek Watershed (PCW), SRW is part of the headwaters of the Ocmulgee River Basin (ORB). ORB is one of the fourteen river basins in Georgia, and there are fifty-two watersheds in the state. The United States Geological Survey (USGS) has divided ORB into three sub-basins: Upper, Lower, and Little Ocmulgee with distinct hydrologic unit codes (HUCs) 03070103, 03070104, and 03070105, respectively. SRW can be found in the Upper ORB, which is in the Piedmont physiographic province.

Studies on the impact of urbanization on the hydrology of watersheds in Atlanta seem to have neglected SRW. For instance, Ferguson & Suckling, (1990), Peters (2009), Rose (2002), Rose (2003), and Rose & Peters (2001), respectively are a subset of several investigations that have been conducted in Atlanta involving PCW, even though it is the smaller watershed in DeKalb County. Unlike the preceding studies, Diem et al. (2018) investigated the entire SRW in their recent study of eight urbanized watersheds within Atlanta. Several reaches or segments of South River have not been meeting water quality standards. As such, the river as a whole is not supporting its designated use (GA-EPD, 2018). DeKalb County is currently under a consent decree, just like the City of Atlanta, due to sewage spills. The GA-EPD (2018) 305(b)/303(d) Integrated Report shows that certain tributaries to the river, including Pole Bridge Creek, Snapfinger Creek at Decatur, Intrenchment Creek, Shoal Creek, and South River at Klondike have violated the state's water quality standards. The report is an evaluation of the state of health of lakes, rivers, streams, and other water bodies in Georgia in terms of compliance with established water quality criteria.

Within the SRW basin in DeKalb County, there are nine USGS gauging stations. However, seven have been selected for this study. The selection criteria were based on the availability of

continuous streamflow data for all of 2012 through 2016 and the size of the drainage area. Catchments with an area greater than or equal to 22km^2 with reasonable streamflow records were chosen. Figure 3 shows the origin of South River in East Point in Fulton County and the nine streamflow monitoring stations south of the county. The lack of study that exclusively focuses on the hydrology of SRW and results from the study by Diem et al. (2018) make the watershed an excellent choice to investigate the dynamics of catchment water storage in an urban setting.
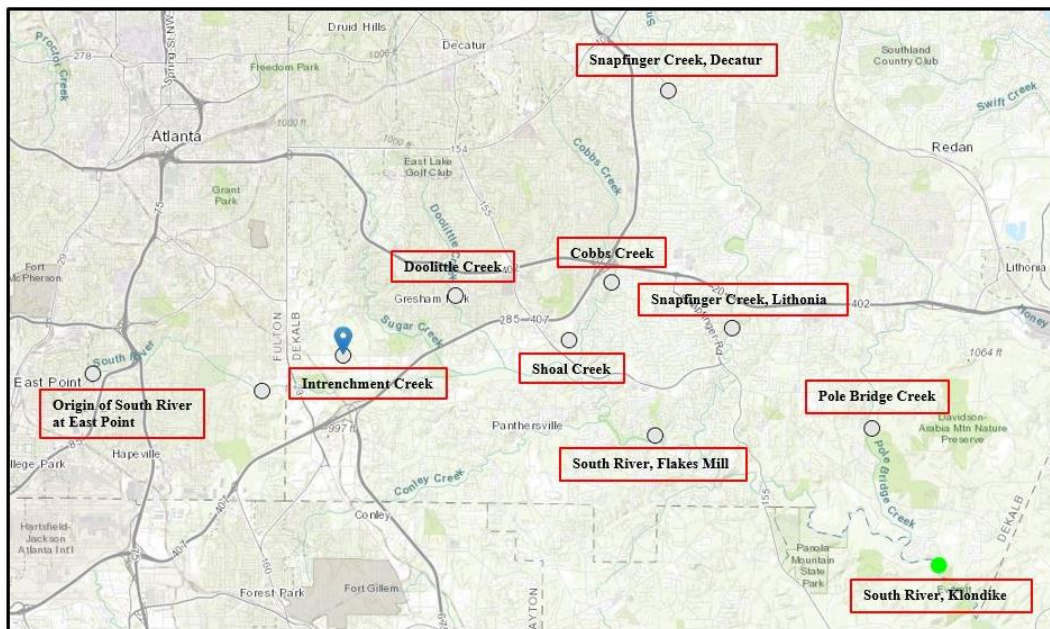
Figure 3. Origin of South River and nine USGS gauging stations south of DeKalb County. Source: http://waterwatch.usgs.gov

The study catchments range in size from ~22km^2 to ~485km^2 (Table 1). The mean elevation varies from 265m to 299m above mean sea level (a.m.s.l). The areas are characterized by gentle slopes with mean values of 7.2% - 8.9%. Figure 4 is the delineated SRW mainly within DeKalb County and six of its sub-watersheds listed in increasing area: Shoal Creek (SC), Intrenchment Creek (IC), Snapfinger Creek Decatur (SFCD), Pole Bridge Creek (PBC), Snapfinger Creek Lithonia (SFCL), South River Flakes (SRF), and South River Klondike (SRK) respectively. From this point onward in this document, the parent catchment (SRW, red outline)

will also be denoted by SRK and used alternately with SRW. The USGS gauging stations within the basin where continuous discharge and precipitation data were collected are also shown in green triangles with filled circles at the center. The application of Strahler (1957) stream ordering method revealed that SRK is a fifth-order river.

Table 1. Topographic attributes of each catchment. Elevation and slope are mean values.

Catchment	USGS Station	Area (km^2)	Elevation (m)	Slope (%)
Shoal Creek (SC)	2203863	22.36	287	8.3
Intrenchment Creek (IC)	2203700	27.85	291	8.9
Snapfinger Creek, Decatur (SFCD)	2203950	34.21	299	8.0
Pole Bridge Creek (PBC)	2204037	41.62	265	7.2
Snapfinger Creek, Lithonia (SFCL)	2203960	86.15	286	8.1
South River, Flakes (SRF)	2203900	267.26	278	8.2
South River, Klondike (SRK)	2204070	485.41	273	8.3

The bedrock geology of SRW consists of seven rock units of Precambrian-Paleozoic age. Figure 5 illustrates the spatial distribution of these units across the watershed. By visual inspection, mica schist (MS), biotite gneiss (BG), and granitic gneiss (GG) in that order are the dominant rock types. MS is present in 54% (274 km^2) of the whole catchment area, while BG and GG, respectively, cover 16% (79 km^2) and 14% (66 km^2) of the drainage basin. Other less dominant bedrock types are gneiss, granite, quartzite, and intrusive ultramafic rock. Table 2 summarizes the percentage area covered by each bedrock type. Individual sub-catchment comprises of at least a mix of three rock units, as seen, for example, in SC, SFCD, and SFCL, respectively (Figure 5). All the sub-catchments have BG and MS; only PBC and SRK have granite bedrock.
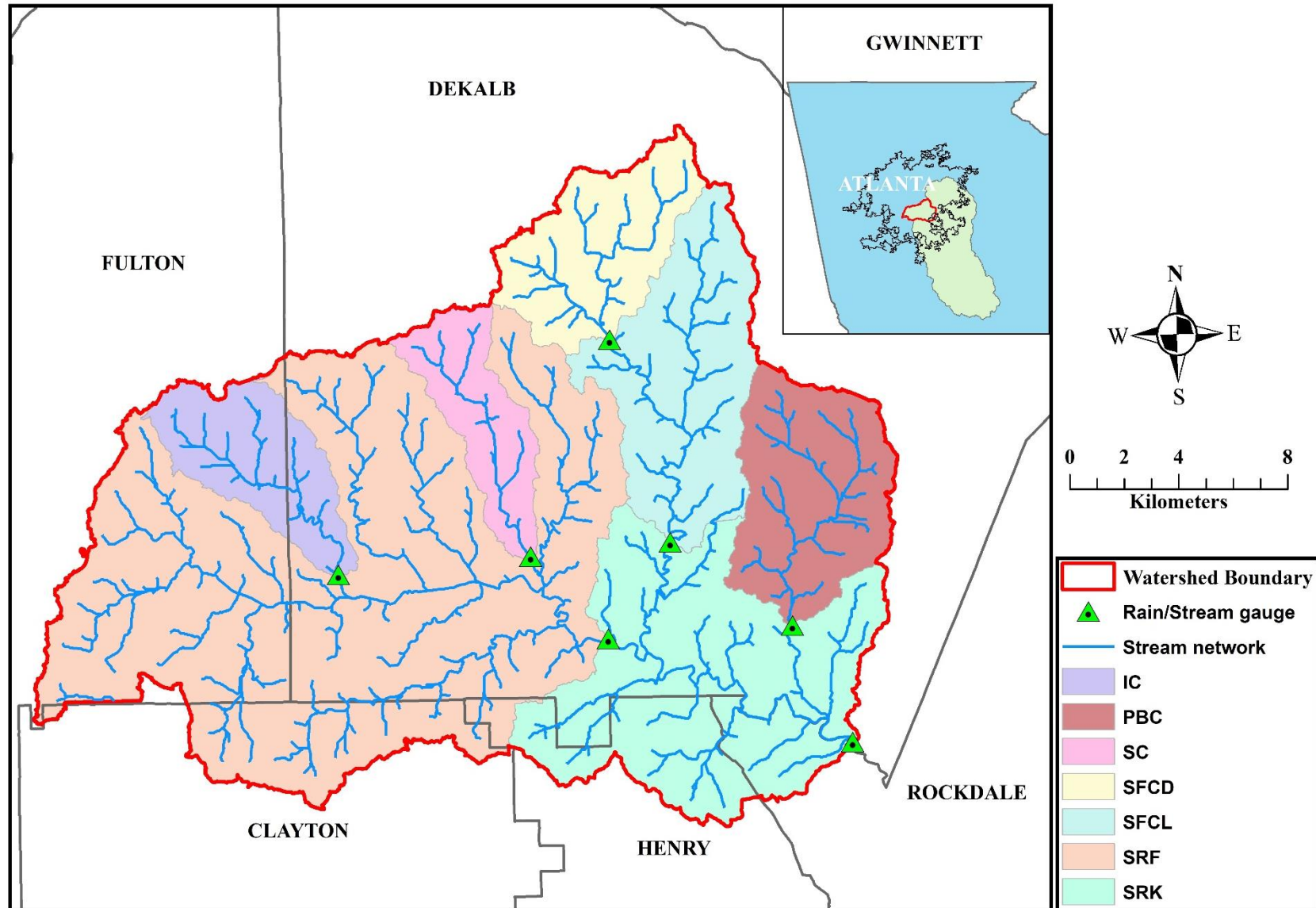
Figure 4. *Study area and the sub-catchments bounded by six counties. The green triangles with filled circles represent stream and rain gauge stations. Inset map shows the study catchment within the Upper Ocmulgee River Basin in metropolitan urban Atlanta (black outline).*
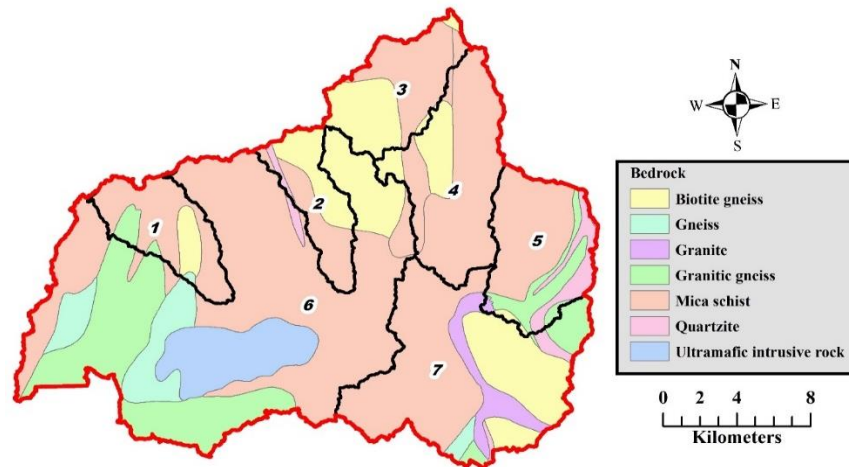
Figure 5. Geological map of South River Watershed. The numbers correspond to catchment IDs and are not ranked.1=IC, 2=SC, 3 = SFCD, 4 = SFCL, 5 = PBC, 6 = SRF, and 7 = SRK.

Table 2. Bedrock geology as a percentage of the catchment area.

ID	Catchment	Bedrock Type (%)						
		Biotite gneiss	Gneiss	Granite	Granitic gneiss	Mica schist	Quartzite	Ultramafic intrusive
1	IC	14.76	1.21	-	9.81	74.22	-	-
2	PBC	2.68	-	0.37	3.42	73.07	20.46	-
3	SC	44.61	-	-	-	50.75	4.64	-
4	SFCD	44.06	-	-	-	55.90	-	0.04
5	SFCL	28.92	-	-	-	71.07	-	0.01
6	SRF	10.70	6.93	-	19.19	53.20	0.81	9.17
7	SRK	16.30	4.19	2.11	13.69	56.36	2.30	5.05

The percentage composition of soils by hydrologic soil group (HSG) for each catchment and the areal estimation of their depths are provided in Tables 3 and 4, respectively. The basin is predominantly occupied by HSG_B (64%, 309 km^2) and those classified as undefined (HSG_U: 24%, 115 km^2). Soils in the HSG_B group are moderately well-drained with good infiltration capacity compared to HSGs C and D. HSG_A soils have excellent drainage characteristics and very high infiltration capacity relative to others. HSG_U is a miscellaneous area delineated at some scale, presumably for mapping convenience. However, gSSURGO describes it as comprising rock

outcrop, urban land, some soils, and water bodies that do not support vegetation. In SRW, urban land (streets, parking lots, and buildings) dominates the HSG_U group, having an area of ~89 km^2 (77%). Jointly, HSG_B and HSG_U account for roughly 88% of the soil types in the basin. The HSG_B has a soil depth of ~19cm, and the total depth for the watershed is ~129cm.

Table 3. Catchment hydrologic soil group in percentage.

ID	Catchment	Hydrologic Soil Group (%)							
		A	A/D	B	B/D	C	C/D	D	Undefined
1	IC	2.54	0.85	29.32	-	1.30	-	0.03	65.91
2	PBC	1.88	9.17	73.99	0.62	0.56	-	1.04	12.74
3	SC	6.98	1.36	72.76	0.21	0.09	-	-	18.61
4	SFCD	3.22	3.38	70.94	-	0.29	-	-	22.18
5	SFCL	3.89	5.00	76.45	0.26	0.67	-	0.15	13.56
6	SRF	3.11	4.74	51.68	0.35	0.54	1.06	3.49	35.04
7	SRK	3.41	5.40	63.63	0.38	0.54	0.59	2.38	23.68

Table 4. The areal estimate of soil depth in SRW.

HSG	Area (km^2)	Soil Depth (cm)
A	16.56	16.62
A/D	26.19	17.35
B	308.63	18.53
B/D	1.83	26.21
C	2.6	20.26
C/D	2.85	19.61
D	11.53	6.76
Undefined	114.83	3.32
TOTAL	485	129

The land cover/land use and impervious surface descriptor maps of the study watersheds are shown in Figures 6(a) and (b), respectively. The development of the basin is concentrated in the northern and western parts (around the headwaters) and not the basin outlet. In Figure 6(a), the red patches indicate highly developed sections of the watershed. The developed impervious descriptor (DID) map shows the different types of roads within the basin (Figure 6(b)). The black

patches in Figure 6(b) labeled as unclassified are vegetated areas with zero percent imperviousness. The reclassified LCLU categories and estimated percent impervious surface area for each watershed are presented in Table 5. The table shows that developed land and forest are the major land-use types across all catchments in SRW. Developed land ranges from 64% to 82%, while forest land varies between 14% and 30%. The most developed sub-catchment is IC and PBC is the most forested. Similarly, percent impervious area varies from 35% for the IC catchment to 22% for PBC catchment. These values depict the urban-to-suburban gradient that characterizes the sub-watersheds. Other categories of LCLU are presented in Table 5.
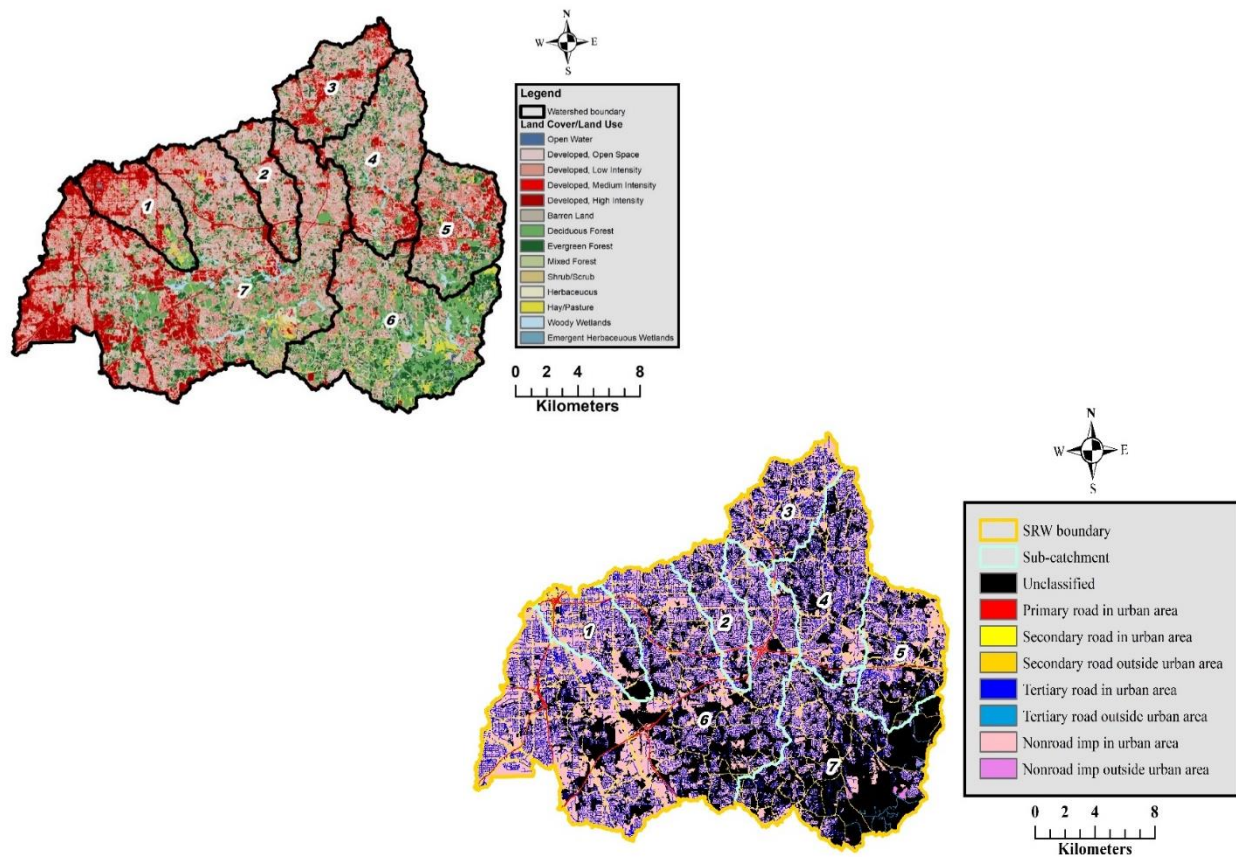
Figure 6. (a) Land use map and (b) Impervious surface descriptor map of SRW.

Table 5. Land cover/land use properties of SRW. Values in parentheses are in percent (%) and others are in km².

Category	Catchment						
	IC	PBC	SC	SFCD	SFCL	SRF	SRK
Developed	22.68 (81.62)	26.83 (64.46)	17.60 (78.70)	27.36 (80.01)	64.15 (74.54)	198.75 (74.43)	323.91 (66.73)
Forest	3.96 (14.26)	12.66 (30.41)	4.43(19.82)	6.52 (19.07)	19.90 (23.13)	56.84 (21.28)	136.06 (28.03)
Open Water	0.08 (0.29)	0.29 (0.70)	0.04 (0.18)	0.10 (0.30)	0.45 (0.52)	0.81 (0.30)	2.19 (0.45)
Barren Land	0.24 (0.86)	0.03 (0.08)	0.01 (0.04)	0.01 (0.03)	0.03 (0.03)	0.67 (0.25)	1.28 (0.26)
Vegetation	0.83 (2.97)	0.97 (2.33)	0.14 (0.64)	0.17 (0.50)	0.75 (0.87)	6.22 (2.33)	14.73 (3.03)
Wetlands	-	0.84 (2.02)	0.14 (0.64)	0.03 (0.09)	0.78 (0.91)	3.75 (1.40)	7.25 (1.49)
Impervious area	**(35.39)**	**(20.25)**	**(21.08)**	**(26.22)**	**(21.71)**	**(27.00)**	**(22.22)**

The estimated population and population density for year 2017 are presented in Table 6. The parent watershed has a population density of 919 persons/km². The sub-watersheds have population densities that vary from 991 persons/km² to 1,612 persons/km². Total annual precipitation for five years (2012 – 2016) is similar in magnitude among the sub-watersheds and varies between 4436mm and 6344mm. Correspondingly, total annual discharge over the same period was between 6623 mm/h and 9537 mm/h.

Table 6. Estimated catchment population and population density for year 2017.

Catchment	IC	PBC	SC	SFCD	SFCL	SRF	SRK
Population	40,001	40,261	27,211	55,163	106,794	264,970	445,946
Population Density (ppskm)	1,436	967	1,217	1,612	1,240	991	919

4   DATA SOURCE AND METHODS

Several geospatial datasets were utilized to characterize the catchments and obtain attributes or properties that will aid the interpretation of results and the understanding of streamflow recession and storage-discharge dynamics. Section 4.1 provides a detailed description of the datasets, while Section 4.2 describes the methods used in this study.

4.1   Data Source

The datasets were acquired from publicly available sources and include a digital elevation model (DEM), geology, land cover and impervious surface, population, precipitation, soil, and streamflow. DEM used was acquired from the National Elevation Dataset (NED) of the United States Geological Survey (USGS) at 10-m resolution. It was used to delineate the catchments, derive topographic variables (elevation and slope), and generate geomorphic descriptors (hypsometry and slope-area relationship). Georgia geologic map data, which is a GIS database of geologic units and structural features in the state, was downloaded from the USGS mineral resources program (https://mrdata.usgs.gov/geology/state) at a scale of 1:500,000. National Land Cover Dataset (NLCD) for 2016 was obtained from the Multi-Resolution Land Cover Characteristics (MRLC) Consortium (Yang et al., 2018; - https://www.mrlc.gov) at 30-m resolution. The NLCD 2016 dataset comprises land cover/use (LCLU), percent developed imperviousness (PDI), and developed imperviousness descriptors (DID), respectively. The latter is a new addition to this version, and it describes impervious areas by identifying types of roads and important urban areas for each impervious pixel for detailed analysis of the extent of development in a given catchment.

The DID data consists of the following layers: primary and secondary roads in urban areas, secondary road outside urban area, tertiary roads in and outside urban areas, and nonroad

impervious in and outside urban areas. According to Dewitz (Personal Communication, 2019), "primary roads are interstates, secondary roads are not interstate but larger transportation roads, tertiary roads can be anything from small gravel roads to suburban roads, and nonroad impervious is impervious that is not associated with any road." The LCLU raster has 14 classes that describe the entire SRW. These classes include open water, developed (open space, low, medium, and high intensity), barren land, forest (deciduous, evergreen and mixed), shrub/scrub, herbaceous, hay/pasture and wetlands (woody and emergent herbaceous).

Oak Ridge National Laboratory (ORNL) has a yearly population dataset through its LandScan platform (https://landscan.ornl.gov). Population data were downloaded at 1 km^2 spatial resolution in grid format for year 2017. The LandScan data (i.e., population data) is susceptible to changes in coordinate systems, and it may even result in an increased or reduced population estimate without the knowledge of the user. Bringing the data into a projected view in the GIS environment (ArcMap) causes the data to be re-projected and resampled 'on the fly.' Therefore, it is suggested that the data should be brought first into the GIS environment to set the projection because of its sensitivity and to avoid loss of data or disparity (lower/higher value) between the estimated population and that published.

High frequency (quarter-hourly, i.e., 15 min) precipitation and streamflow data were retrieved from USGS rain and streamflow gauges (https://waterdata.usgs.gov/ga/nwis) located at the study catchments from 2012 to 2016. It is important to emphasize that the stream discharge used in this study is in a calendar year and not water year as defined by the USGS. The water year is designated as the time between October 1 in the previous year and September 30 in the next year. Soil data was downloaded from the Gridded Soil Survey Geographic (gSSURGO) database of the National Resources Conservation Service (NRCS) provided by the United States

Department of Agriculture (USDA) (https://gdg.sc.egov.usda.gov/) in ArcGIS file geodatabase in raster format at a spatial resolution of 10-m. It represents soil attributes classified by soil series (with percent slope), hydrologic soil groups (HSGs), and available water storage (AWS) in the range 0-150cm of the soil depth weighted average (aws0150wta).

4.2   Methods

Diverse tools within ESRI (Environmental Systems Research Institute) ArcMap were utilized in this project to delineate the catchments and manipulate the various geospatial datasets to obtain catchment properties. Georgia State is between Universal Traverse Mercator (UTM) Zones 16N and 17N; the study area falls under Zone 16N. Hence, all the spatial datasets are set to UTM Zone 16N Projected Coordinate System (PCS), except for the population dataset, which retains its original projection (World Geodetic System, WGS) due to its sensitivity to changes in spatial reference, as explained in Section 4.1.

4.2.1   Catchment Delineation and Topography

The DEM described in Section 4.1 was used to delineate the catchments' boundaries using USGS gauging station coordinates as pour points (outlet/mouth). As a first step in the delineation process, the fill function under the hydrology tool in ArcGIS (Figure 7) was used to process the DEM data to remove any pits or sinks and to guarantee proper delineation of the catchments and generation of stream networks. Pits and sinks are depressions in DEM data due to differences in elevation between points and biases that arise during data acquisition and processing. If they are not filled, they form small basins and can introduce error or uncertainty in terms of flow direction. After filling the DEM, the flow direction tool was activated to determine the direction of flow from each cell in the raster to one cell or more cells downslope. Flow accumulation was the next tool

used to create a raster of accumulated flow into each raster cell from upslope areas, thus generating stream channels recognized by cells with high flow accumulation values.

The watershed tool was executed together with flow direction and pour point (USGS gauge station) as input parameters to finally delineate the catchments. It was ensured that the pour point was situated on a cell/pixel with high flow accumulation value for proper delineation. The stream network was determined by setting a threshold of 5,000 for the flow accumulation raster using a raster calculator. This generated stream links (cells) with a high accumulated flow. This value was chosen after several threshold values were tested because of the size of the parent catchment. After that, (Strahler, 1957) method of stream ordering in ArcGIS was chosen to determine the hierarchy of the stream network. In this method, stream order increases as a result of the intersection of two streams having the same order. For instance, the intersection of a first-order stream and another first-order stream yields a second-order stream, whereas the stream order remains the same when two streams of dissimilar orders intersect.

Finally, the raster products from the catchment delineation and stream network generated were converted to polygon and saved as shapefiles. The parent catchment is South River, Klondike (SRK), the respective sub-catchments are the following: Intrenchment Creek (IC), Pole Bridge Creek (PBC), Shoal Creek (SC), Snapfinger Creek, Decatur (SFCD), Snapfinger Creek, Decatur (SFCL) and South River, Flakes (SRF). The catchment gradient (slope) was derived from the DEM in percent rise (%). The catchment boundaries (shapefiles) were used to clip elevation and slope raster datasets, and their respective mean value was computed. Figure 4 is the flow chart illustrating the main steps.
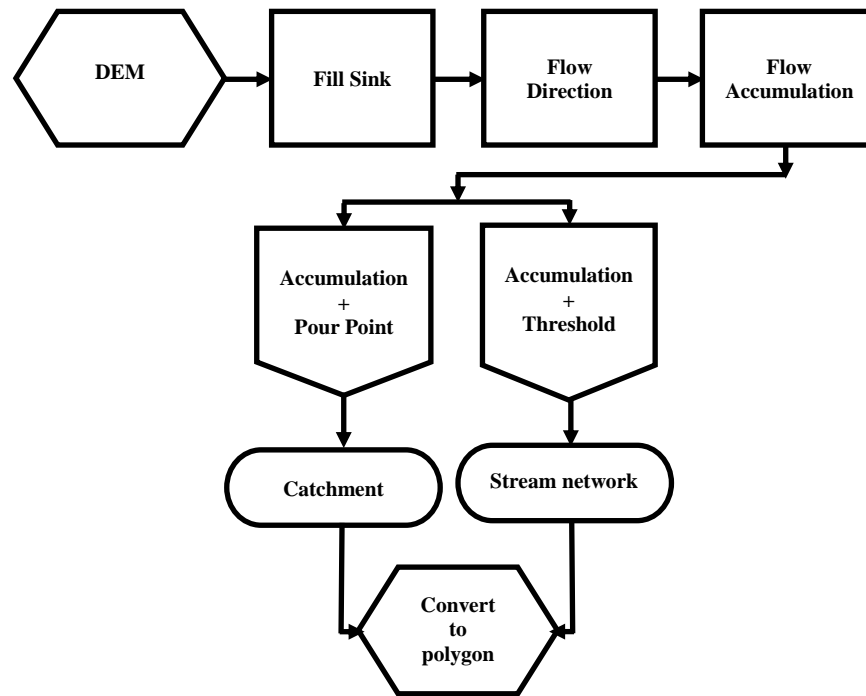
Figure 7. Flow chart illustrating procedure used for delineating catchment using tools in ArcGIS.

4.2.2 Geology and Soil

The geologic map unit of the entire Georgia State was clipped using each catchment's boundary to obtain catchment-specific local geology. The area of the respective rock unit was calculated for each catchment. Similarly, the soil map of Georgia State was clipped to the boundary of each catchment. The soil data are classified by their series names (Gwinnett series, Cecil series, Ashlar series, Appling series et cetera) and hydrologic soil group (HSG). The series names are enormous and contain additional classification schemes such as soil textures, slope values, and flood tendencies, which made the analysis cumbersome and time-consuming. Therefore, the soil data were grouped according to their HSG because the analysis was much easier that way, and their areas were calculated. Areal weighted soil depth for each HSG was also determined for the whole watershed.

4.2.3   Developed Imperviousness Descriptor, Impervious Surface, and Land Use

The land cover types for each catchment in the study area were extracted from the MRLC-NLCD 2016 dataset described in Section 4.1. The LCLU classes were reclassified, hence reducing the number from 14 to 6 classes (open water, developed, barren land, forest, vegetation, and wetlands). After that, the land cover class in each catchment as a percentage of the total catchment area was determined. LCLU and PDI layers were converted to polygons (shapefiles). A spatial intersect operation was performed in ArcGIS to estimate the composite imperviousness of each catchment. The corresponding area for each land cover type was determined, as well. This allowed each land cover class to have a representative impervious surface. After this was executed, the Delaware Method (Kauffman et al., 2009) was used to compute the composite catchment impervious surface in percent. DID layer was used to generate the impervious surface map for the basin rather than the conventional method, where the imperviousness of a catchment is illustrated by using the PDI layer to create a map.

4.2.4   Population and Population Density

ORNL's LandScan is a global population dataset that represents population distribution averaged over 24 hours. In the database, the value field represents the population per cell, while the count field is the number of cells that have a similar population count. The catchment boundary was used to clip a spatial representation of the population for each catchment from the LandScan raster dataset. Population and population density (persons/km^2 – ppskm) were computed to estimate the number of people inhabiting each catchment for year 2017. In the population dataset, the value field was multiplied by the count field to determine the population within a catchment. The estimated population was divided by the catchment area to determine population density.

4.2.5   Construction of Flow Duration Curve (FDC)

A flow duration curve (FDC) is a graphical representation of the cumulative probabilities associated with the exceedance of a given magnitude of discharge. Multiple streamflow and modeling studies across diverse physiographic environments, climate and regions have utilized FDC to understand the behaviors and responses of catchments to precipitation events and for inter-catchment comparisons (Brown, Western, McMahon, & Zhang, 2013; Doulatyari et al., 2015; Rosburg et al., 2017). For instance, Mohamoud (2010) used the FDC method to reconstruct streamflow values in ungauged catchments in Mid-Atlantic Region, USA and upon comparison with observed streamflow values showed high potential for predicting streamflow in such area.

To generate FDC for each catchment, the streamflow data was initially arranged in ascending order (lowest to highest) and then ranked accordingly. The ranking procedure involved assigning the same rank to a discharge value that shows up multiple times in the data and recording the number of times (count or frequency) such discharge value appeared. For instance, if some discharge value of $0.5\text{ft}^3/\text{s}$ appears 200 different times in the discharge data, they get the same rank, say 1, and the count becomes 200. Following this procedure and adhering strictly to the arrangement of the discharge data, the count associated with each discharge value was recorded. The VLOOKUP and IF command in Microsoft Excel were used for this aspect of the data analysis. Next, the discharge probability (or probability of occurrence, P(Q)) was computed for each discharge data point by dividing the count by the total number of streamflow record:

$$P(Q) = \frac{C}{N} \tag{1}$$

where P(Q) = discharge probability, C = count (the number of times a given discharge value appears in the streamflow record), and N = the total number of data points in the record.

Consequently, the probability of occurrence of discharge was cumulated, and the likelihood that that discharge would be equaled or exceeded was calculated as follows:

$$P_e(Q) = 1 - P(Q) \tag{2}$$

where $P_e(Q)$ is the exceedance probability.

Hence, $P_e(Q)$ was plotted against discharge Q on a semi-logarithmic graph to make the relationship as linear as possible.

Finally, flow-duration metrics were employed to estimate baseflow index (BFI) for each catchment to assess the influence of subsurface storage (groundwater contribution) on streamflow. These metrics are commonly applied to characterize streamflow, calculate BFI, and deduce storage capacity in the subsurface (Gordon, McMahon, Finlayson, Gippel, & Nathan, 2004; Price, 2011). These metrics are flows with an exceedance probability of 90% (Q_{90}) and that of 50% (Q_{50}). BFI was calculated from the ratio of the two metrics:

$$BFI = \frac{Q_{90}}{Q_{50}} \tag{3}$$

BFIs were plotted against percent impervious areas to assess their relationships

4.2.6 Geomorphic Descriptors

Geomorphological analyses are important for the understanding of the complex relationships and processes within watersheds. Linear and areal morphometric parameters are usually used to characterize watersheds such as stream order, stream number, mean and total stream length, bifurcation ratio and basin length for the former, and drainage density, stream frequency, drainage texture and texture ratio, elongation ratio, circularity ratio, form factor, infiltration number and length of overland flow for the latter. Geomorphological descriptors have been found to strongly influence the hydrology of catchments in the Piedmont physiographic

province (Mohamoud, 2010). Equally, it has been demonstrated by several studies that recession parameters (i.e., intercept and slope) not only depend on hydraulic characteristics of a catchment, but also on its geomorphologic properties (Biswal & Marani, 2010; Biswal & Nagesh Kumar, 2014; Brutsaert & Nieber, 1977; Troch, Francois, & Brutsaert, 1993). As such, they are catchment regulators influencing flow regimes – low flow and peak flow – and storage. In this work, the area-elevation (hypsometry) and area-slope distributions are employed to characterize and compare catchments.

4.2.6.1 Catchment Hypsometry

Hypsometry, also known as area-altitude relation or area-elevation distribution, is a geomorphological method that is used to describe landscape evolution, quantify landforms (Luo, 2000), compare catchment, and infer surface and hydrological processes (Vivoni, Di Benedetto, Grimaldi, & Eltahir, 2008). It provides information on catchment evolution, for example, due to factors such as tectonic uplift, lithology, climate, and land cover using hypsometric index (HI) and hypsometric curve (HC). The former is a dimensionless quantity that characterizes catchment erosional maturity and flood response as well as landscape evolution, whereas the latter is used to infer a surface process that shapes the catchment.

To generate the hypsometric curves, the maximum, mean, and minimum elevations were determined for each catchment from DEM. The minimum elevation was subtracted from the elevation representing a given data point/cell/pixel. This was then normalized by dividing with the catchment relief/range as presented in Equation 7a:

$$N_i = \frac{E_i - E_{min}}{E_{max} - E_{min}} \qquad\qquad (4a)$$

where N_i and E_i are the respective normalized elevation and elevation of the *ith* pixel, while E_{max} and E_{min} represent the maximum and minimum elevation of the catchment, respectively. Similarly, the area that corresponds to the *ith* pixel was normalized by dividing it with the total catchment area.

$$NA_i = \frac{A_i}{A_{Total}} \tag{5b}$$

where NA_i, A_i, and A_{Total} are respectively normalized area, area of the *ith* pixel and total catchment area. Thus, the standardized area in the hypsometric plot was cumulated over the range of elevation values. HC was constructed for each catchment by plotting a normalized cumulative area on the x-axis against normalized elevation on the y-axis. Normalization of the catchment removes the effect of scale. The area under the hypsometric curve is called the hypsometric index (HI), and it was calculated using the elevation-relief ratio method of (Pike & Stephen, 1971), which is a simple and less cumbersome approach to estimating HI (Singh, Sarangi, & Sharma, 2008). It is expressed as:

$$HI = \frac{E_{mean} - E_{min}}{E_{max} - E_{min}} \tag{6}$$

where E_{mean}, E_{min}, and E_{max} are the mean, minimum, and maximum elevation of the catchment. In Equation (8), the numerator describes dissection and the denominator is the catchment relief or range. If dissection is constant, the hypsometric index could be said to be inversely related to relief.

Strahler (1952 p. 1124) classified the hypsometric index into three stages and assigned values to them: old or monadnock (0 – 0.35), equilibrium, or mature stage (0.35 – 0.6), and young or non-equilibrium stage (≥ 0.6). Catchments that fall under the young category have convex shapes and are vulnerable to erosion since they are still at the early stage of development. Those

under the mature class are stable and S-shaped. The most stable catchments are the ones that are in the old category; they have HC shape that is concave. The HI values range from 0 to 1 and describe the amount of landscape that has been impacted by tectonic activities or geomorphic processes (e.g., erosion) over time (Singh et al., 2008). For instance, a catchment with HI = 0.45 indicates that 45% of the original amount of earth material is still available after erosion.

4.2.6.2 Area-Slope Relationship

Another geomorphic catchment descriptor is the area-slope relationship. Area and slope are both drivers of hydrologic processes, and they possess signatures of past processes in a catchment (Cohen, Willgoose, & Hancock, 2008). The relationship shows the distribution of slope at various points and the area draining to those points in a catchment. A power-law function is used to describe this relationship (Flint, 1974; Willgoose & Hancock, 1998), characterize geomorphic processes, identify channel head, and analyze river/stream profile. The power-law equation relating slope and contributing area of a catchment is expressed as:

$$S = \rho A^{-\mu} \tag{7}$$

where S = slope, ρ = steepness index, A = contributing area and μ = concavity index or scaling exponent. μ is related to catchment hydrology, channel/hydraulic geometry and erosion processes, while ρ has been linked to rock uplift rates and erodibility, which is a function of rock strength and climate. Different values have been reported for μ by different workers: 0.37 to 0.83 (Flint, 1974), -0.4 to 2.3 (Zaprowski, 2005), 0.23 to 0.63 (Ambili & Narayana, 2014), 0.46 (Kirby & Whipple, 2012), and 0.29 to 0.59 (Snyder, Whipple, Tucker, & Merritts, 2000).

This power-law equation with a negative exponent implies that if slope increases with the cumulative upslope area, then hillslope erosion processes (e.g., rain splash) dominate, whereas if it decreases with increasing area, fluvial erosion processes (e.g., incision) dominate. The equation

assumes a steady state (equilibrium) condition in which erosion and uplift rates are equal. Willgoose & Hancock (1998) noted that landscape evolution is caused by two contending forces: tectonic uplift on the one hand, and erosion and mass movement processes on the other hand. They formulated a continuity equation for the evolution of sediment transport:

$$\frac{\partial z}{\partial t} = U - E \tag{8}$$

where z represents the elevation at any point on the landscape, t represents time, U represents tectonic uplift, and E represents the erosion processes. The condition for equilibrium, as stated above, is attained when average erosion equals average tectonic uplift, and there is no change in average elevation, so that $\partial z/\partial t = 0$ in equation (8).

Producing the area-slope plot for each catchment required certain steps, which are described below. First, slope data that contained the gradient at every pixel was generated from the filled DEM, as discussed in Section 4.2.1. A 3 x 3 pixel window smoothing technique that averages the values of a fixed-sized pixel (Cohen et al., 2008) was applied to the slope data to reduce any noise and remove no-data (-9999 values). This exercise was effective in removing a substantial amount of -9999 values. The upslope contributing area was determined using the flow accumulation raster generated previously in Section 4.2.1. A contributing area threshold of 100 pixels was applied to the flow accumulation raster because drainage networks are unstable. Hillslope processes may dominate over fluvial processes, so the transition from hillslope to fluvial occurs at some critical contributing area that is referred to as threshold, turnover, or knick point (Cohen et al., 2008; McNamara, Ziegler, Wood, & Vogler, 2006). Following this, the flow accumulation raster was converted to points, and slope values were extracted to these points in the ArcGIS environment. The data was subsequently exported to Microsoft Excel for further analysis.

The data were additionally examined for the availability of slope with -9999 and 0 values; if present, they were deleted because they cannot be plotted on a log-log scale.

Area-slope plots often appear scattered because of the errors in DEMs and the variability of precipitation, soil type, and morphology (Grimaldi, Teles, & Bras, 2005; Kok, Mohd Sidek, Jung, & Kim, 2018). To reduce this scatter, the slope-area data were binned. Binning procedure for slope-area plots have been performed in previous studies: Brummer & Montgomery, 2003; Ijjasz-Vasquez & Bras, 1995; Lague & Davy, 2003; McNamara et al., 2006, and Stock & Dietrich, 2003. Each data point represents the binned mean of area and slope. The bin width was determined by subtracting the lowest value from the highest in the flow accumulation and slope datasets and dividing by the number of data points. The average slope and flow accumulation pixel for each bin were calculated. Slope data in percent rise was converted to m/m (i.e., rise/run) by dividing by 100. The flow accumulation raster was multiplied by the pixel area (10^{-4} km^2) to get the contributing area in a square kilometer.

In numerous studies involving area-slope (e.g., Kok, 2018 and McNamara, 2006), critical threshold areas are identified, and the stream profile is broken into segments to identify the dominant geomorphic process at work. The power-law regression equation is then fitted to the data to obtain the geomorphic parameters (ρ and μ). In this study, a third-order polynomial regression was fitted to the binned area and slope data because it follows the major features of the data. To remove the influence of catchment size, each contributing drainage area was normalized using the total catchment area. The area-slope data was subsequently plotted on a semi-logarithmic graph. Concavity and steepness indices were retrieved from the linear part of the polynomial regression line.

4.2.7   Simple Dynamical System (SDS) Approach

Kirchner (2009) model applies the simple water balance Equation (9) and assumes   that

discharge Q is a singled-valued function of the volume of water S stored in the catchment. This

relationship is represented by the storage-discharge function (10):

$$\frac{dS}{dt} = P - E - Q \tag{9}$$

$$Q = f(S) \tag{10}$$

where *P* and *E* are precipitation and evapotranspiration, respectively. Since *Q*, which is easily

measured, is an increasing function of *S*, the storage-discharge function given above can be

inverted thus:

$$S = f^{-1}(Q) \tag{11}$$

and differentiating equation (10) with respect to time and combining with Equation (9) yields:

$$\frac{dQ}{dt} = \frac{dQ}{dS} * \frac{dS}{dt} = \frac{dQ}{dS}[P - E - Q)] \tag{12}$$

Because *Q* is invertible, we can differentiate Equation (10) with respect to *S*, and this gives:

$$\frac{dQ}{dS} = f'(S) = f'(f^{-1}(Q)) = g(Q) \tag{13}$$

Kirchner (2009) defined *g(Q)* as the sensitivity function. It is an expression of the sensitivity of

discharge to changes in catchment water storage. However, the function is dependent on discharge

(which can be observed or measured) and not storage (which cannot). By combining Equations

(12) and (13), and rearranging them, an expression for $g(Q)$ can be obtained as follows:

$$g(Q) = \frac{dQ}{dS} = \frac{dQ/dt}{dS/dt} = \frac{dQ/dt}{P - E - Q} \tag{14}$$

Considering periods when precipitation and evapotranspiration are infinitesimal compared to

discharge, *P* and *E* can be neglected, and Equation (14) becomes

$$g(Q) = \frac{dQ}{dS} = \frac{dQ/dt}{dS/dt} \approx -\frac{dQ/dt}{Q} \qquad P \ll Q, E \ll Q \tag{15a}$$

$$g(Q) = -\frac{\frac{dQ}{dt}}{Q} \tag{15b}$$

Thus, the sensitivity function can be estimated from recession data alone, which requires extracting such data from the total streamflow record under the afore-mentioned conditions.

The approach to estimating the catchment sensitivity function, and ultimately the storage-discharge relationship generally follows the procedure outlined by Kirchner (2009), with some deviations noted below. Initially –*dQ/dt* versus mean *Q* was plotted, where *dQ/dt* is approximated as the difference between discharge measured at a moment in time and discharge measured at some preceding time, and *Q* is the calculated average value of discharge at those same two moments in time (Brutsaert & Nieber, 1977):

$$-\frac{dQ(t)}{dt} = \frac{Q_{t-\Delta t} - Q_t}{\Delta t} \tag{16a}$$

$$Q = \frac{Q_{t-\Delta t} + Q_t}{2} \tag{16b}$$

Following Equation 14, the values of *Q* were utilized only at times when *P* and *E* can be assumed negligibly small. For this study, this includes all values of *Q* occurring between 6:00 and 22:00, and when no precipitation was recorded for the previous hour. A review of the recession data extraction procedures in multiple previous studies (Adamovic et al., 2015; Kirchner, 2009; Krier et al., 2012; Majone, Bertagnoli, & Bellin, 2010; Rusjan & Mikoš, 2015; Teuling et al., 2010) shows that diverse time windows have been employed leading ultimately to varying storage-discharge relationships. However, (Adamovic et al., 2015) tested larger time windows (10 and 12h) and found no improvement in *g(Q)* estimation.

Part of the scatter observed in the resulting plot is attributable to an error in the measurement of water depth; additional error is attributable to uncertainty in the depth-discharge relationship for the river channel (Rupp & Selker, 2006). Multiple approaches have been proposed to remove the influence of those values of *dQ/dt* that are lesser in magnitude than the cumulative uncertainty associated with measurements of *Q* (Roques, Rupp, & Selker, 2017; Rupp & Selker, 2006). For comparison, *dQ/dt* versus *Q* is plotted using four scenarios: *dt* = 15 minutes, *dt* = 1 hour, *dt* = 2 hours, and *dt* as a variable quantity following the method of (Rupp & Selker, 2006). The use of that final approach requires some estimate of the cumulative error associated with measurements of *Q*, for the purpose of assigning value to the parameter ε within the equation below:

$$Q_{i-j} - Q_i \geq C[Q(H_i + \varepsilon) - Q_i] \tag{17}$$

where Q_{i-j} and Q_i are discharge at a number of time increments *j* in the past and discharge at the current time step *i*, respectively; *C* is an adjustable calibration parameter; H_i is the river depth at current time step *i*. The value of *j* is adjusted incrementally until the inequality proves true; then *dQ/dt* and *Q* are calculated using values from time steps *i* and *i-j*. For an automated application of the equation above to a time series containing many hydrograph peaks and recessions, it is necessary to limit the maximum value of *j*, so that Q_{i-j} is not associated with the flow recession following an entirely different precipitation event than the one causing Q_i. Therefore, the limit *j* < 12 was imposed, where 12-time steps (at the 15-minute frequency) represents a time span of three hours.

For each of the four scenarios noted above, the individual values of *dQ/dt* and *Q* are separated into bins, and average values calculated within each bin. Following Kirchner (2009), and starting from the largest values, bins were delimited that have a range of values spanning at

least 1% of the logarithmic range of Q, and for which the standard error of $-dQ/dt$ among data within the bin is less than half of the mean value of dQ/dt within the bin:

$$\left[\left(-\frac{dQ}{dt}\right)_{SE}\right] \leq \frac{1}{2}\left[\left(\frac{dQ}{dt}\right)_{MEAN}\right] \tag{18}$$

The catchment sensitivity function is derived by using least-squares regression to fit a line through these binned mean values. Similar to Kirchner (2009), sufficient curvature was found in the relationship between the natural logs of $-dQ/dt$ and Q to warrant a second-order polynomial function (i.e., quadratic equation), of the form shown below:

$$\ln\left(-\frac{dQ}{dt}\right) = c_1 + c_2 \ln(Q) + c_3 \left[\ln(Q)\right]^2 \tag{19}$$

where the subscripted c terms are the constant coefficients of the polynomial function. The catchment sensitivity function, as shown in Equations 15(a)-(b), is a function of Q and is equivalent to $-dQ/dt$ divided by Q. Subtracting $\ln(Q)$ from both sides of the equation above yields the following:

$$\ln\left(-\frac{dQ}{dt}\right) - \ln(Q) = c_1 + c_2 \ln(Q) - \ln(Q) + c_3 \ln(Q)^2 \tag{20}$$

which can be rewritten as below, yielding the sensitivity function $g=f(Q)$ in natural logs:

$$\ln[g(Q)] = \ln\left(\frac{-\frac{dQ}{dt}}{Q}\right) = c_1 + (c_2 - 1)\ln(Q) + c_3 \left[\ln(Q)\right]^2 \tag{21}$$

By taking the exponentials of both sides and invoking the natural logarithmic law for the inverse of the exponentials (i.e., $e^{\ln x} = x, if \ x > 0$) Equation (21) becomes

$$g(Q) = e^{c_1 + (c_2 - 1)\ln(Q) + c_3 [\ln(Q)^2]} \tag{22}$$

The approach to deriving these catchment sensitivity functions deviated from the original method of Kirchner (2009) in one more important way. Likely due to unknown complexities in the runoff response of these highly urbanized watersheds, we found very poor fits of our calibrated

polynomial functions to the binned mean values of $-dQ/dt$ and Q at relatively large values of Q. As such, we imposed a restriction whereby no values of Q greater than 0.5 mm/h were utilized in the calculation of the catchment sensitivity functions. This restriction was imposed uniformly for all study watersheds and limits the overall range of the storage-discharge relationship that we can examine and compare. By substituting Equation (22) into (14) or (15) and taking the integral of both sides, we get

$$\int dS = \int \frac{dQ}{g(Q)} = \int \frac{dQ}{e^{c_1 + (c_2 - 1)\ln(Q) + c_3\,[\ln(Q)]^2}} \tag{23}$$

Dynamic storage was estimated for each catchment by solving Equation (23) using numerical integration, substituting in the minimum and maximum values of Q that were used in fitting the second-order polynomial function to the $-dQ/dt$ versus Q scatter points. Correlation analyses were performed to investigate how dynamic storage is influenced by catchment-wide properties using Spearman's (σ) non-parametric correlation. This correlation method was selected because of the small size of the data.

5   RESULTS

The results section is divided into four parts. In the first part, results regarding flow duration curve (FDC) and baseflow index (BFI) for the catchments are given (Section 5.1). Next, results of catchment geomorphology (concavity index, steepness index, hypsometric curve, and hypsometric index) are presented (Section 5.2). In Section 5.3, results of recession analysis (recession plots, error analysis, and estimation of discharge sensitivity function) are shown. Lastly, the results of estimated dynamic storage, its relationship with discharge, and correlation analyses are reported in Section 5.4.

5.1   Flow Duration Curve (FDC) Characteristics and BFI

The FDC for each watershed from hourly discharge data is illustrated in Figure 8. The shapes of the FDCs are similar, but they also show differences in the behavior of streamflow across the catchments. The inset plots represent the two extremes: high flow and low flow. The high flow is based on the condition imposed for the generation of discharge sensitivity function (Q > 0.5mm/h) in Section 4.2.7, which is equivalent to 1.50% exceedance probability. Low flows are

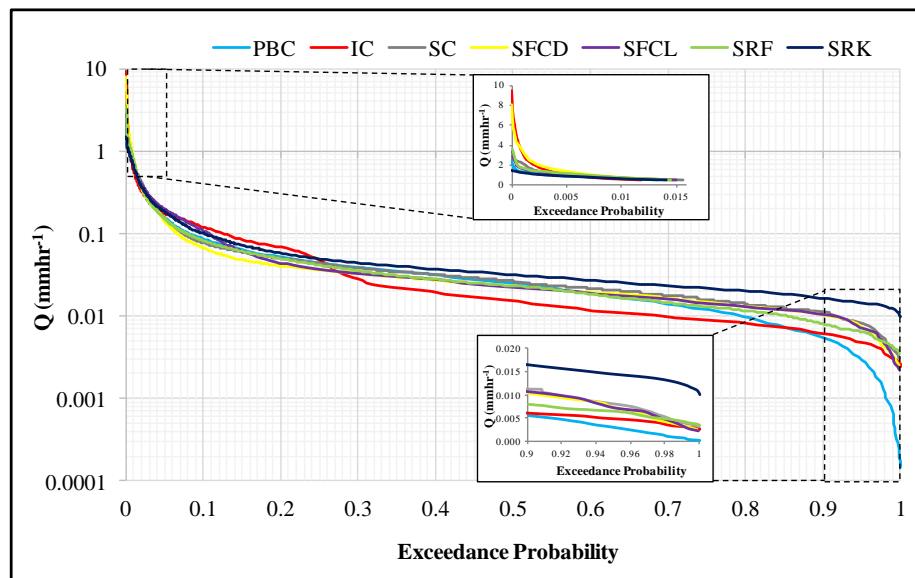*Figure 8. Normalized flow duration curves (FDC) for each of the seven watersheds. Top and bottom inset FDCs show high flow (>0.5mm/h) and low flow (<0.02mm/h).*

those for which exceedance probability is 90% (Q < 0.02mm/h). As shown in Figure 8 and Table 7, IC and SFCD streams had the greatest high flow magnitudes (greater than SRF which is more urbanized than SFCD) (top inset plot). The variability of streamflow across the catchments during low flow is pronounced. SRK had the highest low flow magnitude, whereas IC and PBC had the lowest (bottom inset plot). There is a hump at about the 20% exceedance probability in the flow duration curve of IC. This later fell to 30% exceedance probability and remained flat for the rest of the flow, crossing PBC around 90% exceedance probability. The curve for PBC began to decline at about 50% exceedance probability (not evident in the combined plot) and became pronounced or very steep at 90% exceedance probability.

Table 7. Total discharge (mm/hr) values at high flow ($Q_{1.5}$) and low flow (Q_{90}).

Catchment	High Flow (Q>0.5mm/hr)	Low Flow (Q<0.02mm/hr)
SC	481	0.15
IC	1140	0.07
PBC	307	0.06
SFCD	1099	0.12
SFCL	607	0.14
SRF	637	0.22
SRK	275	0.25

The estimated baseflow index (BFI) for each watershed is small and ranges from 0.03 to 0.13. PBC has the lowest value, 0.03, while SC has the highest, 0.13. The BFI values for SFCL and SRK are 0.12 and 0.11, respectively. Three other catchments, IC, SFCD, and SRF, have identical BFI values: 0.06. The plot of BFIs and catchment impervious surface areas revealed negative association between both catchment variables with a very low R^2 value (Figure 9).
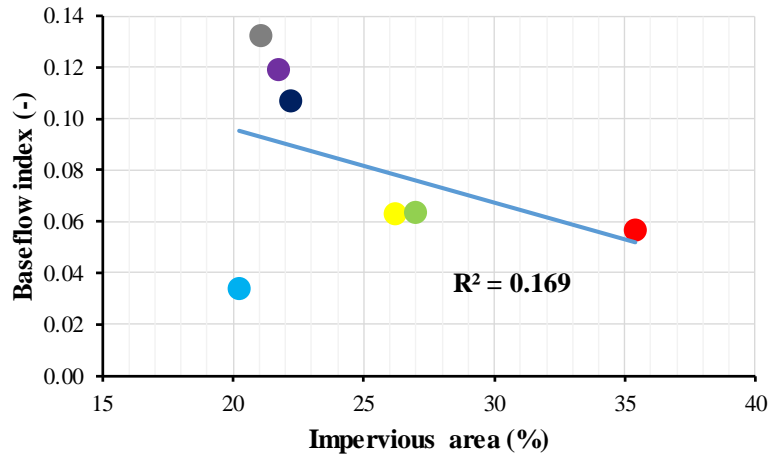
Figure 9. Base-flow index against percent impervious area for seven catchments in the SRW. SC = Grey, IC = Red, SFCD = Yellow, PBC = Light blue, SFCL = Purple, SRF = Light green, and SRK = Dark blue.

5.2   Geomorphic Variables

5.2.1   Concavity and Steepness Indices

The area-slope (A-S) plot for each catchment is presented on a single graph for direct comparison (Figure 10). The individual plot can be found in Appendix A. The regression fit to the A-S data shows a linear relationship but transitions to a non-linear type downslope at 0.8 (see Appendix A for a clearer view). As shown in Table 8, the concavity index (μ) varies across the catchments ranging from 0.40 to 2.17, with a mean of 1.17. Steepness index (ρ) ranges from 0.34 to 0.68, with a mean of 0.49. There are multiple discontinuities or gaps in the A-S plots. Both μ and ρ correlate with the impervious area ($\sigma = 0.71$ and 0.54).
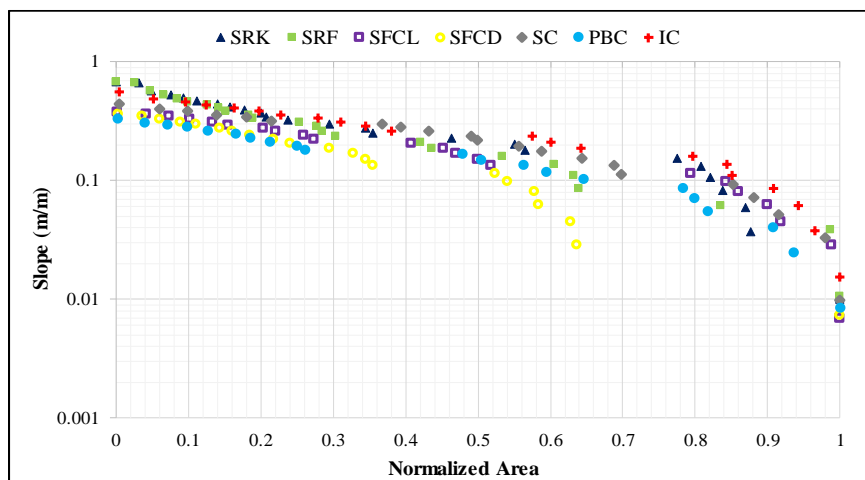
Figure 10. A semi-logarithmic plot of area-slope relationship. The gaps are natural discontinuity depicting geomorphic processes.

Table 8. Magnitudes of catchment concavity and steepness indices.

Catchment	Area (km^2)	Concavity Index (μ)	Steepness Index (ρ)	R2
SC	22.36	0.40	0.43	0.990
IC	27.85	1.26	0.56	0.996
SFCD	34.21	0.76	0.37	0.989
PBC	41.62	0.71	0.34	0.991
SFCL	86.15	0.82	0.40	0.989
SRF	267.26	2.17	0.67	0.989
SRK	485.40	2.10	0.68	0.990
	Average	**1.17**	**0.49**	**0.99**

5.2.2   Hypsometric Curve and Index

The hypsometric curves (HCs) of the watersheds are shown in Figure 11. The HC for the individual catchment is provided in Appendix B. In Table 9, the hypsometric index (HI) gives the proportion of the landscape that has not been eroded. They range from 0.45 to 0.62: IC catchment has the highest HI and PBC catchment has the lowest. All the catchments have similar convex shapes downslope, except PBC that has a concave shape for the most part.
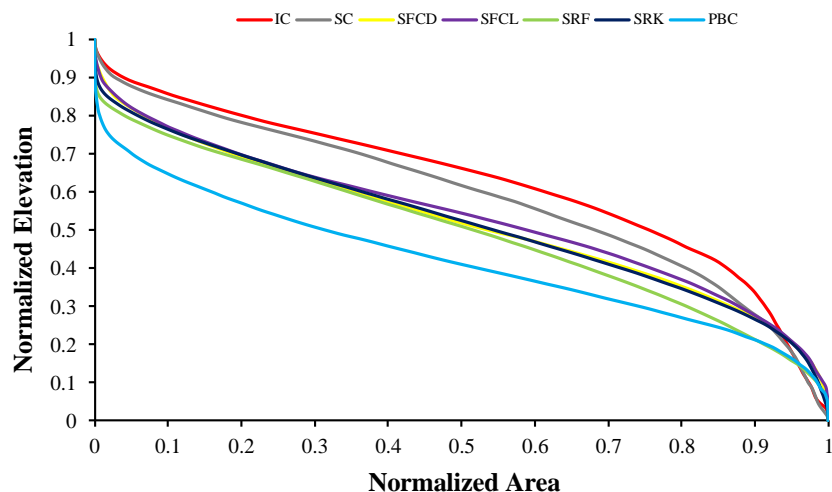
Figure 11. Catchment hypsometric curves.

The hypsometric curves for SFCD and SRK are identical and do not overlap. In addition, they have the same HI value (Table 9). Basically, the catchments in this study do not vary in terms of their geologic stages of development. By invoking Strahler (1952) classification scheme, they are either mature or young. In all, about 90% of the catchment area has an elevation that is less than 35% of the maximum elevation.

Table 6. Values of hypsometric index following Strahler (1952) classification.

Catchment	Hypsometric Index	Classification
SC	0.58	Late mature stage
IC	0.62	Young stage
SFCD	0.51	Mature stage
PBC	0.45	Late monadnock
SFCL	0.53	Mature stage
SRF	0.49	Mature stage
SRK	0.51	Mature stage

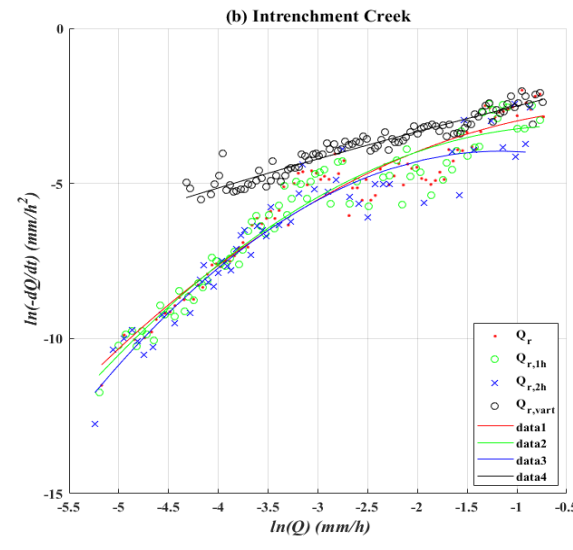## 5.3   Recession Analysis

5.3.1   Recession Plots

Two plots are presented next to each other in Figures 12(a)-(g), showing the results of the recession analysis for each catchment. On the left are the recession plots of flow recession rate [*In(-dQ/dt)*] vs discharge [*In(Q)*] on a linear graph, while on the right are the residual analyses for the different time steps (red = 15-min, green = 1-h, blue = 2-h, and black = variable time step). Residual analysis determines how well the model captures the relationship between *In(-dQ/dt)* and *In(Q)*. The figures are arranged in increasing watershed area from SC to SRK. The catchments differ in their recession behavior. There was considerable scatter in the data that increased with Q for some catchments. For example, at high flow for IC and SFCL (Figures 12(b) and (e)), the regression lines are curved, and the binned *In(Q)* had the greatest variability. Likewise, high discharge variability was also observed at low flow in Figure 12(g).

However, the relationship between *In(-dQ/dt)* and *In(Q)* improved markedly after the data were corrected for errors using the variable time step (VTS) method. There was significantly less scatter for all the streams, and the data points can be seen aligning with the regression line. The residuals did not show any distinct pattern for the VTS data (black circle) and were uniform, aggregating around the horizontal line (zero residual). To closely evaluate how *In(Q)* and *In(-dQ/dt)* vary across the catchments, VTS data from each catchment was used to generate a single recession plot. The recession plot in Figure 13 indicates that flow recession rate decreases with discharge. While IC, SC, and SFCL catchments exhibit linear, one-to-one relationships, the recession curves for the other catchments (PBC, SFCD, SRF, and SRK) are non-linear.

(a) Shoal Creek

(b) Intrenchment Creek

(c) Snapfinger Creek Decatur

(d) Pole Bridge Creek

(e) Snapfinger Creek Lithonia

(f) South River Flakes
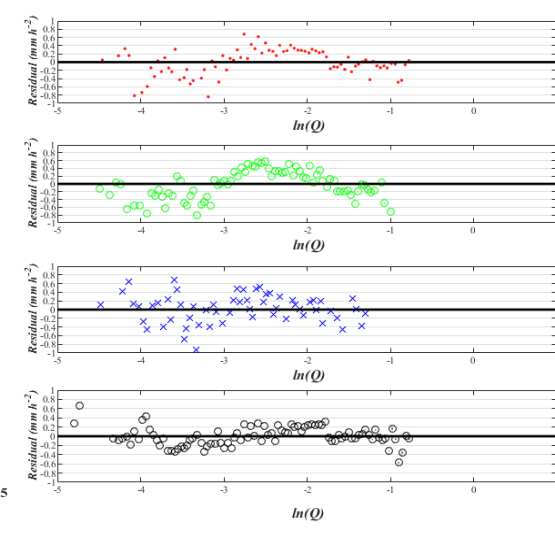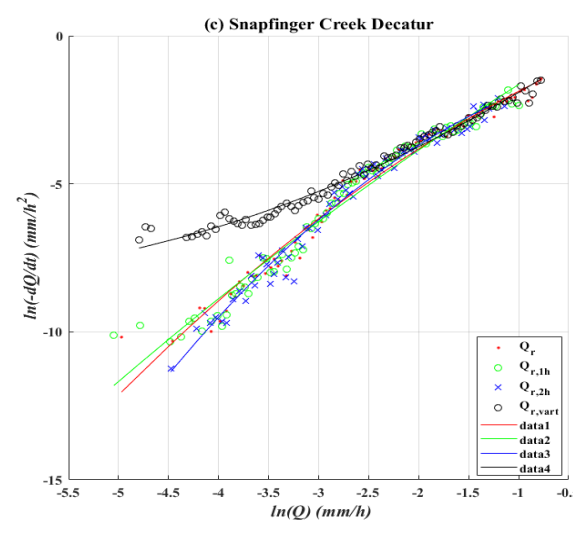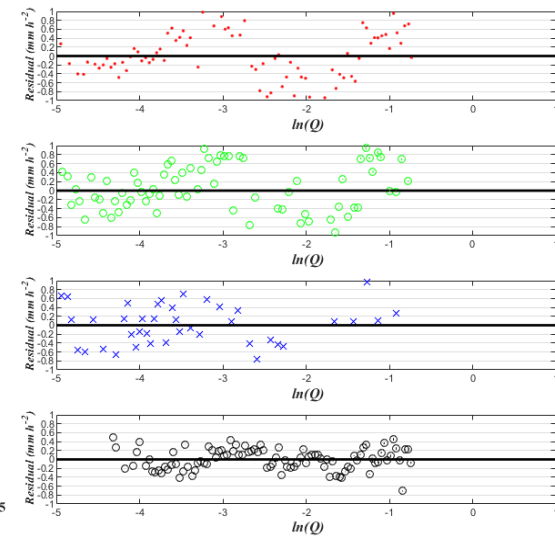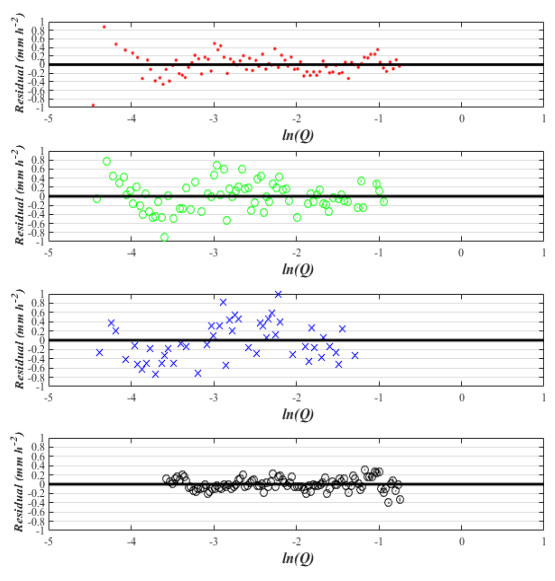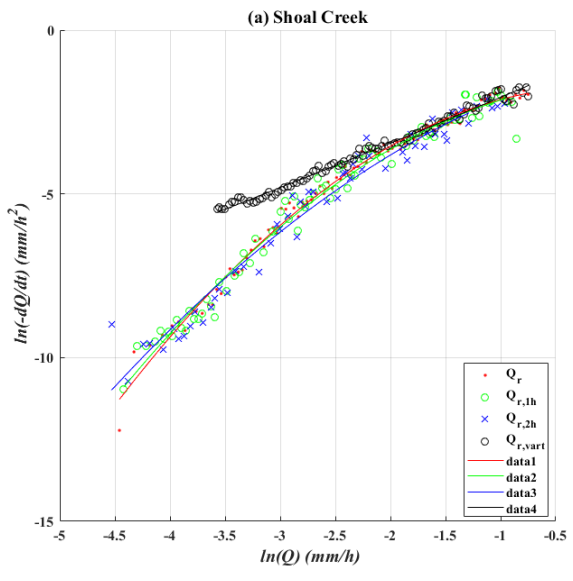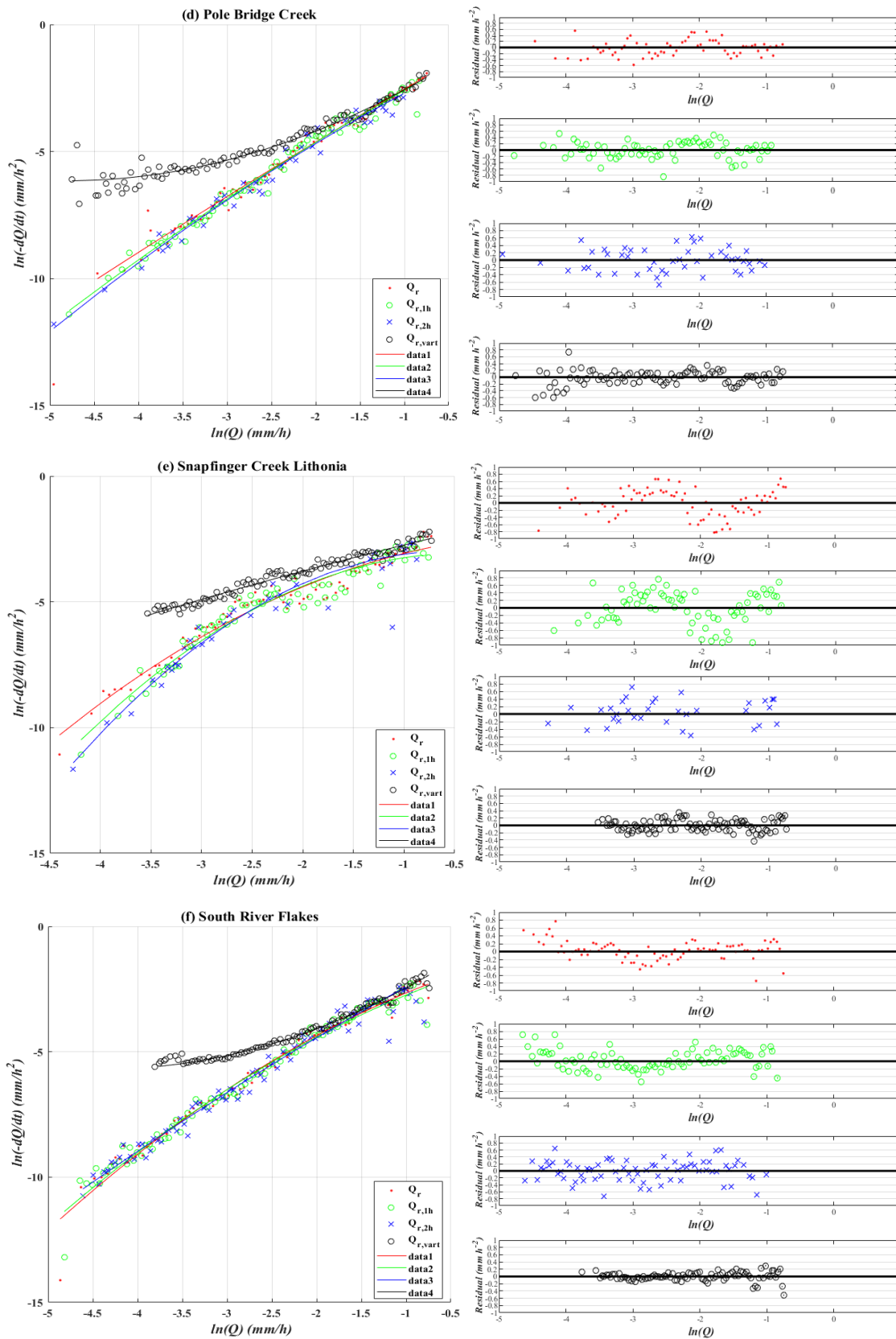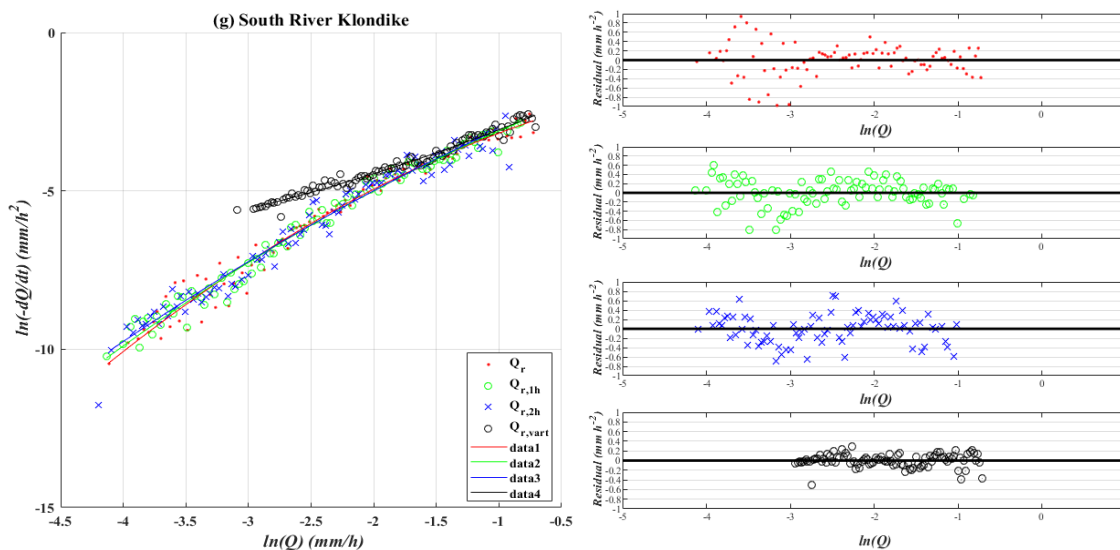
Figures 12(a)-(g). Hydrograph recession analysis together with residual plots for 15-min (red), 1-hour (green), and 2-hour (blue). The streamflow data were corrected using the VTS method of Rupp and Selker (2006).
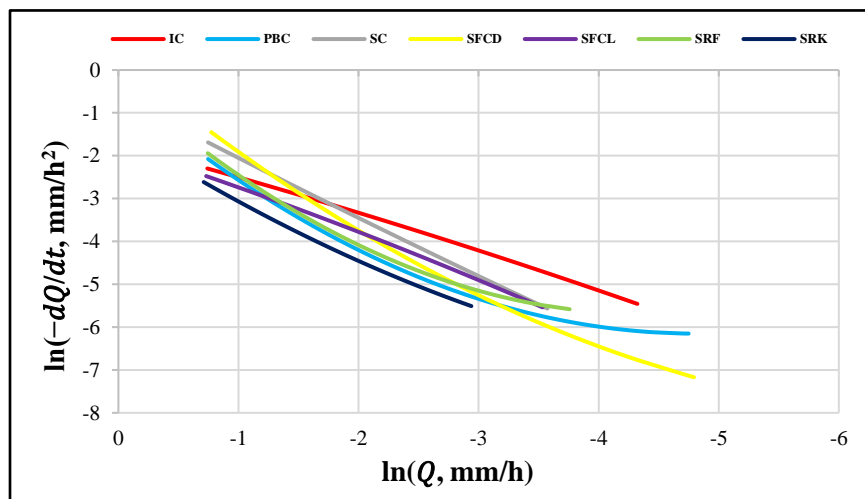
Figure 13. Inter-catchment comparison of recession plot using only variable time step data.

5.3.2   Discharge Sensitivity Function, g(Q)

The relationship between stream discharge (Q) and sensitivity function, g(Q) for each catchment is displayed in Figure 14. The sensitivity function was generated with the model equations in Table 10, and it illustrates the variation of catchment sensitivities to changes in storage. The third most urbanized catchment (i.e., SFCD), as defined by percent impervious area, emerged as the catchment that is most sensitivity to storage changes accompanied by the second least urbanized watershed (SC). The most urbanized catchment (IC) initially showed high sensitivity, but it declined as Q increased.
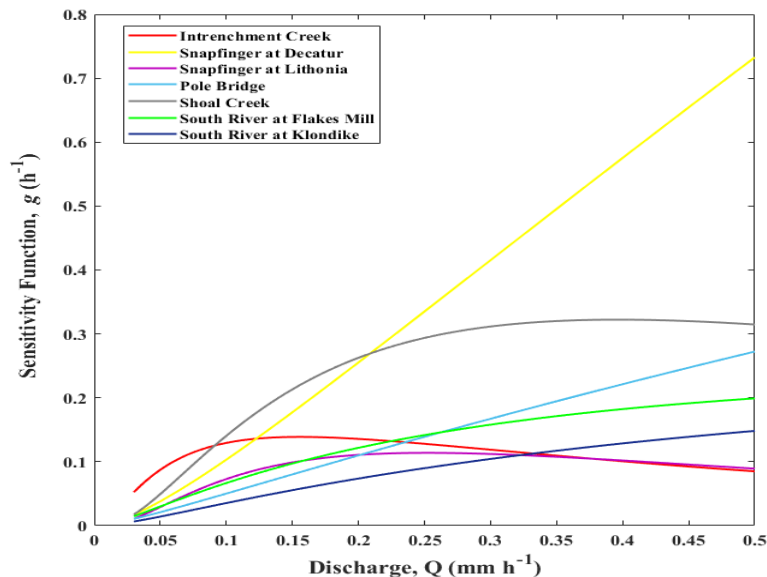
Figure 2. The behavior of discharge sensitivity functions across catchments.

The shape of the $Q - g(Q)$ curves and the sensitivity parameters vary across the catchments. The c_3 parameter influences the concave or convex shape of the $g(Q)$ function and is related to low flow (Adamovic et al., 2015). The values of c_3 in this study varied from -0.044 to 0.283 with just two catchments, IC and SFCL, having negative signs. It is observed that all the catchments except SFCD had positive values for the c_1 parameter (Table 10).

Table 10. Discharge sensitivity function for each study catchment

Catchment	Discharge Sensitivity Function
Shoal Creek (SC)	$g(Q) = 0.022[\text{In}(Q)]^2 + 0.466[\text{In}(Q)] - 0.607$
Intrenchment Creek (IC)	$g(Q) = -0.027[\text{In}(Q)]^2 - 0.252[\text{In}(Q)] - 1.729$
Snapfinger Creek Decatur (SFCD)	$g(Q) = 0.160[\text{In}(Q)]^2 + 1.312[\text{In}(Q)] + 0.242$
Pole Bridge Creek (PBC)	$g(Q) = 0.246[\text{In}(Q)]^2 + 1.372[\text{In}(Q)] - 0.443$
Snapfinger Creek Lithonia (SFCL)	$g(Q) = -0.044[\text{In}(Q)]^2 - 0.094[\text{In}(Q)] - 1.789$
South River Flakes (SRF)	$g(Q) = 0.283[\text{In}(Q)]^2 + 1.483[\text{In}(Q)] - 0.251$
South River Klondike (SRK)	$g(Q) = 0.138[\text{In}(Q)]^2 + 0.803[\text{In}(Q)] - 1.403$

5.4 Catchment Dynamic Storage, Storage-Discharge Characteristics, and Correlation

The estimated dynamic storage in this study ranges from 2.70mm (SC) to 8.83mm (SRK). In Figure 15, a scatter plot of dynamic storage versus impervious area is presented. The family of storage-discharge *(S – Q)* curves derived from the sensitivity function, *g(Q)* is shown in Figure 16. In the former plot, as impervious area decreased, dynamic storage increased from 4.25mm to 4.91mm, and then to 5.79mm for IC (red), SRF (light green), and PBC (light blue) respectively. Dynamic storage appears to increase somewhat significantly from 6.04mm for SFCL (purple) to 8.83mm for SRK (parent catchment, dark blue) with increasing catchment area at about a constant impervious area of 20%. Dynamic storage values are similar in magnitude but vary among the catchments. It is interesting to note that the two most urbanized catchments (by impervious coverage, IC and SRF) have higher storage values than the two catchments with the highest discharge sensitivities. The shapes of the *S–Q* curves are non-linear and similar except for IC in Figure 16. The *S–Q* relationship for IC appears to be linear; the catchment's response to changes in storage is fast, while SRK's response is slow. It is worth emphasizing that in developing the *S–Q* relation from *g(Q)* for the catchments (Figures 14 and 16), observed discharge data in the record

were used. Extrapolation beyond this data will yield false dynamic storage estimate (Ajami et al., 2011).
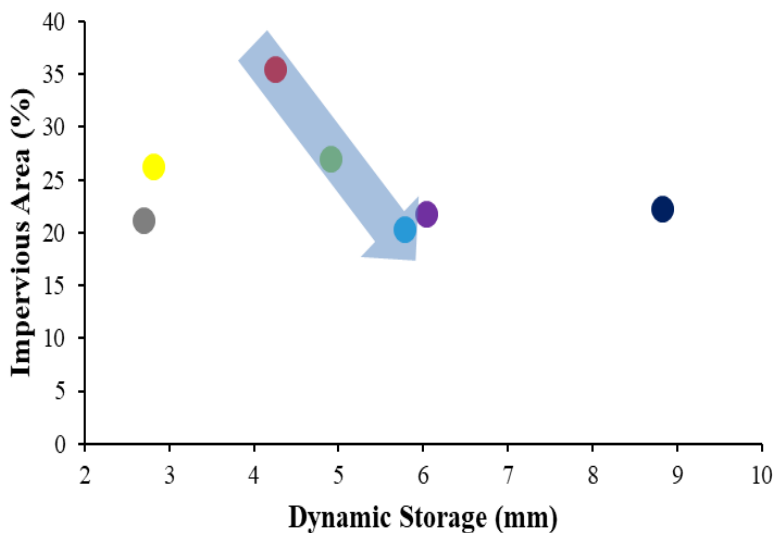
Figure 3. Scatter plot between percent impervious surface and dynamic storage across the seven catchments. Colour coding is the same as Figure 9.
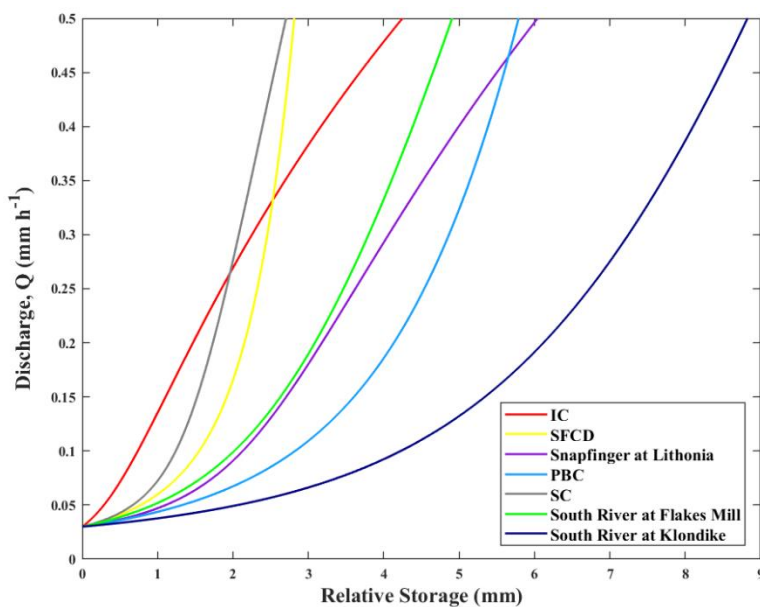
Figure 4. Storage-discharge relations for catchments in South River Watershed.

The results of the correlational analyses between dynamic storage and some catchment properties are illustrated graphically in Figures 17(a)-(f). Drainage area, elevation, forest and, percent developed have strong and statistically significant correlations with dynamic storage ($\sigma =$

0.86, p < 0.01; σ = -0.71, p < 0.05; σ 0.79, p < 0.05 and σ = -0.68, p < 0.05). Geology (BG: σ = -0.46 and MS: σ = 0.43), concavity index (μ: σ = 0.50), and discharge (0.43) all show moderate and statistically insignificant correlation. The correlation between dynamic storage and other catchment properties turned out to be very weak and insignificant (see Appendix C).
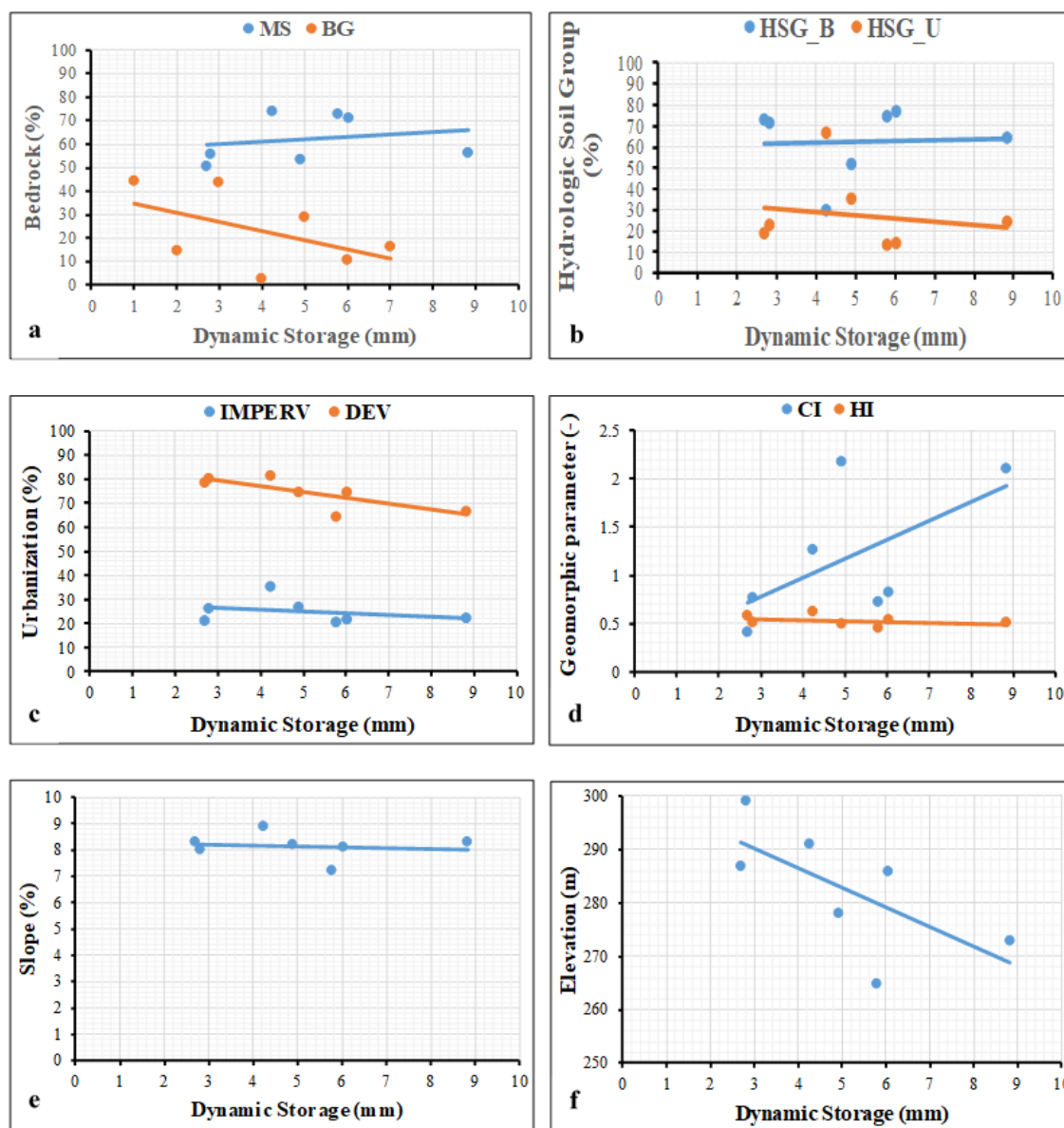
Figure 5. Watershed properties and dynamic storage association in SRW. MS (Mica Schist), BG (Biotite Gneiss), HSG (Hydrologic Soil Group), IMPERV (Impervious area), DEV (Development), CI (Concavity Index) and HI (Hypsometric Index).

To summarize all the results, the shapes of the FDC are similar across the catchments except for IC and PBC that exhibit different flow regimes around 20% and 90% exceedance probabilities, respectively. BFI is low in all the catchments and decline with increasing percentage impervious area. For the area-slope plots, slope decreases as the contributing area increases. The catchments have different discontinuities/gaps in the plots. The HC for all the catchments is similar and convex except for PBC which exhibit a concave HC, but the HI does not vary significantly. Most of the catchments are in the mature stage of geologic development. Recession behavior of the catchments vary as shown by the plots of *In(-dQ/dt)* vs *In(Q)*. Increased variability is observed for both high and low flows. Residual analyses demonstrate that the performance of the quadratic regression model improved only after the errors in the discharge data were corrected with the variable time step technique of Rupp and Selker (2006). By combining the recession plots for all the catchments, it is evident that flow recession rate for IC is the highest and lowest for SRK. In terms of streamflow sensitivity, SFCD is the most sensitive catchment to changes in storage followed by SC. The estimated dynamic storage values are small but similar in magnitude across the catchments, increasing in some (IC, PBC, and SFCL) with decreasing impervious surface coverage. The storage-discharge relationship is non-linear for all the catchment except for IC which appears to be linear. Dynamic storage correlate statistically and significantly with few physical catchment descriptors but was weak and/or insignificant with others.

6   DISCUSSIONS

What explains the dissimilarity in FDC slopes at flow extremes and the downward trend in BFI?

The similarity exhibited by the FDCs in these urban catchments as shown in Figure 8 is because they are geologically and pedologically homogeneous, particularly at low flow (see Tables 2, 3, and 4). Gordon et al. (2004, p. 217) stated that streams that drain the same geologic formations are likely to have similar low flow duration curves. The hump at 20% exceedance probability in the IC curve was due to the catchment's response to a precipitation event, which momentarily altered the flow pattern. The higher impervious surface area (35%) of the catchment caused more rainwater to flow to the stream via the infiltration overland flow mechanism (Meriano et al., 2011, p. 85). The large flow magnitude at the high flow end of the FDCs for IC and SFCD is due to urbanization. Increased impervious surface area has been reported in several studies to cause high streamflow velocities and runoff volumes (Rosburg, Nelson, & Bledsoe, 2017; Rose & Peters, 2001) as a result of overland flow (Meriano et al., 2011). The flow magnitude of SFCD (impervious area = ~26%) is higher than SRF (impervious area = 27%) as shown in Table 7 which is possibly due to the small size of the former's catchment (see Table 1). This is consistent with the results of Rosburg, Nelson, & Bledsoe (2017, p. 501) and they explained that larger catchments are more resistant to hydrologic changes and so have higher mean streamflow compared to smaller catchments. The slope of the SRK curve at the low flow end is flat and high suggesting "flow augmentation" (Rosburg, Nelson, & Bledsoe, 2017) due in part to effluent discharge from two wastewater treatment plants (WWTPs) within urbanized SRK (Diem et al., 2018). Groundwater contribution i.e., high baseflow (Gordon et al., 2004; Priest, 2004) can also be a factor. The steep PBC curve at the low flow end implies small baseflow (Gordon et al., 2004; Priest, 2004). Since the slope of FDCs mirrors the watershed's feedback from rainfall (Gordon et al., 2004), the drought

in Georgia (2012 and 2016) during the study period may have resulted in low rainfall and increased evapotranspiration, especially during summer time (PBC has the highest percent forest area). Urbanization, through paving of recharge zones (Rose & Peters, 2001), has led to decreased rainwater infiltration and reduced contribution from subsurface storage (i.e., groundwater) to streamflow (Price, 2011). It also explains why the BFI for PBC is isolated and the overall inverse relationship between BFI and impervious area in Figure 9. This result agrees with previous studies in Atlanta (Diem et al., 2018 and Calhoun, Frick, & Buell, 2003) and elsewhere (Kauffman, Belden, Vonck, & Homsey, 2009).

What effect do the geomorphic variables have on the watershed hydrology?

The inverse relationship depicted in the area-slope (A-S) plots in Figure 10 implies that fluvial erosive processes are dominant in the catchments i.e., mean slope decreases as contributing area increases. The gaps in A-S plots are natural discontinuities that are indicative of geomorphic process transitions (hillslope to fluvial processes) (Cohen et al., 2008; McNamara et al., 2006). Additionally, channel heads (stream sources) are formed at these transition areas, which are equally locations where the channel has been incised. Stream incision has been linked to the reduction of water table downstream (Micheli & Kirchner, 2002; Neal, 2009). It is hypothesized that the discontinuities observed in each A-S plot is facilitated by catchment urbanization. The strong correlation between the A-S parameters (μ and ρ) and percentage impervious surface area supports this hypothesis. Moreover, discontinuities are required to create fractures in rocks (Chapman, Crawford, & Tharpe, 1999, p. 9). But the poor correlation between the dominant bedrock types and A-S parameters (Appendix C) also suggests that the bedrock is not eroded. The strong correlation between A-S parameters and the dominant soil types suggests that fluvial processes may not depend on catchment bedrock. In Table 8, the R^2 value is greater than 0.98 for

all the catchments implying a good fit of the third order polynomial regression line to the binned A-S data. No literature on A-S study in urban catchments was found. The reason for this may be that urban settings are transformed natural landscapes and have been dramatically impacted by human activities. Hence, this provides an opportunity for further research. Overall, the result demonstrates that the polynomial regression captured the relationship between area and slope.

The IC watershed has the highest hypsometric index (HI) value and belong to the young group because it is less eroded, whereas PBC has undergone significant erosion so it has the lowest HI value and classified as old/late monadnock (Table 9). In Table 7, the high discharge magnitude in IC and low discharge magnitude can also be explained by their respective HI values in Table 9. A convex watershed that has experienced minimal erosion will display higher total runoff compared to a more eroded concave watershed (Vivoni, Di Benedetto, Grimaldi, & Eltahir, 2008). In addition, hypsometric distribution controls catchment water balance and runoff partitioning (Vivoni, Di Benedetto, Grimaldi, & Eltahir, 2008). Therefore, the convex shape of the hypsometric curve (HC) for all the catchments, with the exception of PBC, suggests that they will experience more erosion and transport processes, less soil moisture, and less infiltration (Willgoose & Hancock, 1998). PBC has a concave HC implying depositional processes, more soil moisture, and higher infiltration. The travel time of water in a catchment has been linked to the catchment hypsometric attributes (Luo & Harlin, 2003). This explains why HI (a quantitative measure of HC) strongly correlates with discharge and catchment development (see Appendix C).

How do discharge recession and sensitivity function vary across catchments?

The homogeneity of the geology, soil, climate, and overall extent of catchment development can be attributed to the clustering of the recession curves in the study watersheds despite differing spatial scales. This clustering is also indicative of similar recession pattern and

hydrological processes across the catchments (Figure 12). There was no systematic pattern of deviation in the *In(-dQ/dt)–In(Q)* relationship from linearity relative to catchment size. In a previous study within Atlanta, Clark et al. (2009) had demonstrated that *In(-dQ/dt)–In(Q)* relationship for the Panola Mountain Research Watershed (PMRW) deviated from linearity with increasing catchment scales. The authors attributed this to the nonlinearity of upslope (hillslope) hydraulics and spatial heterogeneity of recession properties. Gottschalk, Tallaksen, & Perzyna (1997) believed that such deviation could be attributed to the uncertainty associated with the choice of the model and fitting procedure for the estimation of recession parameters. The deviation of the recession curve of IC from the cluster shows that the catchment has a faster discharge rate, which is attributed to the high percent land impervious surface area facilitating Hortonian overland flow**.** The concave shapes of PBC and SFCD recession curves at low flow are possibly the result of human factors – the addition of effluent waters from the wastewater treatment plants at the two catchments (Wang & Cai, 2010).

The sign of the quadratic coefficient in the polynomial regression does not seem to be the only factor determining the convexity or concavity of the discharge sensitivity curve of the watersheds in this study. As reported by Adamovic et al. (2015) and observed in Kirchner (2009) and Teuling (2010), the shape of the *Q vs. g(Q)* plot is convex if a quadratic polynomial regression has a negative quadratic coefficient and concave otherwise. In this study, only two catchments (IC and SFCD) had negative quadratic coefficients resulting in convex sensitivity curves. The third catchment (SC) shape had a positive quadratic coefficient. The remaining four catchments have positive quadratic coefficients, yet the shape of the sensitivity function is linear and not concave. This implies that this observation may not hold for all catchments, and other factors like land cover/land-use change, hydrologic properties, and geology can explain the shape of the discharge

sensitivity function other than the sign of the quadratic coefficient. The result of the sensitivity analysis in this study is consistent with the result obtained by Bhaskar & Welty (2015) in urban catchments in Maryland, another Piedmont physiographic province with a similar climate as Atlanta. Though the authors found that the most urbanized catchment had the highest sensitivity to changes in storage, the most urbanized sub-catchment (IC) was not the most sensitive to changes in storage in SRW. The high sensitivity initially displayed by IC may be attributed to the catchment's response to a sudden change in subsurface storage after a precipitation event, as noted in the hump in the FDC plot in Figure 8. Still, it was found that $g(Q)$ had high values for two highly developed sub-catchments (IC and SFCD). The difference in the result between the two studies may be due to the size of the catchment and the regression model adopted to derive $g(Q)$: the previous study employed a power-law fitting technique, whereas the present study utilized a polynomial quadratic fitting model. Nevertheless, these results agree with the conclusion of Brown et al. (2009) that the response of a hydrologic variable to urbanization varied among metropolitan areas across the U. S.

How do the dynamic storage estimates in these urban watersheds compare to those from more natural watersheds?

The estimated dynamic storage values from the SDS model were small and varied among these urbanized catchments, but they had the same order of magnitude. The result in this study is consistent with the catchment storage estimated (4.88mm) by Meriano, Howard, & Eyles (2011, p. 91) in Frenchman's Bay watershed (>75% urbanized) in Ontario, Canada. Within Georgia State University (GSU) campus in downtown Atlanta, Waguespack (2019) estimated water depth in a well to be ~1m (1000mm) using ground penetrating radar (GPR). This figure suggests that absolute or total storage was estimated at this well and not dynamic storage. Catchment dynamic storage

study in urban systems is very limited, if available, and so comparison with previous studies is challenging. Nevertheless, a comparison is made with results from this study and those from some more natural, undisturbed catchments.

In the undisturbed Panola Mountain Recharge Watershed (PMRW) in Atlanta, Peters & Aulenbach (2011) estimated dynamic (active) storage to be in the range 40-70mm. For the Severn and Wye catchments in mid-Wales, Kirchner (2009) estimated dyanmic storage for the former to be 98mm and the latter 62mm. In the Rietholzbach catchment in Switzerland, Teuling et al. (2010) found that yearly average dynamic storage was 104mm, while over the whole 32-year period of record, the maximum estimated storage was 205mm. Ajami et al. (2011) considered mountain block recharge (MBR) to be equal to the lower bound of storage derived from the S-Q relationship. The storage value estimated for Marshall Gulch, which is a headwater to the Sabino Creek in Arizona in the Santa Catalina Mountains ranged from 14.8mm to 25.7mm for observed streamflow data. Birkel, Soulsby, & Tetzlaff (2011) estimated mean dynamic storage for two nested catchments in the Cairngorms National Park, Scotland to be 35mm for smaller Bruntland Burn catchment and 15mm for the larger Girnock catchment, respectively. Buttle (2016) provided estimates of the dynamic storage at five catchments in Ontario, Canada with similar catchment properties to range from 30mm to 77mm. Pfister (2017) estimated the dynamic storage in sixteen nested catchments (0.45 to 410 km^2) within the 1078 km^2 Alzette River basin in Luxembourg to vary from 107mm to 373mm. Staudinger et al. (2017) quantified the dynamic storage in twenty-one prealpine and alpine catchments (0.7 to 351 km^2) in Switzerland to vary between 12mm and 974mm, respectively. Dralle et al. (2018) estimated the direct (dynamic) storage of Elder Creek in the Northern California Eel River Critical Zone Observatory (ERCZO) to be 78mm. Finally, Carrer

et al. (2019) found that the dynamic storage for the experimental Weierbach catchment in Luxembourg ranged from range 64mm to 101mm between 2007 and 2014.

The estimated dynamic storage values from the preceding studies show that dynamic storage in these natural watersheds are 10^1 - 10^2 orders of magnitude greater than those estimated in urban watersheds. As demonstrated by Waguespack (2019) and Pfister (2017), absolute or total catchment storage can even be up to 10^3 order of magnitude greater than dynamic storage in urban settings. However, the SDS method employed in this study cannot be applied to estimate total catchment storage due to subsurface boundary problems (Dralle et al., 2018; Kobayashi & Yokoo, 2013; Tetzlaff et al., 2011). This comparative analysis of results also points to the huge effect of urbanization in estimating dynamic catchment storage. Rainwater that would have infiltrated the soil to recharge groundwater are either transported quickly to streams or rivers due to high impervious surface or are conveyed via storm sewer to wastewater treatment plants (WWTPs). However, several other factors such as aquifer properties, geology, soil and climate contribute in controlling storage dynamics. For example, the geology of a catchment moderates storage (Pfister et al., 2017) and baseflow (Tague & Grant, 2004). BG and MS are the two dominant bedrock types in all the catchments (Table 2) but they did not correlatte with storage (Appendix C). This pattern was observed with BFI, which is not unexpected given the layering/stratification of subsurface materials with each substratum exhibiting distinct hydrologic behavior. The non-correlatin implies that water is not released from the bedrock.

As recently reported by Waguespack (2019), the bedrock underlying urban Atlanta is close to the land surface and has a non-uniform topography. Depth to bedrock ranges from ~9m to ~12m below land surface. These bedrocks are fractured horizontally with a vertical extent between ~0.03m and ~0.20m (Cressler, Thurmond, & Hester, 1993). Waguespack (2019) confirmed this

when he estimated the water depth in a well within the Georgia State University (GSU) campus to be ~1m. Therefore, deeper percolation of infiltrated event water is very minimal, even if possible. Thus, the infiltration of precipitation progresses until it reaches the bedrock, where further infiltration of event water is halted due to low hydraulic conductivity since it reduces exponentially with depth. Hence, flow path changes and flow becomes lateral at the bedrock-soil interface. This is the runoff generation mechanism in the subsurface (saturation excess overland flow/lateral flow/interflow) at these catchments. The low values of dynamic storage inferred from streamflow data suggests little contribution from the bedrock, implying that saturated and unsaturated zones are not hydraulically connected. This explains the poor relationship between storage, BG, and MS. Further research is required in this regard. Most water in the Piedmont physiographic province is stored in the thick regolith (soils and saprolite layers) that overlies the bedrock. The downward flow of water through the vadose (unsaturated) zone is regulated by soil matric potential and hydraulic conductivity (Kirchner, 2009). Soils in HSG_B (dominant soil type) have good infiltration capacity, but there was no correlation with dynamic storage. The small estimated dynamic storage values suggest that the water stored in the regolith is not contributing to streamflow. Therefore, it is hypothesized that water in the unsaturated zone is held under very strong matric potential which inhibits its contribution to streamflow. Perhaps, the water forms part of a regional groundwater flow system.

7   CONCLUSIONS

Storage is an important component of a watershed's water budget, and its study is critical for understanding watershed hydrologic functions, ecosystem dynamics, and biogeochemical processes. However, few studies have quantified this key state variable in urban watersheds. In this study, storage-discharge relation was evaluated, and dynamic storage estimated among variably urbanized watersheds within South River Watershed, Atlanta, GA using the simple dynamical system approach developed by Kirchner (2009). Results show that two less developed sub-watersheds, in terms of impervious surface area (SC, 21% and SFCD, 26%), out of the seven investigated demonstrated high sensitivities to changes in storage. Storage-discharge relations across all the watersheds were non-linear, exhibiting threshold-like tendency except the most developed sub-watershed (IC - 35% impervious surface area), which displayed a one-to-one linear relationship. The non-linear storage-discharge relations exhibited by these urban watersheds are consistent with results from previous studies that applied the Kirchner (2009) approach, mostly in non-urbanized settings, in terms of recession characteristics (recession plots and curves) and storage-discharge relations.

Dynamic storage values in this nested urban watershed are small and vary with the same order of magnitude ranging from ~3mm to ~9mm. Inter-catchment differences in dynamic storage can be attributed to each catchment's subsurface property, flow recession rate, recession time, and extent of human activities. Compared to natural watersheds, estimated dynamic catchment storage for urban watersheds can be 10^1 - 10^2 and the absolute or total catchment storage can be 10^3 orders of magnitude lower. Interestingly, the dynamic storage value of the most developed sub-watershed was more than the two watersheds that showed the highest sensitivities. The small dynamic storage values observed across the watersheds are linked to watershed urbanization; however, other

factors, namely geology, low aquifer properties, and high soil matric potential may also account for this small dynamic storage values. Correlation analysis revealed that watershed properties such as topographic descriptors (drainage area and elevation), land use and land cover (forest and percent development), and geomorphology (concavity index) were significantly correlated with dynamic storage. Results in the current study agrees with previous investigations in urban catchments that groundwater recharge is feasible. Overall, the study shows that the simple dynamical system model which asserts that discharge is a single-valued function of watershed storage can be applied in urban catchments. Consequently, the South River Watershed (SRW), along with its sub-watersheds, can be regarded as dynamical systems.

REFERENCES

Adamovic, M., Braud, I., Branger, F., & Kirchner, J. W. (2015). Assessing the simple dynamical systems approach in a Mediterranean context: application to the Ardèche catchment (France). *Hydrology and Earth System Sciences, 19*(5), 2427-2449. doi:10.5194/hess-19-2427-2015

Ajami, H., Troch, P. A., Maddock, T., Meixner, T., & Eastoe, C. (2011). Quantifying mountain block recharge by means of catchment-scale storage-discharge relationships. *Water Resources Research, 47*(4). doi:10.1029/2010wr009598

Ambili, V., & Narayana, A. C. (2014). Tectonic effects on the longitudinal profiles of the Chaliyar River and its tributaries, southwest India. *Geomorphology, 217*, 37-47. doi:10.1016/j.geomorph.2014.04.013

Arnold, C. L., & Gibbons, C. J. (1996). Impervious Surface Coverage: The Emergence of a Key Environmental Indicator. *Journal of the American Planning Association, 62*(2), 243-258. doi:10.1080/01944369608975688

Atlanta Regional Commission (ARC) (2018). Population Estimates for the Atlanta Region: A Slightly Slow(er) Grow for Most

Aulenbach, B. T., Landers, M. N., Musser, J. W., & Painter, J. A. (2017). Effects of Impervious Area and BMP Implementation and Design on Storm Runoff and Water Quality in Eight Small Watersheds. *JAWRA Journal of the American Water Resources Association, 53*(2), 382-399. doi:10.1111/1752-1688.12501

Aulenbach, B. T., & Peters, N. E. (2018). Quantifying Climate-Related Interactions in Shallow and Deep Storage and Evapotranspiration in a Forested, Seasonally Water-Limited

Watershed in the Southeastern United States. *Water Resources Research, 54*(4), 3037-3061. doi:10.1002/2017wr020964

Basso, S., Schirmer, M., & Botter, G. (2015). On the emergence of heavy-tailed streamflow distributions. *Advances in Water Resources, 82*, 98-105. doi:10.1016/j.advwatres.2015.04.013

Berghuijs, W. R., Hartmann, A., & Woods, R. A. (2016). Streamflow sensitivity to water storage changes across Europe. *Geophysical Research Letters, 43*(5), 1980-1987. doi:10.1002/2016gl067927

Bhaskar, A. S., & Welty, C. (2015). Analysis of subsurface storage and streamflow generation in urban watersheds. *Water Resources Research, 51*(3), 1493-1513. doi:10.1002/2014wr015607

Birkel, C., Soulsby, C., & Tetzlaff, D. (2011). Modelling catchment-scale water storage dynamics: reconciling dynamic storage with tracer-inferred passive storage. *Hydrological Processes, 25*(25), 3924-3936. doi:10.1002/hyp.8201

Biswal, B., & Marani, M. (2010). Geomorphological origin of recession curves. *Geophysical Research Letters, 37*(24), n/a-n/a. doi:10.1029/2010gl045415

Biswal, B., & Nagesh Kumar, D. (2014). What mainly controls recession flows in river basins? *Advances in Water Resources, 65*, 25-33. doi:10.1016/j.advwatres.2014.01.001

Black, P. E. (1997). Watershed Functions. *Journal of The American Water Resources Association, 33(1)*.

Bosch, D. D., Arnold, J. G., Allen, P. G., Lim, K.-J., & Park, Y. S. (2017). Temporal variations in baseflow for the Little River experimental watershed in South Georgia, USA. *Journal of Hydrology: Regional Studies, 10*, 110-121. doi:10.1016/j.ejrh.2017.02.002

Brandes, D., Cavallo, G. J., & Nilson, M. L. (2005). Base Flow Trends in Urbanizing Watersheds of the Delaware River Basin. *Journal of the American Water Resources Association (JAWRA), 41(6)*, 1377-1391.

Brauer, C. C., Teuling, A. J., Torfs, P. J. J. F., & Uijlenhoet, R. (2013). Investigating storage-discharge relations in a lowland catchment using hydrograph fitting, recession analysis, and soil moisture data. *Water Resources Research, 49*(7), 4257-4264. doi:10.1002/wrcr.20320

Brown, A. E., Western, A. W., McMahon, T. A., & Zhang, L. (2013). Impact of forest cover changes on annual streamflow and flow duration curves. *Journal of Hydrology, 483*, 39-50. doi:10.1016/j.jhydrol.2012.12.031

Brown, L. R., Cuffney, T. F., Coles, J. F., Fitzpatrick, F., McMahon, G., Steuer, J., . . . May, J. T. (2009). Urban streams across the USA: lessons learned from studies in 9 metropolitan areas. *Journal of the North American Benthological Society, 28*(4), 1051-1069. doi:10.1899/08-153.1

Brummer, C. J., & Montgomery, D. R. (2003). Downstream coarsening in headwater channels. *Water Resources Research, 39*(10). doi:10.1029/2003wr001981

Brutsaert, W., & Nieber, J. L. (1977). Regionalized Drought Flow Hydrographs From a Mature Glaciated Plateau. *Water Resources Research, 13(3)*, 637 - 643.

Buttle, J. M. (2016). Dynamic storage: a potential metric of inter-basin differences in storage properties. *Hydrological Processes, 30*(24), 4644-4653. doi:10.1002/hyp.10931

Calhoun, D. L., Frick, E. A., & Buell, G. R. (2003). Effects of Urban Development on Nutrient Loads and Streamflow, Upper Chattahooche River Basin, Georgia, 1976–2001. *Proceedings of the 2003 Georgia Water Resources Conference, held April 23–24, 2003, at*

the University of Georgia. Kathryn J. Hatcher, editor, Institute of Ecology, The University of Georgia, Athens, Georgia.

Carrer, G. E., Klaus, J., & Pfister, L. (2019). Assessing the Catchment Storage Function Through a Dual-Storage Concept. *Water Resources Research, 55*(1), 476-494. doi:10.1029/2018wr022856

Chapman, J. M., Crawford, J. T., & Tharpe, W. T. (1999). Geology and Ground-Water Resources of the Lawrenceville Area, Georgia. *U. S. Geological Survey, Water-Resources Investigations Report, 98 - 4233*. doi:https://doi.org/10.3133/wri984233

Chen, X., Kumar, M., Basso, S., & Marani, M. (2018). On the effectiveness of recession analysis methods for capturing the characteristic storage-discharge relation: An intercomparison study. *Hydrology and Earth System Sciences Discussions*, 1-30. doi:10.5194/hess-2018-65

Chen, X., & Wang, D. (2013). Evaluating the effect of partial contributing storage on the storage–discharge function from recession analysis. *Hydrology and Earth System Sciences, 17*(10), 4283-4296. doi:10.5194/hess-17-4283-2013

Cheng, L., Zhang, L., Chiew, F. H. S., Canadell, J. G., Zhao, F., Wang, Y.-P., . . . Lin, K. (2017). Quantifying the impacts of vegetation changes on catchment storage-discharge dynamics using paired-catchment data. *Water Resources Research, 53*(7), 5963-5979. doi:10.1002/2017wr020600

Clark, M. P., Rupp, D. E., Woods, R. A., Tromp-van Meerveld, H. J., Peters, N. E., & Freer, J. E. (2009). Consistency between hydrological models and field observations: linking processes at the hillslope scale to hydrological responses at the watershed scale. *Hydrological Processes, 23*(2), 311-319. doi:10.1002/hyp.7154

Cohen, S., Willgoose, G., & Hancock, G. (2008). A methodology for calculating the spatial distribution of the area-slope equation and the hypsometric integral within a catchment. *Journal of Geophysical Research, 113*(F3). doi:10.1029/2007jf000820

Cressler, C. W., Thurmond, C. J., & Hester, W. G. (1993). Ground Water in the Greater Atlanta Region, Georgia. *Georgia Geologic Survey Information Circular 63, Georgia Department of Natural Resources, Environmental Protection Division, Georgia Geologic Survey*. Retrieved from https://www2.usgs.gov/water/southatlantic/ga/publications/ggs/ic-63/

Creutzfeldt, B., Troch, P. A., Güntner, A., Ferré, T. P. A., Graeff, T., & Merz, B. (2014). Storage-discharge relationships at different catchment scales based on local high-precision gravimetry. *Hydrological Processes, 28*(3), 1465-1475. doi:10.1002/hyp.9689

Dai, D., Neal, F. B., Diem, J., Deocampo, D. M., Stauber, C., & Dignam, T. (2019). Confluent impact of housing and geology on indoor radon concentrations in Atlanta, Georgia, United States. *Sci Total Environ, 668*, 500-511. doi:10.1016/j.scitotenv.2019.02.257

Diem, J. E., Hill, T. C., & Milligan, R. A. (2018). Diverse multi-decadal changes in streamflow within a rapidly urbanizing region. *Journal of Hydrology, 556*, 61-71. doi:10.1016/j.jhydrol.2017.10.026

Doulatyari, B., Betterle, A., Basso, S., Biswal, B., Schirmer, M., & Botter, G. (2015). Predicting streamflow distributions and flow duration curves from landscape and climate. *Advances in Water Resources, 83*, 285-298. doi:10.1016/j.advwatres.2015.06.013

Dralle, D. N., Hahm, W. J., Rempe, D. M., Karst, N. J., Thompson, S. E., & Dietrich, W. E. (2018). Quantification of the seasonal hillslope water storage that does not drive streamflow. *Hydrological Processes, 32*(13), 1978-1992. doi:10.1002/hyp.11627

Ebrahimian, A., Wilson, B. N., & Gulliver, J. S. (2016). Improved methods to estimate the effective impervious area in urban catchments using rainfall-runoff data. *Journal of Hydrology, 536*, 109-118. doi:10.1016/j.jhydrol.2016.02.023

Ferguson, K. B., & Suckling, W. P. (1990). Changing Rainfall-Runoff Relationships in the Urbanising Peachtree Creek Watershed, Atlanta, Georgia. *Water Resources Bulletin, 26(2)*, 313 - 322.

Flint, J. J. (1974). Stream Gradient as a Function of Order, Magnitude, and Discharge. *Water Resources Research, 10(5)*, 969 - 973.

Georgia Environmental Protection Division (2018). Water Quality in Georgia 2017-2018 (2016 – 305(b)/303(d) Integrated Report) (2016 Rivers/Streams), Georgia Department of Natural Resources, Environmental Protection Division. Retrieved from https://epd.georgia.gov/georgia-305b303d-list-documents

Gordon, D. N., McMahon, A. T., Finlayson, L. B., Gippel, J. C., & Nathan, J. R. (2004). Stream Hydrology: An Introduction for Ecologists. *John Wiley & Sons Ltd, The Atrium, Southern Gate, Chichester, West Sussex PO19 8SQ, England*.

Gordon, D. W., & Painter, J. A. (2018). Groundwater conditions in Georgia, 2015–16: U.S. Geological Survey Scientific Investigations Report 2017–5142, 59 p. doi:10.3133/sir20175142

Gottschalk, L., Tallaksen, M. L., & Perzyna, G. (1997). Derivation of low flow distribution functions using recession curves. *Journal of Hydrology, 194*, 239–262.

Grimaldi, S., Teles, V., & Bras, R. L. (2005). Preserving first and second moments of the slope area relationship during the interpolation of digital elevation models. *Advances in Water Resources, 28*(6), 583-588. doi:10.1016/j.advwatres.2004.11.014

Hailegeorgis, T. T., Alfredsen, K., Abdella, Y. S., & Kolberg, S. (2016). Evaluation of storage–discharge relationships and recession analysis-based distributed hourly runoff simulation in large-scale, mountainous and snow-influenced catchment. *Hydrological Sciences Journal, 61*(16), 2872-2886. doi:10.1080/02626667.2016.1170939

Hall, R. F. (1968). Base-Flow Recessions - A Review. *Water Resources Research, 4(5)*, 973-983.

Hayashi, M., & Rosenberry, O. D. (2002). Effects of Ground Water Exchange on the Hydrology and Ecology of Surface Water. *Groundwater, 40(3)*, 309-316.

Hector, B., Séguis, L., Hinderer, J., Cohard, J. M., Wubda, M., Descloitres, M., . . . Boy, J. P. (2015). Water storage changes as a marker for base flow generation processes in a tropical humid basement catchment (Benin): Insights from hybrid gravimetry. *Water Resources Research, 51*(10), 8331-8361. doi:10.1002/2014wr015773

Hrachowitz, M., Soulsby, C., Tetzlaff, D., Dawson, J. J. C., & Malcolm, I. A. (2009). Regionalization of transit time estimates in montane catchments by integrating landscape controls. *Water Resources Research, 45*(5). doi:10.1029/2008wr007496

Ijjasz-Vasquez, J. E., & Bras, L. R. (1995). Scaling regimes of local slope versus contributing area in digital elevation models. *Geomorphology, 12*, 299-311.

Jakeman, A. J., & Hornberger, G. M. (1993). <Jakeman_Hornberger -1993.pdf> How Much Complexity Is Warranted in a Rainfall-Runoff Model? *Water Resources Research, 29(8)*, 2637-2649.

Karlsen, R. H., Bishop, K., Grabs, T., Ottosson-Löfvenius, M., Laudon, H., & Seibert, J. (2019). The role of landscape properties, storage and evapotranspiration on variability in streamflow recessions in a boreal catchment. *Journal of Hydrology, 570*, 315-328. doi:10.1016/j.jhydrol.2018.12.065

Katsuyama, M., Tani, M., & Nishimoto, S. (2010). Connection between streamwater mean residence time and bedrock groundwater recharge/discharge dynamics in weathered granite catchments. *Hydrological Processes, 24*(16), 2287-2299. doi:10.1002/hyp.7741

Kauffman, J. G., Belden, C. A., Vonck, J. K., & Homsey, R. A. (2009). Link between Impervious Cover and Base Flow in the White Clay Creek Wild and Scenic Watershed in Delaware. *Journal of Hydrologic Engineering, 14(4)* 324-334. doi:10.1061/(ASCE)1084-0699(2009)14:4(324)

Kirby, E., & Whipple, K. X. (2012). Expression of active tectonics in erosional landscapes. *Journal of Structural Geology, 44*, 54-75. doi:10.1016/j.jsg.2012.07.009

Kirchner, J. W. (2009). Catchments as simple dynamical systems: Catchment characterization, rainfall-runoff modeling, and doing hydrology backward. *Water Resources Research, 45*(2). doi:10.1029/2008wr006912

Kobayashi, S., & Yokoo, Y. (2013). Estimating watershed-scale storage changes from hourly discharge data in mountainous humid watersheds: toward a new way of dominant process modeling. *Hydrological Research Letters, 7*(4), 97-103. doi:10.3178/hrl.7.97

Kok, K., Mohd Sidek, L., Jung, K., & Kim, J.-C. (2018). Application of Geomorphologic Factors for Identifying Soil Loss in Vulnerable Regions of the Cameron Highlands. *Water, 10*(4). doi:10.3390/w10040396

Krakauer, N. Y., & Temimi, M. (2011). Stream recession curves and storage variability in small watersheds. *Hydrology and Earth System Sciences, 15*(7), 2377-2389. doi:10.5194/hess-15-2377-2011

Krier, R., Matgen, P., Goergen, K., Pfister, L., Hoffmann, L., Kirchner, J. W., . . . Savenije, H. H. G. (2012). Inferring catchment precipitation by doing hydrology backward: A test in 24

small and mesoscale catchments in Luxembourg. *Water Resources Research, 48*(10). doi:10.1029/2011wr010657

Lague, D., & Davy, P. (2003). Constraints on the long-term colluvial erosion law by analyzing slope-area relationships at various tectonic uplift rates in the Siwaliks Hills (Nepal). *Journal of Geophysical Research: Solid Earth, 108*(B2). doi:10.1029/2002jb001893

Lerner, D. N. (2002). Identifying and quantifying urban recharge: a review. *Hydrogeology Journal, 10*(1), 143-152. doi:10.1007/s10040-001-0177-1

Li, W., & Nieber, J. L. (2017). A modified simple dynamic model: Derived from the information embedded in observed streamflows. *Journal of Hydrology, 552*, 198-209. doi:10.1016/j.jhydrol.2017.06.014

Liu, G., Schwartz, F. W., & Kim, Y. (2013). Complex baseflow in urban streams: an example from central Ohio, USA. *Environmental Earth Sciences, 70*(7), 3005-3014. doi:10.1007/s12665-013-2358-3

Lo, C. P., & Yang, X. (2002). Drivers of Land-Use/Land-Cover Changes and Dynamic Modeling for the Atlanta, Georgia Metropolitan Area. *Photogrammetric Engineering & Remote Sensing, 68(10)*, 1073-1082.

Long, D. D., & Badwin, M. (1914). Soil Survey of DeKalb County, Georgia. Retrieved from https://www.nrcs.usda.gov/Internet/FSE_MANUSCRIPTS/georgia/dekalbGA1914/dekalbGA1914.pdf

Luo, W. (2000). Quantifying groundwater-sapping landforms with a hypsometric technique. *Journal of Geophysical Research: Planets, 105*(E1), 1685-1694. doi:10.1029/1999je001096

Luo, W. L., & Harlin, M. J. (2003). A Theoretical Travel Time Based on Watershed Hypsometry. *Journal of The American Water Resources Association, 39(4)*, 785-792.

Majone, B., Bertagnoli, A., & Bellin, A. (2010). A non-linear runoff generation model in small Alpine catchments. *Journal of Hydrology, 385*(1-4), 300-312. doi:10.1016/j.jhydrol.2010.02.033

McNamara, J. P., Tetzlaff, D., Bishop, K., Soulsby, C., Seyfried, M., Peters, N. E., . . . Hooper, R. (2011). Storage as a Metric of Catchment Comparison. *Hydrological Processes, 25*(21), 3364-3371. doi:10.1002/hyp.8113

McNamara, J. P., Ziegler, A. D., Wood, S. H., & Vogler, J. B. (2006). Channel head locations with respect to geomorphologic thresholds derived from a digital elevation model: A case study in northern Thailand. *Forest Ecology and Management, 224*(1-2), 147-156. doi:10.1016/j.foreco.2005.12.014

Melsen, L. A., Teuling, A. J., van Berkum, S. W., Torfs, P. J. J. F., & Uijlenhoet, R. (2014). Catchments as simple dynamical systems: A case study on methods and data requirements for parameter identification. *Water Resources Research, 50*(7), 5577-5596. doi:10.1002/2013wr014720

Méndez-Barroso, L. A., Zárate-Valdez, J. L., & Robles-Morúa, A. (2018). Estimation of hydromorphological attributes of a small forested catchment by applying the Structure from Motion (SfM) approach. *International Journal of Applied Earth Observation and Geoinformation, 69*, 186-197. doi:10.1016/j.jag.2018.02.015

Meriano, M., Howard, K. W. F., & Eyles, N. (2011). The role of midsummer urban aquifer recharge in stormflow generation using isotopic and chemical hydrograph separation techniques. *Journal of Hydrology, 396*(1-2), 82-93. doi:10.1016/j.jhydrol.2010.10.041

Micheli, E. R., & Kirchner, J. W. (2002). Effects of wet meadow riparian vegetation on streambank erosion. 1. Remote sensing measurements of streambank migration and erodibility. *Earth Surface Processes and Landforms, 27*(6), 627-639. doi:10.1002/esp.338

Mohamoud, Y. M. (2010). Prediction of daily flow duration curves and streamflow for ungauged catchments using regional flow duration curves. *Hydrological Sciences Journal, 53*(4), 706-724. doi:10.1623/hysj.53.4.706

Neal, G. E. (2009). Channel Incision and Water-Table Decline Along a Recently Formed Proglacial Stream, Mendenhall Valley, Southeastern Alaska. *in Haeussler, P.J., and Galloway, J.P., Studies by the U.S. Geological Survey in Alaska, 2007: U.S. Geological Survey Professional Paper 1760-E, 15 p.* Retrieved from http://pubs.usgs.gov/pp/1760/e/

O'Driscoll, M., Clinton, S., Jefferson, A., Manda, A., & McMillan, S. (2010). Urbanization Effects on Watershed Hydrology and In-Stream Processes in the Southern United States. *Water, 2*(3), 605-648. doi:10.3390/w2030605

Ockenden, M. C., Chappell, N. A., & Neal, C. (2014). Quantifying the differential contributions of deep groundwater to streamflow in nested basins, using both water quality characteristics and water balance. *Hydrology Research, 45*(2), 200-212. doi:10.2166/nh.2013.035

Ourso, R. T., & Frenzel, S. A. (2003). Identification of linear and threshold responses in streams along a gradient of urbanization in Anchorage, Alaska∗. *Hydrobiologia, 501*, 117-131.

Peters, N. E. (2009). Effects of urbanization on stream water quality in the city of Atlanta, Georgia, USA. *Hydrological Processes, 23*(20), 2860-2878. doi:10.1002/hyp.7373

Peters, N. E., & Aulenbach, B. T. (2011). Water storage at the Panola Mountain Research Watershed, Georgia, USA. *Hydrological Processes, 25*(25), 3878-3889. doi:10.1002/hyp.8334

Pfister, L., Martínez-Carreras, N., Hissler, C., Klaus, J., Carrer, G. E., Stewart, M. K., & McDonnell, J. J. (2017). Bedrock geology controls on catchment storage, mixing, and release: A comparative analysis of 16 nested catchments. *Hydrological Processes, 31*(10), 1828-1845. doi:10.1002/hyp.11134

Pike, R. J., & Stephen, E. W. (1971). Elevation-Relief Ratio, Hypsometric Integral, and Geomorphic Area-Altitude Analysis. *Geological Society of America Bulletin, 82*, 1079-1084.

Price, K. (2011). Effects of watershed topography, soils, land use, and climate on baseflow hydrology in humid regions: A review. *Progress in Physical Geography: Earth and Environment, 35*(4), 465-492. doi:10.1177/0309133311402714

Priest, S. (2004). Evaluation of Ground-Water Contribution to Streamflow in Coastal Georgia and Adjacent Parts of Florida and South Carolina. *U.S. Geological Survey Scientific Investigations Report 2004-5265, p. 46.* Retrieved from http://pubs.usgs.gov/

Ragab, R., Rosier, P., Dixon, A., Bromley, J., & Cooper, J. D. (2003). Experimental study of water fluxes in a residential area: 2. Road infiltration, runoff and evaporation. *Hydrological Processes, 17*(12), 2423-2437. doi:10.1002/hyp.1251

Riegger, J., & Tourian, M. J. (2014). Characterization of runoff-storage relationships by satellite gravimetry and remote sensing. *Water Resources Research, 50*(4), 3444-3466. doi:10.1002/2013wr013847

Roques, C., Rupp, D. E., & Selker, J. S. (2017). Improved streamflow recession parameter estimation with attention to calculation of $- dQ/dt$. *Advances in Water Resources, 108*, 29-43. doi:10.1016/j.advwatres.2017.07.013

Rosburg, T. T., Nelson, P. A., & Bledsoe, B. P. (2017). Effects of Urbanization on Flow Duration and Stream Flashiness: A Case Study of Puget Sound Streams, Western Washington, USA. *JAWRA Journal of the American Water Resources Association, 53*(2), 493-507. doi:10.1111/1752-1688.12511

Rose, S. (2002). Comparative major ion geochemistry of Piedmont streams in the Atlanta, Georgia region: possible effects of urbanization. *Environmental Geology, 42*(1), 102-113. doi:10.1007/s00254-002-0545-8

Rose, S. (2003). Comparative solute–discharge hysteresis analysis for an urbanized and a 'control basin' in the Georgia (USA) Piedmont. *Journal of Hydrology, 284*(1-4), 45-56. doi:10.1016/j.jhydrol.2003.07.001

Rose, S. (2007). The effects of urbanization on the hydrochemistry of base flow within the Chattahoochee River Basin (Georgia, USA). *Journal of Hydrology, 341*(1-2), 42-54. doi:10.1016/j.jhydrol.2007.04.019

Rose, S., & Peters, N. E. (2001). Effects of urbanization on streamflow in the Atlanta area (Georgia, USA): a comparative hydrological approach. *Hydrological Processes, 15*(8), 1441-1457. doi:10.1002/hyp.218

Rupp, D. E., & Selker, J. S. (2006). On the use of the Boussinesq equation for interpreting recession hydrographs from sloping aquifers. *Water Resources Research, 42*(12). doi:10.1029/2006wr005080

Rusjan, S., & Mikoš, M. (2015). A catchment as a simple dynamical system: Characterization by the streamflow component approach. *Journal of Hydrology, 527*, 794-808. doi:10.1016/j.jhydrol.2015.05.050

Sayama, T., McDonnell, J. J., Dhakal, A., & Sullivan, K. (2011). How much water can a watershed store? *Hydrological Processes, 25*(25), 3899-3908. doi:10.1002/hyp.8288

Schwartz, S. S., & Smith, B. (2014). Slowflow fingerprints of urban hydrology. *Journal of Hydrology, 515*, 116-128. doi:10.1016/j.jhydrol.2014.04.019

Shuster, W. D., Bonta, J., Thurston, H., Warnemuende, E., & Smith, D. R. (2005). Impacts of impervious surface on watershed hydrology: A review. *Urban Water Journal, 2*(4), 263-275. doi:10.1080/15730620500386529

Singh, O., Sarangi, A., & Sharma, M. C. (2008). Hypsometric Integral Estimation Methods and its Relevance on Erosion Status of North-Western Lesser Himalayan Watersheds. *Water Resources Management, 22*(11), 1545-1560. doi:10.1007/s11269-008-9242-z

Smucygz, B., Clayton, J. A., & Comarova, Z. (2010). Comparison of Changes in Runoff and Channel Cross-sectional Area as a Consequence of Urbanization for Three Chattahoochee River Subbasins, Georgia, USA. *Southeastern Geographer, 50(4)*, 468–483.

Snyder, N. P., Whipple, K. X., Tucker, G. E., & Merritts, D. J. (2000). Landscape response to tectonic forcing: Digital elevation model analysis of stream profiles in the Mendocino triple junction region, northern California. *Geological Society of America Bulletin, 112(8)*, 1250–1263.

Stankowski, S.J., 1972. Population density as an indirect indicator of urban and suburban land-surface modifications. Geological survey research 1972. U.S. Geological Survey, Trenton, NJ, USA, Chapter B, p. 0800-B, pp. B219–B224.

Staudinger, M., Stahl, K., Seibert, J., Clark, M. P., & Tallaksen, L. M. (2011). Comparison of hydrological model structures based on recession and low flow simulations. *Hydrology and Earth System Sciences, 15*(11), 3447-3459. doi:10.5194/hess-15-3447-2011

Staudinger, M., Stoelzle, M., Seeger, S., Seibert, J., Weiler, M., & Stahl, K. (2017). Catchment water storage variation with elevation. *Hydrological Processes, 31*(11), 2000-2015. doi:10.1002/hyp.11158

Stewart, M. K. (2015). Promising new baseflow separation and recession analysis methods applied to streamflow at Glendhu Catchment, New Zealand. *Hydrology and Earth System Sciences, 19*(6), 2587-2603. doi:10.5194/hess-19-2587-2015

Stock, J., & Dietrich, W. E. (2003). Valley incision by debris flows: Evidence of a topographic signature. *Water Resources Research, 39*(4). doi:10.1029/2001wr001057

Stoelzle, M., Stahl, K., Morhard, A., & Weiler, M. (2014). Streamflow sensitivity to drought scenarios in catchments with different geology. *Geophysical Research Letters, 41*(17), 6174-6183. doi:10.1002/2014gl061344

Strahler, A. N. (1952). Hypsometric (Area-Altitude) Analysis of Erosional Topography. *Bulletin of the Geological Society of America, 63*, 1117-1142.

Strahler, A. N. (1957). Quantitative analysis of watershed geomorphology. *Transactions, American Geophysical Union, 38(6).*

Tague, C., & Grant, G. E. (2004). A geological framework for interpreting the low-flow regimes of Cascade streams, Willamette River Basin, Oregon. *Water Resources Research, 40*(4). doi:10.1029/2003wr002629

Tetzlaff, D., McNamara, J. P., & Carey, S. K. (2011). Measurements and modelling of storage dynamics across scales. *Hydrological Processes, 25*(25), 3831-3835. doi:10.1002/hyp.8396

Teuling, A. J., Lehner, I., Kirchner, J. W., & Seneviratne, S. I. (2010). Catchments as simple dynamical systems: Experience from a Swiss prealpine catchment. *Water Resources Research, 46*(10). doi:10.1029/2009wr008777

Thomas, J. G. J. (1979). Soil Survey of DeKalb County, Georgia. *United States Department of Agriculture, Soil Conservation Service*.

Troch, P. A., Berne, A., Bogaart, P., Harman, C., Hilberts, A. G. J., Lyon, S. W., . . . Verhoest, N. E. C. (2013). The importance of hydraulic groundwater theory in catchment hydrology: The legacy of Wilfried Brutsaert and Jean-Yves Parlange. *Water Resources Research, 49*(9), 5099-5116. doi:10.1002/wrcr.20407

Troch, P. A., Francois, P. D. T., & Brutsaert, W. (1993). Effective Water Table Depth to Describe Initial Conditions Prior to Storm Rainfall in Humid Region. *Water Resources Research, 29(2)*, 427-434.

United Nations. (2019). World Urbanization Prospects: The 2018 Revision (ST/ESA/SER.A/420). *Department of Economic and Social Affairs, Population Division (2019). New York: United Nations.*

Vivoni, E. R., Di Benedetto, F., Grimaldi, S., & Eltahir, E. A. B. (2008). Hypsometric control on surface and subsurface runoff. *Water Resources Research, 44*(12). doi:10.1029/2008wr006931

Vogel, R. M., & Kroll, C. N. (1992). Regional Geohydrologic-Geomorphic Relationships for the Estimation of Low-Flow Statistics. *Water Resources Research, 28(9)*, 2451-2458.

Waguespack, J. (2019). Characterization of a Shallow Urban Aquifer in Atlanta, Georgia. *Thesis, Georgia State University*. Retrieved from https://scholarworks.gsu.edu/geosciences_theses/129

Walsh, C. J., Roy, A. H., Feminella, J. W., Cottingham, P. D., Groffman, P. M., & Morgan, R. P. I. (2005). The urban stream syndrome: current knowledge and the search for a cure. *Journal of the North American Benthological Society, 24(3)*, 706-723. doi:10.1899/04-028.1

Wang, D., & Cai, X. (2010). Comparative study of climate and human impacts on seasonal baseflow in urban and agricultural watersheds. *Geophysical Research Letters, 37*(6), n/a-n/a. doi:10.1029/2009gl041879

Weill, S., Altissimo, M., Cassiani, G., Deiana, R., Marani, M., & Putti, M. (2013). Saturated area dynamics and streamflow generation from coupled surface–subsurface simulations and field observations. *Advances in Water Resources, 59*, 196-208. doi:10.1016/j.advwatres.2013.06.007

Wenger, S. J., Peterson, J. T., Freeman, M. C., Freeman, B. J., & Homans, D. D. (2008). Stream fish occurrence in response to impervious cover, historic land use, and hydrogeomorphic factors. *Canadian Journal of Fisheries and Aquatic Sciences, 65*(7), 1250-1264. doi:10.1139/f08-046

Wickham, J. D., Wade, T. G., & Norton, D. J. (2014). Spatial patterns of watershed impervious cover relative to stream location. *Ecological Indicators, 40*, 109-116. doi:10.1016/j.ecolind.2014.01.013

Willgoose, G. (1994). A physical explanation for an observed area-slope-elevation relationship for catchments with declining relief. *Water Resources Research, 30(2)*, 151-159.

Willgoose, G., & Hancock, G. (1998). Revisiting the Hypsometric Curve as an Indicator of Form and Process in Transport-Limited Catchment. *Earth Surface Processes and Landforms, 23*, 611–623.

Wittenberg, H. (1999). *Hydrological Processes, 13*, 715-726.

Xu, N., Saiers, J. E., Wilson, H. F., & Raymond, P. A. (2012). Simulating streamflow and dissolved organic matter export from a forested watershed. *Water Resources Research, 48*(5). doi:10.1029/2011wr011423

Yang, L., Jin, S., Danielson, P., Homer, C., Gass, L., Bender, S. M., . . . Xian, G. (2018). A new generation of the United States National Land Cover Database: Requirements, research priorities, design, and implementation strategies. *ISPRS Journal of Photogrammetry and Remote Sensing, 146*, 108-123. doi:10.1016/j.isprsjprs.2018.09.006

Zaprowski, B. J. (2005). Climatic influences on profile concavity and river incision. *Journal of Geophysical Research, 110*(F3). doi:10.1029/2004jf000138

Zecharias, Y. B., & Brutsaert, W. (1988). Recession Characteristics of Groundwater Outflow and Base Flow From Mountainous Watersheds. *Water Resources Research, 24(10)*, 1651-1658.

Zhou, B., He, H. S., Nigh, T. A., & Schulz, J. H. (2012). Mapping and analyzing change of impervious surface for two decades using multi-temporal Landsat imagery in Missouri. *International Journal of Applied Earth Observation and Geoinformation, 18*, 195-206. doi:10.1016/j.jag.2012.02.003

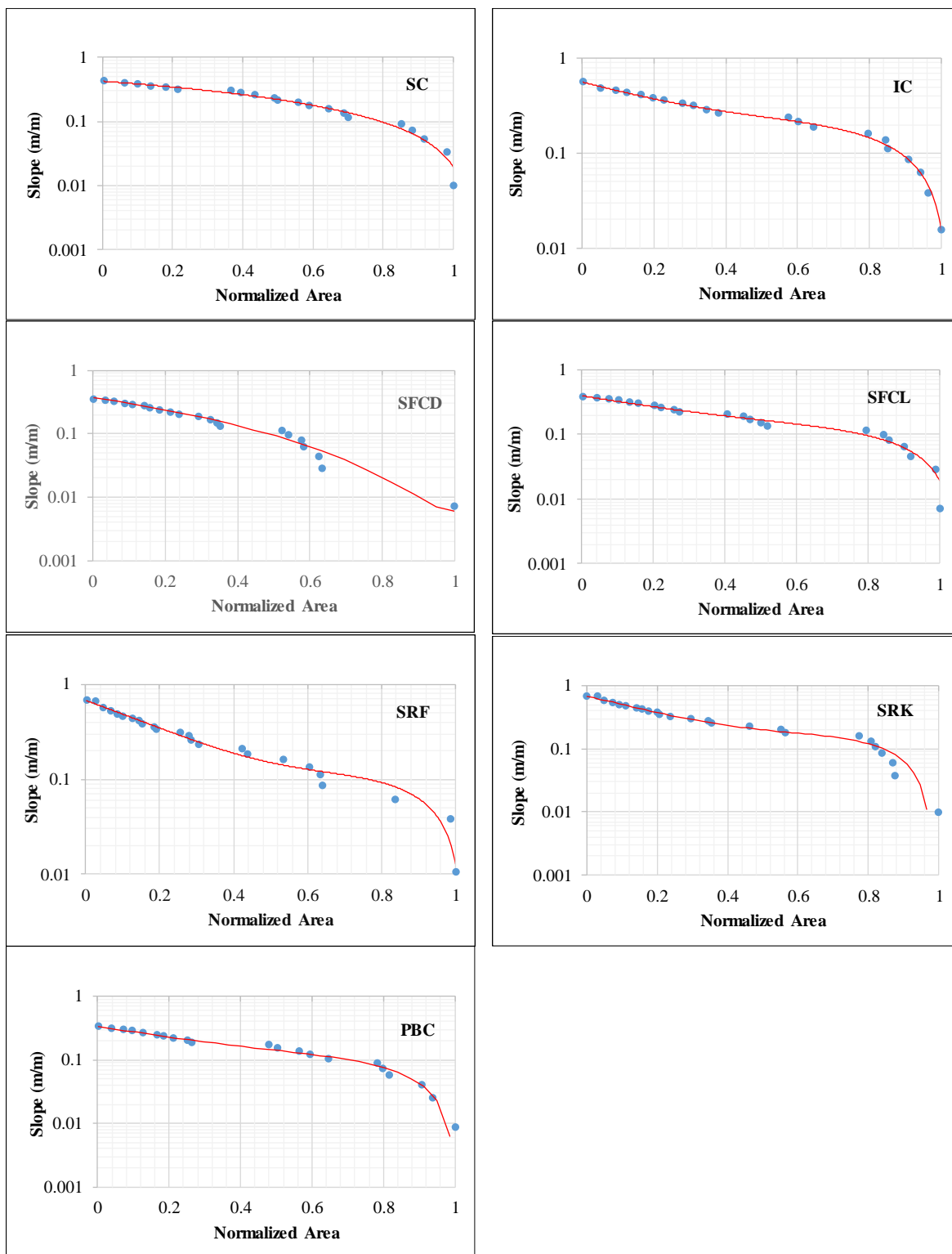# APPENDICES

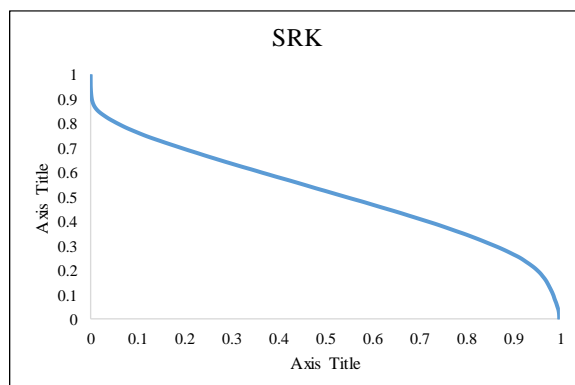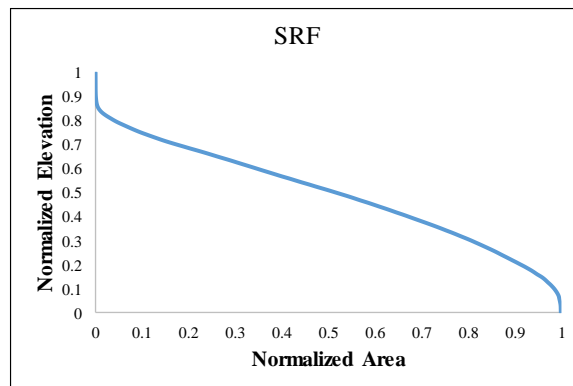**Appendix A: Area-slope relationship plot for each catchment**

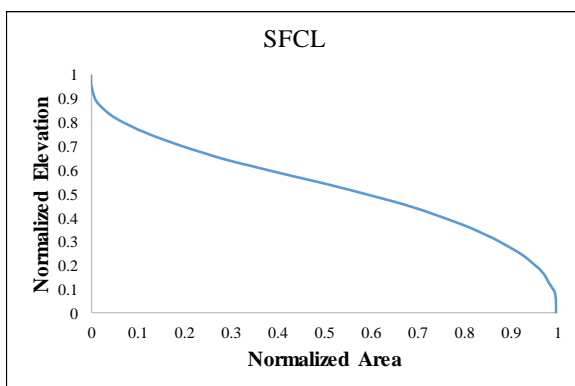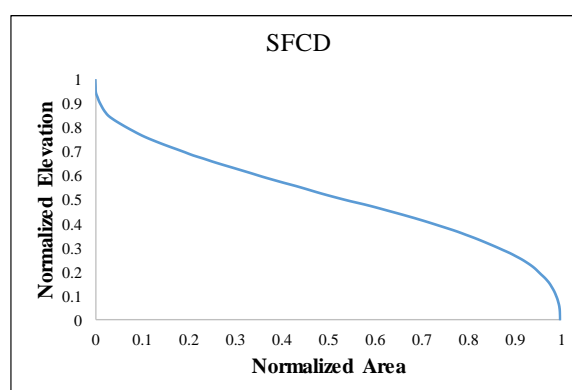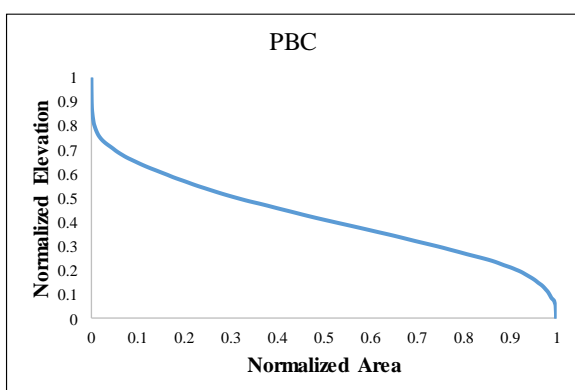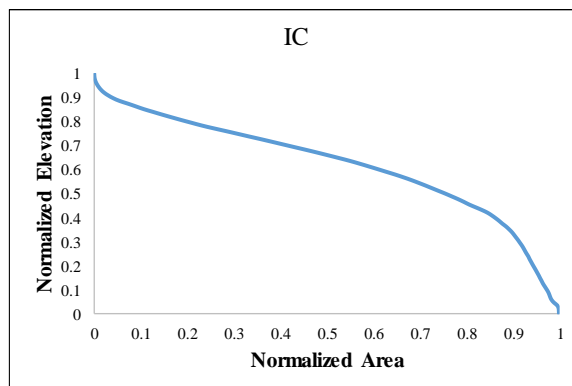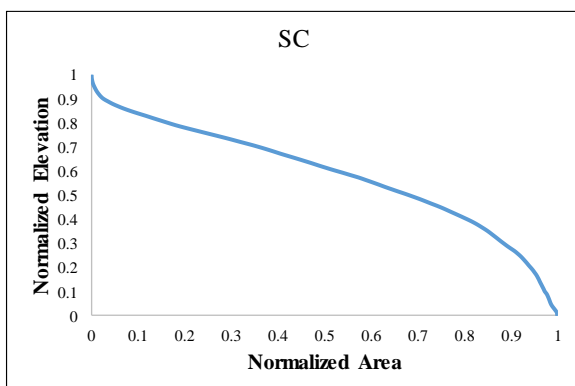**Appendix B: Hypsometric curve for each catchment**

Appendix C: Non-parametric correlation result

Appendix A

Appendix B

SC

IC

PBC

SFCD

SFCL

SRF

SRK

Appendix C

Nonparametric Correlations

			Area	Impervious Area	Developed	Forest	Storage	Population Density Change	Concavity Index	Steepness Index	Elevation	Slope	BG	MS	BFI	HI	HSG_B	HSG_U	Precipitation	Discharge
Spearman's rho (σ)	Area	Correlation Coefficient	1.000	0.071	-.679*	.714*	.857**	-0.321	.714*	0.429	-0.643	-0.180	-0.429	0.036	0.036	-0.377	-0.036	0.071	0.179	0.286
		Sig. (1-tailed)		0.440	0.047	0.036	0.007	0.241	0.036	0.169	0.060	0.350	0.169	0.470	0.470	0.231	0.470	0.440	0.351	0.267
	Impervious	Correlation Coefficient	0.071	1.000	0.571	-0.571	-0.143	0.321	.714*	0.536	0.500	0.505	-0.107	0.107	-0.214	0.464	-.857**	.929**	-0.393	0.643
		Sig. (1-tailed)	0.440		0.090	0.090	0.380	0.241	0.036	0.108	0.127	0.124	0.410	0.410	0.322	0.177	0.007	0.001	0.192	0.060
	Developed	Correlation Coefficient	-.679*	0.571	1.000	-.929**	-.679*	.750*	-0.107	0.000	.964**	0.450	0.536	0.000	0.071	.812*	-0.357	0.464	-0.286	0.321
		Sig. (1-tailed)	0.047	0.090		0.001	0.047	0.026	0.410	0.500	0.000	0.155	0.108	0.500	0.440	0.025	0.216	0.147	0.267	0.241
	Forest	Correlation Coefficient	.714*	-0.571	-.929**	1.000	.786*	-0.536	0.071	-0.179	-.857**	-0.613	-0.464	0.179	-0.143	-0.638	0.500	-0.571	0.250	-0.143
		Sig. (1-tailed)	0.036	0.090	0.001		0.018	0.108	0.440	0.351	0.007	0.072	0.147	0.351	0.380	0.087	0.127	0.090	0.294	0.380
	Storage	Correlation Coefficient	.857**	-0.143	-.679*	.786*	1.000	-0.143	0.500	0.250	-.714*	-0.144	-0.464	0.429	-0.036	-0.116	0.179	-0.143	0.071	0.429
		Sig. (1-tailed)	0.007	0.380	0.047	0.018		0.380	0.127	0.294	0.036	0.379	0.147	0.169	0.470	0.413	0.351	0.380	0.440	0.169
	PopulationChange	Correlation Coefficient	-0.321	0.321	.750*	-0.536	-0.143	1.000	-0.036	-0.036	.714*	0.306	0.571	0.214	0.321	.928**	0.071	0.143	0.000	0.536
		Sig. (1-tailed)	0.241	0.241	0.026	0.108	0.380		0.470	0.470	0.036	0.252	0.090	0.322	0.241	0.004	0.440	0.380	0.500	0.108
	ConcavityIndex	Correlation Coefficient	.714*	.714*	-0.107	0.071	0.500	-0.036	1.000	.750*	-0.179	0.342	-0.429	0.107	-0.071	0.174	-0.643	.714*	-0.107	0.607
		Sig. (1-tailed)	0.036	0.036	0.410	0.440	0.127	0.470		0.026	0.351	0.226	0.169	0.410	0.440	0.371	0.060	0.036	0.410	0.074
	SteepnessIndex	Correlation Coefficient	0.429	0.536	0.000	-0.179	0.250	-0.036	.750*	1.000	-0.107	.775*	-0.036	-0.214	0.357	0.261	-.679*	.750*	-0.214	0.429
		Sig. (1-tailed)	0.169	0.108	0.500	0.351	0.294	0.470	0.026		0.410	0.020	0.470	0.322	0.216	0.309	0.047	0.026	0.322	0.169
	Elevation	Correlation Coefficient	-0.643	0.500	.964**	-.857**	-.714*	.714*	-0.179	-0.107	1.000	0.270	0.643	-0.143	0.107	0.667	-0.250	0.357	-0.214	0.214
		Sig. (1-tailed)	0.060	0.127	0.000	0.007	0.036	0.036	0.351	0.410		0.279	0.060	0.380	0.410	0.074	0.294	0.216	0.322	0.322
	Slope	Correlation Coefficient	-0.180	0.505	0.450	-0.613	-0.144	0.306	0.342	.775*	0.270	1.000	0.198	-0.018	0.324	0.638	-0.649	.721*	-0.414	0.450
		Sig. (1-tailed)	0.350	0.124	0.155	0.072	0.379	0.252	0.226	0.020	0.279		0.335	0.485	0.239	0.087	0.057	0.034	0.178	0.155
	BG	Correlation Coefficient	-0.429	-0.107	0.536	-0.464	-0.464	0.571	-0.429	-0.036	0.643	0.198	1.000	-0.536	.714*	0.551	0.250	-0.107	0.107	-0.107
		Sig. (1-tailed)	0.169	0.410	0.108	0.147	0.147	0.090	0.169	0.470	0.060	0.335		0.108	0.036	0.129	0.294	0.410	0.410	0.410
	MS	Correlation Coefficient	0.036	0.107	0.000	0.179	0.429	0.214	0.107	-0.214	-0.143	-0.018	-0.536	1.000	-0.643	0.406	-0.036	0.000	-0.429	0.607
		Sig. (1-tailed)	0.470	0.410	0.500	0.351	0.169	0.322	0.410	0.322	0.380	0.485	0.108		0.060	0.212	0.470	0.500	0.169	0.074
	BFI	Correlation Coefficient	0.036	-0.214	0.071	-0.143	-0.036	0.321	-0.071	0.357	0.107	0.324	.714*	-0.643	1.000	0.319	0.286	-0.107	0.500	-0.179
		Sig. (1-tailed)	0.470	0.322	0.440	0.380	0.470	0.241	0.440	0.216	0.410	0.239	0.036	0.060		0.269	0.267	0.410	0.127	0.351
	HI	Correlation Coefficient	-0.377	0.464	.812*	-0.638	-0.116	.928**	0.174	0.261	0.667	0.638	0.551	0.406	0.319	1.000	-0.232	0.464	-0.348	.899**
		Sig. (1-tailed)	0.231	0.177	0.025	0.087	0.413	0.004	0.371	0.309	0.074	0.087	0.129	0.212	0.269		0.329	0.177	0.250	0.007
	HSGB	Correlation Coefficient	-0.036	-.857**	-0.357	0.500	0.179	0.071	-0.643	-.679*	-0.250	-0.649	0.250	-0.036	0.286	-0.232	1.000	-.964**	0.607	-0.464
		Sig. (1-tailed)	0.470	0.007	0.216	0.127	0.351	0.440	0.060	0.047	0.294	0.057	0.294	0.470	0.267	0.329		0.000	0.074	0.147
	HSGU	Correlation Coefficient	0.071	.929**	0.464	-0.571	-0.143	0.143	.714*	.750*	0.357	.721*	-0.107	0.000	-0.107	0.464	-.964**	1.000	-0.500	0.571
		Sig. (1-tailed)	0.440	0.001	0.147	0.090	0.380	0.380	0.036	0.026	0.216	0.034	0.410	0.500	0.410	0.177	0.000		0.127	0.090
	Precipitation	Correlation Coefficient	0.179	-0.393	-0.286	0.250	0.071	0.000	-0.107	-0.214	-0.214	-0.414	0.107	-0.429	0.500	-0.348	0.607	-0.500	1.000	-0.536
		Sig. (1-tailed)	0.351	0.192	0.267	0.294	0.440	0.500	0.410	0.322	0.322	0.178	0.410	0.169	0.127	0.250	0.074	0.127		0.108
	Discharge	Correlation Coefficient	0.286	0.643	0.321	-0.143	0.429	0.536	0.607	0.429	0.214	0.450	-0.107	0.607	-0.179	.899**	-0.464	0.571	-0.536	1.000
		Sig. (1-tailed)	0.267	0.060	0.241	0.380	0.169	0.108	0.074	0.169	0.322	0.155	0.410	0.074	0.351	0.007	0.147	0.090	0.108	

**. Correlation is significant at the 0.01 level (1-tailed).

*. Correlation is significant at the 0.05 level (1-tailed).